Materials for Molecular Electronics Devices: Anchoring Azulene Derivatives to A Gold Surface via Molecular Self-Assembly

By

Monisola Khadijat Okeowo

Submitted to the graduate degree program in the Department of Chemistry and the Graduate Faculty of the University of Kansas in partial fulfillment of the requirements for the degree of Doctor of Philosophy.

Co-Chair: Dr. Mikhail V. Barybin

Co-Chair: Dr. Cindy L. Berrie

Dr. Timothy A. Jackson

Dr. Christopher Elles

Dr. Kyle V. Camarda

Date Defended: December 4, 2018

The dissertation committee for Monisola Khadijat Okeowo
certifies that this is the approved version of the following dissertation:

Materials for Molecular Electronics Devices: Anchoring Azulene Derivatives to A Gold Surface via Molecular Self-Assembly

Co-Chair: Dr. Mikhail V. Barybin

Co-Chair: Dr. Cindy L. Berrie

Date Approved: December 4, 2018

Abstract

The use of molecular electronics to build nano-scale devices is potentially applicable to the development of electronic components, such as wires, switches, or diodes. The work described herein involves the self-assembly of azulene-based materials on atomically flat gold substrates with emphasis placed on the formation, stability, orientation, topography, thickness, and molecular packing of isocyano and thiolate junctions as well as the underlying gold films. The techniques employed in this study include Reflection-Absorption Infrared (RAIR) spectroscopy, optical ellipsometry, and Atomic Force Microscopy (AFM).

In chapter I, a review of self-assembly and the coordination of organic molecules to gold substrates are discussed. An emphasis is placed on the use of the azulenic linker for electron transport, which may be a useful building block for molecular wires. The isocyano-azulenic and biazulenic self-assembled monolayers (SAMs) on Au (111) studied in the Barybin group are discussed with emphasis placed on the junction groups' nature and their influence on the physicochemical properties of the azulenic SAMs.

The methods of characterization and sample preparation of gold substrates for SAM formation are discussed in chapter II. New azulenic SAMs featuring nitrile-substituted isocyanoazulene adsorbed on Au (111) are described in this chapter. Ellipsometry and RAIR techniques were utilized in the characterization of these new nitrile-substituted isocyanoazulenic SAMs. The positions of the nitrile and isocyanide groups on the azulene framework were varied to control the binding orientation of the azulene molecules adsorbed on Au (111). Nitrile groups incorporated into the azulenic scaffold acted as remote spectroscopic reporters, while the isocyanide groups were used in anchoring the molecules to the gold surface. The results revealed

that remote nitrile vibrational reporters are sensitive to electronic perturbations exerted by the coordination of isocyanoazulenic motif to the gold surface.

The first examples of employing both isocyanide and thiolate junction groups within the same molecule are described in chapters III and IV. In Chapter III, isocyanoazulenylthiolate derivatives' SAMs are addressed. The study involves first π-linker featuring both -N≡C and -SH termini in the same molecule self-assembled on gold by employing the 2,6-azulenic framework. A direct comparison of the new asymmetric system to the analogous symmetric di-isocyano azulenic system adsorbed on gold was performed.

Chapter IV describes an extension of the azulenic framework studied in the previous chapter. In Chapter IV, a biazulene linker, featuring both -N≡C and -SH termini within the same molecule, was adsorbed on Au (111), utilizing the bi-6,6′-azulenic core, for the purpose of electron transport from one electrode to the other. Characterization of the azulenic and biazulenic monolayer films in chapter III and IV was performed using ellipsometry and RAIR spectroscopy. The isocyano and thiolate junction groups were used in the SAM formation. The study of the competitive adsorption that emphasizes the stronger binding affinity of the thiolate junction group to gold is also addressed. The carbonyl groups of the zero-valent chromium pentacarbonyl-$Cr(CO)_5$ motif anchored to the azulenic scaffold were employed as remote spectroscopic reporters in probing the 6-mercaptoazulenic and 2-mercaptobiazulenic motif on the Au(111) surface in both chapters. Overall, the various spectroscopic and physical methods showed similar result: isocyano and thiol containing azulenes were bound to Au (111) surfaces in an upright orientation.

In chapter V, AFM techniques are used to investigate the molecular packing, and geometry, of the underlying gold and the functionalized azulene molecular layer on the film. The first AFM

topography images of isocyano- and mercaptozulene SAMs are studied. Contact mode AFM was utilized in ambient conditions to investigate the atomically and molecularly resolved images. Optimal packing of the molecular films of 2-mercaptoazulene SAM was achieved using a displacement route of 2-isocyanoazulene preform in the self-assembly, and the AFM images of 2-mercaptoazulene SAMs indicate well-ordered molecules formed on the film. The 2-isocyanoazulene SAMs AFM image was not as clear as the 2-mercaptoazulene analogue. The upright-oriented 2-mercaptoazulene molecules are arranged face-to-face, tilted in a similar direction, and aligned in a π-stacking repeated pattern.

Acknowledgment

First, I would like to give thanks to Almighty God for the opportunity He has provided me. Without God, none of these would be achievable. He has been my pillar, my stone, my every moment. God in my every day has made me stronger, more confident, and more at peace.

My profound gratitude goes to my two advisors and mentors for their unrelenting support, understanding, and guidance throughout this project. It is with great honor I say thank you. Thank you for making sure I become a better scientist, colleague, writer, and person. I have learned a great deal from both of you. Misha, words fail me when it comes to describing you. Cindy, you are better than the best! I appreciate both of you with all my heart.

I want to show my gratitude to the Department of Chemistry, the University of Kansas for the opportunity, scholarship, and facilities provided towards the completion of this research. I would like to thank my committee members, Dr. Kyle V. Camarda, Dr. Christopher Elles, and Dr. Timothy Jackson for their guidance and invaluable constructive criticism of this research.

Working with both the Barybin and Berrie group has been remarkable. I would like to thank the past members of Barybin and Berrie group, Dr. Brad Neal, Dr. Andrew Spaeth, Dr. Jen Settle, and Dr. Mason Hart for helping me begin my career path in both Labs. Thank you for answering all my random questions. Dr. Brad, thank you for training me and also for replying to all my messages whenever I am confused on what to do about my research. Dr. Jen, thank you for your encouragement, you always believed I could do it. Dr. Mason Hart, thank you for your support and training in the Barybin Lab when I first started. Also, I would like to thank my present colleagues Jason, Nate, Nilan, Sasanka, and Jen in the Barybin and Berrie Lab for your support, advice, and friendship. Thank you for putting up with me in the group and for being awesome friends.

My support and push come mostly from my parent especially my mother, you all are my backbone. Thank you for letting me go to the other side of the world to pursue my career. Thank you for always reaching out and never making me feel alone. To my three brothers, Hammed, Hafiz, and Hakeem, I love you guys. I could not imagine a week without communicating with you all. Also, I want to thank Sam Steuart, Camina Mendis, Abraham Opalade, Oluwaseun Mesele, Gbemisola Ojo, Mariam Balogun, and anyone else I may have unintentionally forgotten for listening to my complaints and for providing their friendship here at KU. I want to thank Tutu Martins for being a great "friend adopted as sister", for the encouragement, support and most of all, for listening to every one of my complaints. You are the best, I love you.

Table of Contents

List of Figures

List of Tables

Chapter I:

Self-assembled monolayer films relevant to organic electronic

I.1. Research overview

The design, characterization, and applications of molecular electronic devices in recent years have become very vast. Many researchers are interested in molecular electronics, a branch of nanotechnology, to investigate how molecular building blocks are used for the fabrication of electronic components such as molecular switches, molecular wires, molecular diodes, or molecular transistors.[1-3] These molecular electronic components are said to be 60,000 times smaller than the conventional macroscopic devices.[3] Most electronic devices, as of 2015, are packed with high density of transistors in chips and the density has increased rapidly as illustrated by Gordon Moore's law. Moore's observation, four decades ago, about the density packing of transistors doubling every year is reaching its limits.[4] Although there is a desire to increase the density packing of transistors in modern devices, alternative designs - molecular electronics - have become a promising area of research.[3] Since the density packing of transistors is near fundamental limits with the current materials and fabrication technology, it has become necessary to explore alternatives like molecular electronics for the purposes of advancing technology.[1-3] Researchers' interest in molecular electronics is to mirror the properties of macroscopic devices so that molecular electronics can perform in better or similar ways. These properties include but not limited to stability, readability, controllability, reversibility, and ability to have multiple different states.[2] Molecules that possess the ability to switch from two or more states, for instance, change conductivity upon changes in molecular charge, configuration, pH, etc. to another are called molecular switches.[3] Fabrication of molecular electronics, such as molecular switches, is usually done by building structures up from a substrate. This fabrication is the bottom-up approach which involves assembling molecules to the desired design as opposed to the top-down fabrication strategy used in conventional designs.[3] In choosing molecules for such design of interest, it is essential that the molecule has delocalized electronic systems (such as in π-conjugated organic

molecules) that can connect the source to the drain.[2] The broad synthetic methodology and structural flexibility of organic-based molecules make them interesting for studying charge or electron transfer in molecular electronics.[3] To control the charge transfer or conductivity of these molecular devices, altering the geometry of the molecule by raising or lowering the energy levels of the molecular orbitals are done.[2] The frontier orbital energy levels of azulene can be selectively tuned since they have complementary orbital densities.[5] The frontier orbitals are the highest occupied molecular orbital (HOMO) and the lowest unoccupied molecular orbital (LUMO). The complementary orbital density property makes it possible to have several synthetic capabilities and flexibilities, i.e., an introduction of a substituent on the azulene can selectively raise or lower the energy of the HOMO or the LUMO.[5-7] A significant interest of azulene in this study is its predicted intrinsic diode-like characteristics.[8] Azulene has a dipole moment of approximately 1 Debye, aligned along its molecular axis as shown in Figure 1.0.[1, 5, 9] A theoretical study done by Trebeaux and his co-workers in 1998 showed that bridging aligned with azulene's molecular axis (Figure 1.0) would lead to fascinating charge transport features due to azulene's diode-like behavior.[9] My labs - the Barybin and Berrie labs collaborated on studying azulene-based organic molecules for molecular electronic applications and has done tremendous work till date.[1, 5-8, 10-14] Throughout this work, nonbenzenoid azulene-based organic molecules useful for nanotechnology development in designing molecular electronics are employed. This work entails the design, formation, and extensive study of self-assembled monolayers of azulene derivatives useful in organic electronics.

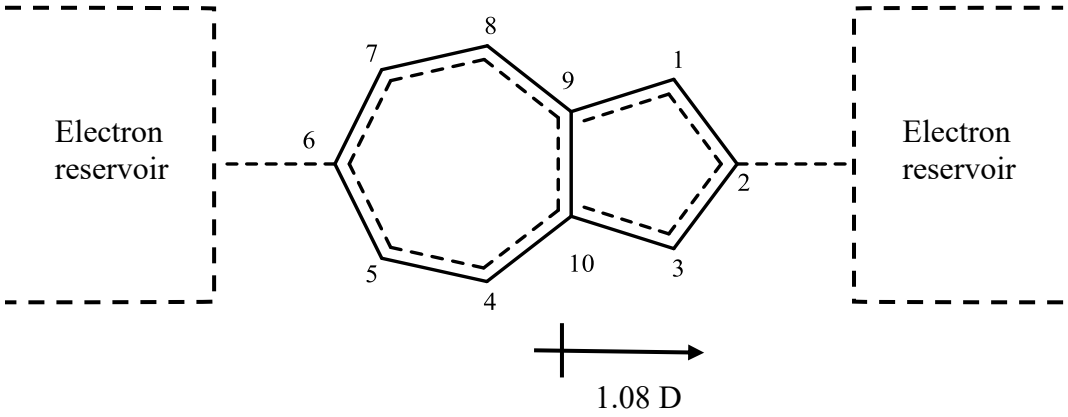

Figure 1.0. Schematic representation of the azulene molecule with a reservoir of states that can allow charge transport.[9]

I.2. Chemistry of self-assembled monolayers (SAMs)

According to literature, self-assembled monolayers (SAMs) are highly-ordered patterns formed by the adsorption of organic molecules, from gas or solution phase, onto a surface called substrate to create 2-D crystalline structures.[15-19] Some intermolecular interactions occur within the adsorbates or molecules which helps in the reorganization of the individual adsorbates into thermodynamically more stable and ordered SAMs.[19] This phenomenon of self-assembly is attractive for further research at the interface of interdisciplinary fields such as chemistry and physics, biology, or surface engineering.[17, 20] Owing to SAMs' potential use in several technological applications, for instance in protecting surfaces from corrosion, wetting, molecular recognition, biosensors, lithography, and electronic devices, SAMs have become very popular in literature.[18, 20-23] The SAM formation proceeds as follows: first, the molecules are known to come in parallel to the surface of the substrate and then bind to a step edge, or sometimes, defect site. This is then followed by chemisorption to the substrate before aligning into well-ordered patterns via intermolecular interactions as illustrated in Figure 1.1.[24] A defect site may be an adatom, a step

edge, a kink, etc. Once an island of well-packed monolayers starts to nucleate, intermolecular interactions accommodates the formation of the highly-ordered monolayers. Sometimes, physisorption may happen (Figure 1.2) where some molecules get intercalated between monolayers which may change the properties of the monolayer. Rinsing off physisorbed molecules on a monolayer film may help remove unwanted materials.

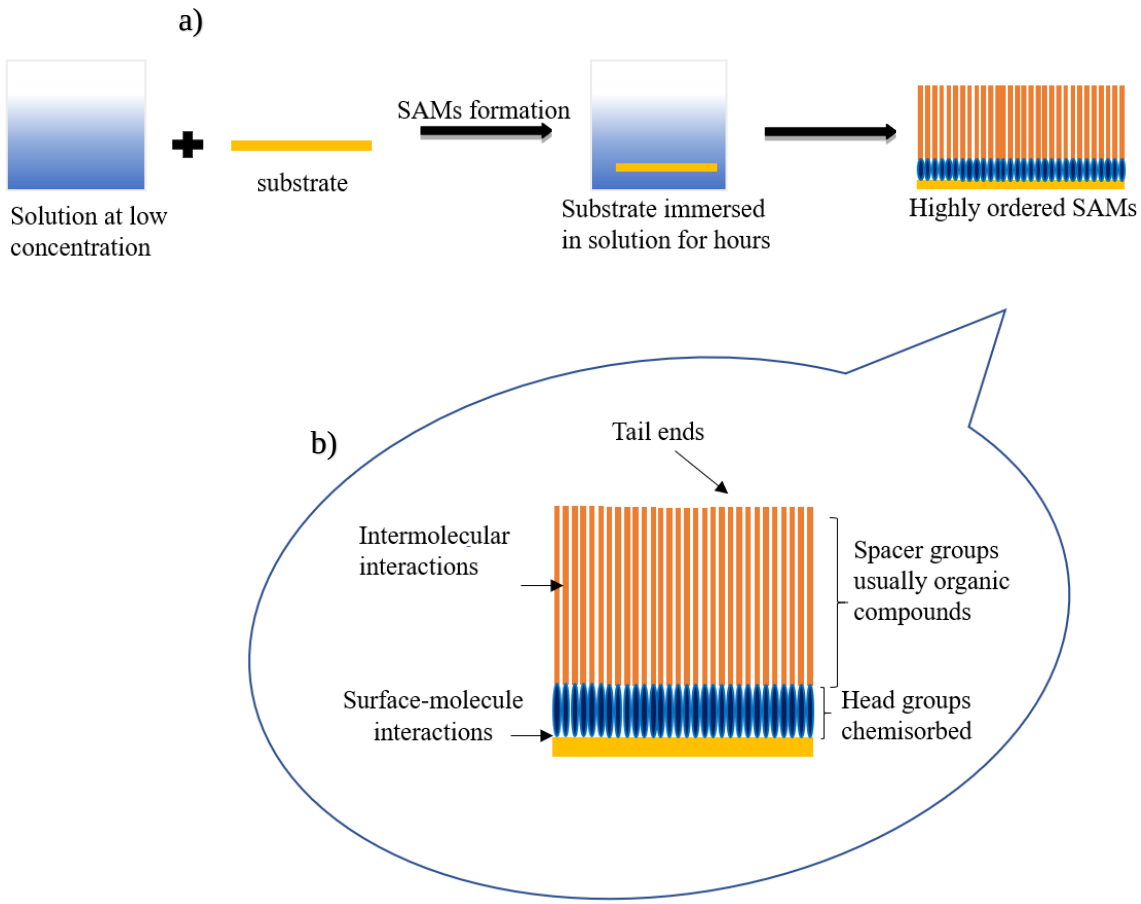

Figure 1.1. a) Schematic representation of highly-ordered SAM formation at low concentration b) Image showing SAM features.

These SAMs are known to have three specific features as shown in Figure 1.1. The head group which is the junction group bound to the substrate, a spacer group, and a terminal group at the end of the monomer.[24] The bonding interactions between the head group and the substrates and also intermolecular interactions between the adjacent adsorbates are the most critical interactions created during SAM formation.[20, 24] Fundamental study of molecule-substrate interaction, intermolecular interactions, and molecule-solvent interactions are key to understanding the phenomenon of self-assembly.[20] Some of these interactions are non-covalent or weak covalent interactions such as van der Waals interactions, hydrophobic effects, electrostatic interactions, hydrogen bonding, or coordination bonds. Defects in monolayers result in less-ordered or loosely-packed SAMs, and this could be due to SAM preparation (low concentrations and impure solutions), insufficient time permitted for the monolayer formation, or defects in the substrates used for the SAM formation.[25] This structural disorder and abnormalities as described in Figure 1.2 were disparities between the van der Waal's radii of the tail groups and head groups.[24]

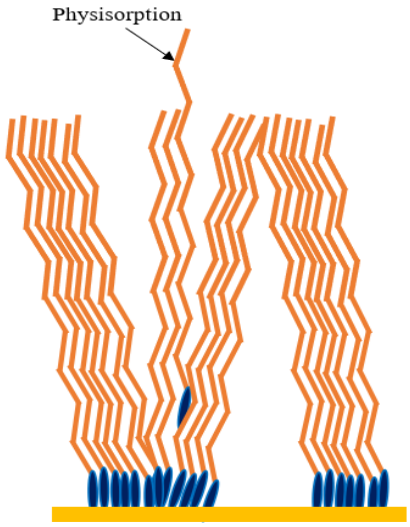

Figure 1.2. Example of disordered or abnormalities as well as physisorbed molecules in SAM.

I.3. Historical background on self-assembly

Though self-assembly was first studied by Zisman in 1946, the field gained more insight in the 80s when Allara and Nuzzo studied alkanethiol monolayers on metallic gold substrates.[15-17, 24] Allara *et al.* first showed that alkanethiol monolayers on the gold substrate could be prepared from alkanethiol or dialkyldisulfide solutions.[15-17, 24] Consequently, work on aliphatic hydrocarbon-containing-sulfur compounds like alkanethiol, dialkylsulfides, and dialkyldisulfides monolayers were extensively reported in the early literature due to simplicity, chemical stability, and ease of preparation.[18, 20-22, 24] The most common substrates for SAM formation are planar surfaces due to ease of preparation and compatibility with the most common analytical techniques used for surface characterization. Thin films of metals coated on mica, glass or silicon wafer substrates are the most popular planar substrates.[26-28] Several metal-coated thin films like gold, silver, copper, platinum, palladium, nickel, rhodium, and chromium have been employed.[29] The thin films are prepared via physical vapor deposition, electrodeposition or electroless deposition methods of the metal onto the substrate.[26-28] The gold thin film is the most widely studied substrate due to its inertness towards oxidation and corrosion.[15-17, 24] In addition, the gold thin film is practical due to its compatibility with several analytical techniques such as Reflection-Absorption IR, high resonance XPS, Scanning Probe Microscopy, etc. In addition, the preparation of gold thin films is relatively straightforward.[8-10]

The method of preparation of thin film is dependent on its application. The most common method of preparing gold film is by electron beam or thermal evaporation, sputtering, or by electrodeposition.[18] The most studied gold thin films used for SAMs formation are those prepared under high vacuum via thermal evaporation of gold onto an adhesive substrate like glass, silicon wafer, or mica.[15-18, 20-21, 24-25, 28] The gold is evaporated directly on a freshly cleaved mica while

glass or silicon wafer is first coated with an adhesion layer before gold is deposited. Gold is a face-centered cubic metal. The (111) face of the gold surface was employed throughout the studies reported in this dissertation.

The SAMs formation is typically achieved by immersing the cleaned gold substrate into a low concentration solution of the compound to be deposited for hours to enable well- ordered SAM formation. The monolayers can be characterized using spectroscopic techniques such as Reflection-Absorbtion Infrared Spectroscopy (RAIRS), X-ray Photoelectron Spectroscopy (XPS), Auger Electron Spectroscopy (AES), Thermal Desorption Spectroscopy (TDS), X-ray diffraction, High-Resolution Electron Energy Loss Spectroscopy (HREELS), Raman spectroscopy, contact angle goniometry, optical ellipsometry, surface plasmon resonance spectroscopy, and Scanning Probe Microscopy (SPM).[18, 20-21, 23]

Allara and Nuzzo used XPS, AES, HREELS, and TDS characterizations to carry out the study on aforementioned SAMs of dialkyldisulfides. They concluded that the S–S bond of dimethyldisulfide cleaves and chemisorbs on gold to form monolayers indistinguishable from those obtained from methanethiol, with the formation of Au–S bonds although the mechanisms for both reactions are not the same.[15, 17-18, 20, 23-24] While the proposed mechanism for the adsorption of dialkyldisulfides involves oxidative addition of the S–S bond, the mechanism for forming alkylthiolate films is thought to involve oxidative addition of the S–H bond to the gold surface followed by reductive elimination of the hydrogen, either as H_2 or H_2O (in the presence of oxygen).[15, 17, 23]

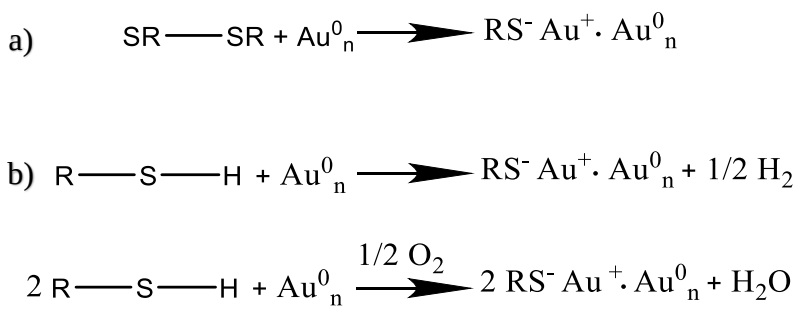

Figure 1.3. Proposed mechanisms for SAM formation of a) dialkyldisulfides and b) alkanethiols.

The adsorption kinetics suggested the occurrence of a fast step which happens within a few minutes of the monolayer formation. During this step, the monolayer thickness is almost entirely formed. A slow step then follows, taking several hours for the monolayer to reach a maximum coverage. The thiolate ($-S^-$) is the most studied junction groups, i.e., a head group, in SAMs.[15, 17-18, 20, 23-24] For longer alkyl thiol chains, increase in van der Waals interaction between the molecules causes slower adsorption kinetics. Although the shorter chains are known to adsorb faster, a thermodynamically controlled adsorption experiment shows that competitively, longer chains preferentially adsorb on the substrate.[30-32] The first SAM formation for these alkyl thiols generally occurs in a disordered fashion before reorganization into an ordered monolayer, spaced by 5 Å mostly in a $(\sqrt{3} \times \sqrt{3})R30^\circ$ geometry.[32-35] Though reports have been made that SAMs with -SH head groups can occupy different adsorption geometries, for instance c(4 x 2) or (22 x $\sqrt{3}$) due to minimization of intermolecular repulsion, the energy difference between various geometries for thiol is minimal.[36-37]

Depending on the application of the SAM film, one can tweak the structure or packing in the monolayer formation. For instance, the building of molecular wires will require charge transfer behavior and study of the charge tunneling mechanism becomes essential. Study of the charge

transport properties in molecules, for designing molecular wires, involve the use of conjugated organic molecules. For the purpose of conductivity in molecular wires, tunneling currents across the molecule is necessary. Alkyl chains are known to support non-resonant tunneling while resonant tunneling has been documented for conjugated molecules.[38] STM measurements were employed on conjugated molecules, the tunneling currents in conjugated molecules were three orders of magnitude higher than the straight alkyl chains.[38] One of the vital keys to fabricating molecular wires using SAMs is the presence of a series of conjugated bonds in the SAM due to the relatively small HOMO-LUMO gap in the conjugated molecules. Aromatic thiols SAMs on gold due to their electronic conductivity and optical properties of the SAM film have been trending in literature. Benzenethiol, the simplest aromatic thiol, is the most popular nolecule used in SAM formation on gold but is known to form disordered phase as observed when the films are studied with scanning tunneling microscopy (STM) studies.[34, 39-40] Moreover, some studies show conflicting conclusions on the orientation of the phenyl rings of benzenethiol. Figure 1.4 shows the predictions about the orientation of the phenyl rings. The Au-S-C bond angle of 180 ° will enable a highly ordered monolayer while the other bond angle of about 104 ° may lead to slightly lower density resulting in less ordered monolayer when compared to the 180 ° bond angle as seen in Figure 1.4.[40]

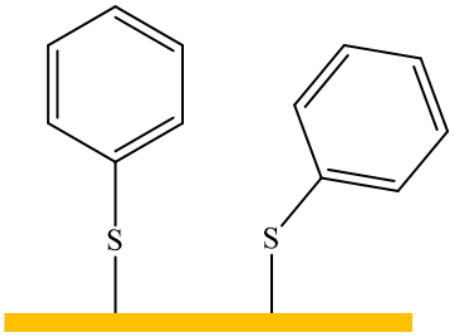

Figure 1.4. Predicted orientation of phenylthiolate monolayer.[40]

While some spectroscopic studies showed the phenyl ring in the pheylthiolate molecule is parallel to the gold film,[41-42] others concluded that it is perpendicular to the gold film.[43] Moreover, the STM studies by J. Noh *et al.* suggested that disordered monolayers are formed from benzenethiol as opposed to the highly-ordered phenylthiolate monolayers, where the methylene (CH_2) group was inserted between the phenyl ring and the thiol head group.[39] Studies have shown that the CH_2 - spacer can significantly improve the SAMs by creating better flexibility around the phenyl rings [39-40] to enhance the intermolecular interactions present the SAMs as shown in Figure 1.5. In work done by J. Noh and coworkers, thermal desorption experiments further supported the benzyl thiol binds stronger to the gold films and have well-ordered phases as compared to phenyl thiolate, though the XPS signatures for both samples were quite similar.[39] The -CH_2 spacer allows the monolayer's Au–S–C tilt angle of 105 ° with enhanced packing order.[39-40] The increase in the π-π interaction enhances the stability, durability, and the packing of the monolayers. Some benzenoid thiols like benzene(di)thiols, biphenyl(di)thiols, oligophenyl(di)thiols, terphenylthiols, naphthalene(di)thiols, etc. have been studied [36, 44-45] and the obtained results reinforce the importance of the π-π interaction.

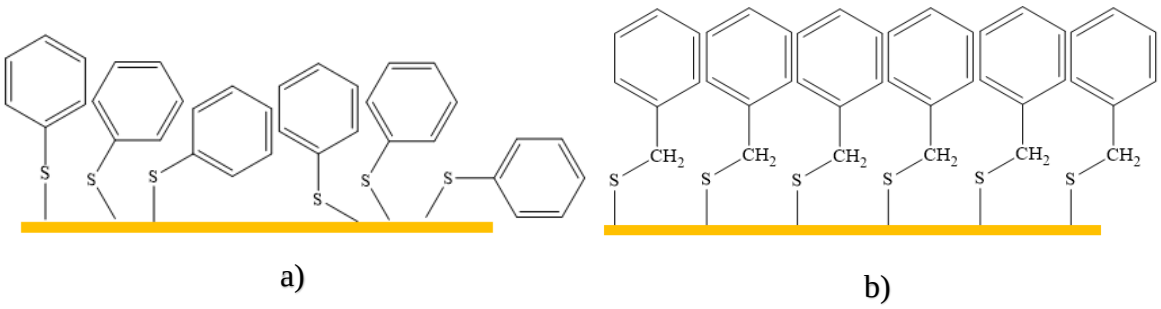

Figure 1.5. Schematic representation of a) disordered phenylthiolate and b) highly-ordered benzylthiolate on Au(111).[39]

The tilt angle experienced in the monolayer varies from SAM to SAM, and the ordering of the monolayer may depend on the type of molecule used in the formation. In the case of SAMs of naphthalene-2-thiol on Au, three different structural arrangements were suggested where the naphthalene is either lying flat, standing, or facing up with respect to the gold surface.[44] The standing and the lying phases were proposed as the most stable phase which defined the packing arrangement that was observed. A (3 x 3√3)R30° and (3 x 6√3)R30° packing geometries were observed.[45] The thickness characterization of these benzenoid aromatic thiols are usually studied by XPS, HRXPS, NEXAFS, and ellipsometry (most popular) and most observed thicknesses correspond to the calculated monolayer thicknesses oriented in an upright manner.[36, 44-45]

Not many nonbenzenoid aromatic systems have been studied. A typical nonbenzenoid aromatic molecule is Azulene. Benzenoid congeners have alternant aromatic properties with an even distribution of their π-electrons, unlike Azulene framework that possesses an uneven distribution of its π-electrons in the fused 5- and 7- membered rings.[1, 5, 46] Azulene, $C_{10}H_8$ though is an isomer of naphthalene, has electronic properties that are different from the benzene-like

naphthalene system. Azulene and its derivatives, as potential candidates, in designing molecular wires for organic electronics have not been explored as thoroughly when compared to benzenoid systems. Azulene has an unusually small frontier molecular orbitals energy gap, that might be useful for charge transport studies for the design of molecular wire.[6, 10-12] The theoretical study by S. K. Pati and coworkers showed that azulene has higher conductive ability as compared to its isomer, naphthalene, due to the relatively small HOMO-LUMO gap of the former.[47]

I.4. Diode-like Nonbenzenoid scaffolds self-assembled on Gold film

Azulene, a nonbenzenoid aromatic framework, fabricated on gold films was first studied in our lab where Barybin *et al.* focused on SAM formation, stability, orientation, thickness, and the influence of the junction group for the design of advanced materials relevant to nanotechnological applications.[1, 5, 46] The conductive probing of the azulenic scaffold on gold as depicted in Figure 1.6b may give charge transport information useful for molecular electronics. The charge transport could be between the conductive probe and the monolayer end, along the conjugated azulene spacer molecule, or between the head-group and the gold substrates. The design features a hybrid metal-organic ensemble where the electronically ambivalent azulenic framework behaves like an acceptor, a donor, or structural and electronical bridge.[1] All the azulene derivatives discussed have been synthesized in our lab. Like other SAMs, azulenic SAM has three distinct parts; a head group, a spacer group and a terminal group as shown below in Figure 1.6a. The head groups, otherwise called the junction groups, studied in our lab employ the use of thiolate, the isocyanide, and the carboxylate groups with preference majorly on the thiolate and the isocyanide group.[1, 8, 11-12, 14, 46]

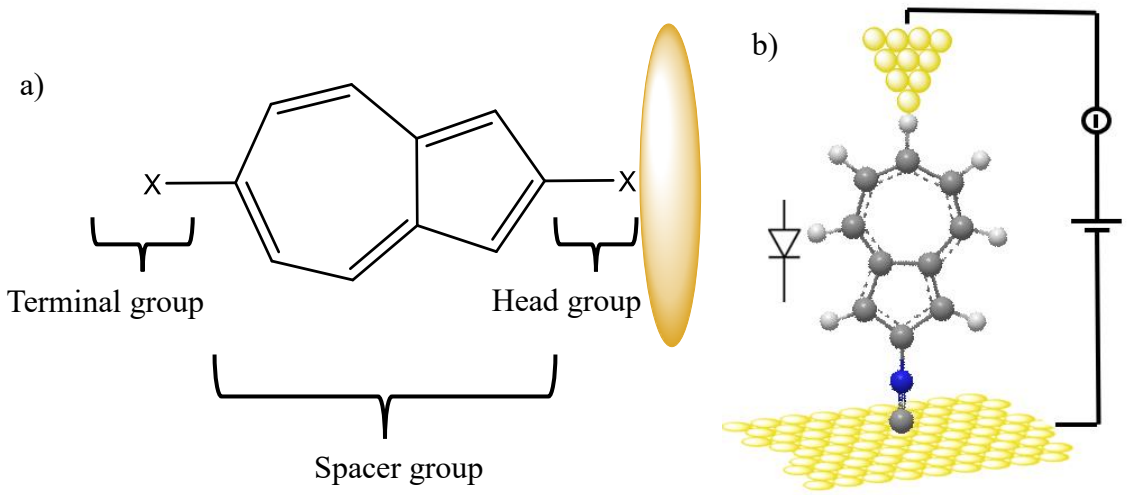

Figure 1.6. Schematic representation of a) azulenic scaffold monolayer showing three distinct parts. b) Conductance of an electron through the diode-like azulene scaffold on gold via a molecular junction.

Azulene dipole moment is about one Debye, and the dipole is aligned along the azulene's molecular axis.[1, 5, 9, 46] Consequently, introducing junction groups along the azulene molecular axis, marked as X in Figure 1.6a, is essential in designing azulenic SAMs. This way, one can take advantage of the direction of the dipole, enhancing the ability of the azulenic scaffold in organic electronics application. The information on packing, orientation, and stability of these SAMs is very important for understanding the monolayer formation. In addition, molecularly resolved images and conductance analysis of the SAMs are necessary to gain insights into the packing and periodicity, and conductivity of the molecules. Extensive characterization of the binding and orientation of the SAMs and further characterization of the SAMs using AFM and STM to give insights into the packing and conductivity are employed throughout this work. FTIR, and ellipsometry have been used to study the structure, stability of the molecules in these SAM films.[1, 5-6, 10, 12, 14] Theoretical and experimental studies of isocyanides and mercaptans, as stable molecular

electronic junctions have been achieved in literature.[1, 12-14] Upon coordination of mercapto- and isocyanoazulene to gold film, an Au–S and Au–C bond is formed respectively. The Au–S bond is typically estimated as 2.45 Å, longer than an Au–C estimate of 2.0 Å bond length.[5, 6, 36-39] Confirmation of the SAM formation by ellipsometry and grazing angle reflection FTIR affords information about the upright orientation of the monolayer and binding mode which is via the junction group adsorbed in the η^1 coordination mode on the gold surface. The work that was done by Dr. Brad Neal, a previous member of the group, comparing the junction groups of some azulenic derivatives on gold supported the Au–S bond being more energetically favorable than the Au–C.[14] The study showed a complete displacement of the monolayers of Au–C by the Au–S monolayer. The Au-S bond strength, 44 to 50 kcal/mol, are twice of an Au–C bond strength.[14, 22-23] Azulene derivatives with thiol end at positions 2, 6, or both for monolayer formation have been studied in the Barybin and Berrie labs. Unfortunately, most of the mercaptoazulene derivatives on gold film lack distinct spectroscopic characteristics in their IR spectra since the Au–S stretching frequency is very weak and occurs around 400 cm^{-1} which is not included in the FTIR window eployed in our lab (600 cm^{-1} - 4000 cm^{-1}). Ellipsometry measurements though calculate thickness for the azulenylthiolate monolayer; FTIR characterization has proven challenging, unlike the isocyano junction groups that have identifiable spectroscopic handles in the IR spectrum.

The first kinds of azulenic derivatives SAMs featuring isocyano junction groups were studied by past members of the Berrie and Barybin groups. Figure 1.7 shows some of the azulenic derivatives on gold. FTIR and ellipsometric measurements were employed in studying the SAMs made. FTIR provides information on the binding and orientation of molecules formed in the SAMs. Depending on the position of the junction group, the vibrational energy changes. Typically, free isocyanide at the position 2 on the azulene gives an infrared stretching frequency (*ν(CN)*) of

ca. 2127 cm^{-1} in CH_2Cl_2 solution. The stretching frequency then experiences a hypsochromic (blue) shift when the Au–C is formed gaining about 38 - 65 cm^{-1}.[1, 1, 14] Whereas free isocyanide at most of the 6 positions gives *v(CN)* of *ca.* 2115 cm^{-1} in CH_2Cl_2 solution and experiences a blue shift to higher energy gaining about 42 - 60 cm^{-1} (see Table 1.1) when bound to the gold substrate. The FTIR studies show that a lone pair on the carbon atom of the free isocyanide on the azulene derivative, which occupies antibonding orbital energy, is donated to the gold film resulting in a η^1 binding mode leading to the *v(CN)* having higher energy. Table 1.1 shows free and bound infrared stretching frequencies of some of the isocyano monoazulenic derivative that has been made in the Barybin and Berrie labs. The synthesis of these azulenic derivatives can be found in our publications. These azulenic derivatives are highly colored, crystalline and air-stable.[1, 5-6, 10, 12, 14]

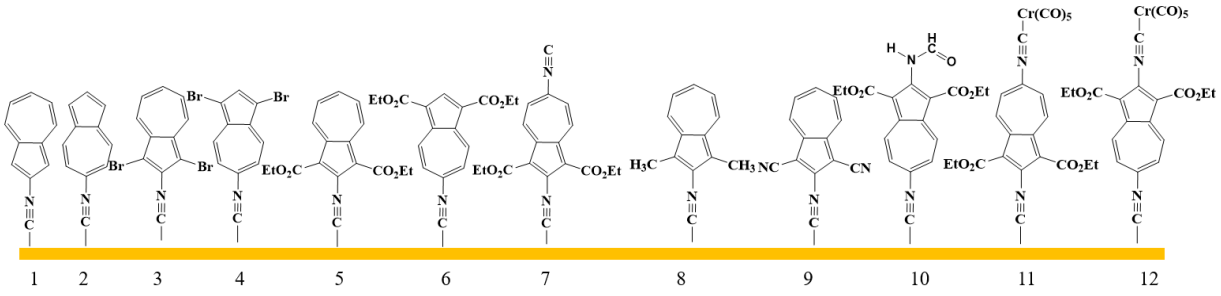

Figure 1.7. A variety of monoazulenic derivatives featuring isocyano junction groups coordinated to gold thin film. The numbers directly below correspond to above SAMs.[1, 12]

Table 1.1. Free (CH_2Cl_2 solutions) and bound (SAM on gold) Infrared stretching frequencies of isocyano groups on isocyanide azulenic derivatives and the ellipsometry thickness.

	SAM on gold, *v(CN)* (cm^{-1})	CH_2Cl_2 solution, *v(CN)* (cm^{-1})	Ellipsometry thickness (Å)	Expected/Theoretical thickness(Å)	Ref./*viz.*
1	2174	2127	9.2±2.7	10.5	1
2	2176	2117	Not reported	Not reported	1
3	2168	2121	11.9±0.6	10.8	Appendix 1
4	2179	2115	Not reported	Not reporteed	1
5	2169	2127	8±1	10.5	1
6	2178	2115	11.3±3	12.5	1
7	2117, 2163	2116, 2125	14±1	12.5	1
8	2167	2115	10.5±0.6	10.7	50
9	2156	2114	11.7±0.6	10.7	14
10	2170	2116	Not reported	Not reported	1
11	2120, 2171	2123, 2123	21±3	17	1
12	2132, 2174	2115, 2135	18±2	17	1

The SAMs of 2-isocyanoazulene labeled as 1 in Figure 1.7 binds to the gold film in an upright orientation via the coordination of the antibonding lone pair on the carbon of -NC end, donating the lone pair to the gold. The FTIR in CH_2Cl_2 solution before coordination shows a 2127 cm^{-1} of the free isocyanide and a 2174 cm^{-1} for the bound isocyanide indicative that all the isocyanide coordinates to the gold film.[1] This SAM was prepared in ambient conditions and no other peaks support any oxidation of the isocyanide to isocyanate (NCO) occurred in the data. The obtained result supports a stable, robust, all-bound isocyanide to gold SAM formation without deterioration in the air as compared to the unstable benzenoid isocyanides.[1] The FTIR derivatives for SAM 1 (i.e., SAM 3, 5, 8, and 9) supports that the SAMs formed did not experience any oxidation of the isocyanide either.[1, 14] A blue shift in energy seen in the FTIR spectra for all the

SAM derivatives is indicative of the donation of the lone pair on the carbon of the -NC end to the gold film. The ellipsometry data for all these SAMs was consistent with the upright orientation of the monolayer formed (see Table 1.1).

Similarly, the 6-isocyanoazulene (SAM 2) on the gold film was via the coordination of the carbon's lone pair on the isocyanide during monolayer formation. The derivatives of SAM 2 (that is 4, 6, and 10) based on FTIR results supported that all the isocyanides present on the gold film were bound to the gold substrates and an upright orientation of the monolayer, without any physisorption or oxidation, is present. Comparing the expected monolayer thicknesses and measured thicknesses, the results from ellipsometry as seen in Table 1.1 for these SAMs shows that the SAMs are one layer thick and an upright orientation of the monolayer formed. The expected thicknesses are calculated from the crystallograhy of the azulene derivative used in monolayer formation or from chembioDraw and a Au–C bond length of 2 Å is included to account for the coordinated bond.

For the isocyano monoazulenic derivatives featuring SAM in Figure 1.7, formation of the monolayer was relatively similar and easily achieved except for SAM 3. The molecule used in SAM 3 is an isomer of SAM 4, bound via the position 2 instead of 6, to the gold substrate. The molecule used in formation of SAM 3, recently synthesized by Dr. Mason Hart and Zack Wood, initially gave thicknesses that suggested a bilayer at 2 mM distilled dichloromethane (detailed synthesis and FTIR data can be retrieved from appendix 1). The UV-Vis of this sample, a greenish-blue solution, was performed and the result showed a significant broad absorbance band at 632 nm. The Ellipsometer in our lab uses a HeNe laser at a wavelength of 632.8 nm, assuming the incident laser radiation is not absorbed by the film. The result may have been altered if the laser radiation got absorbed. Upon reduction of the concentration to 0.6 mM, the averaged measured

thicknesses were 11.9 Å, supporting the formation of an upright monolayer. The concentration for monolayer formation plays a vital role in the formation of SAM 3.

A diisocyanide azulene derivative (SAM 7 in Figure 1.7.) featuring a rigid linear motif which leads to the small HOMO-LUMO gap was made in the Barybin and Berrie labs for metal-bridge-metal charge transport systems useful in electronic applications.[1, 10] The *v(CN)* isocyanides at positions 2 and 6 when the FTIR of the free molecule of SAM 7 in Figure 1.7. was measured showed overlapping C–N stretching frequency bands at 2125 and 2116 cm^{-1} attributed to positions 2 and 6 respectively because of electronic inhomogeneity of the azulenic framework.[1, 5] When the SAMs 7 were made, an observation made was a preferential binding of the isocyanide in position 2 to the gold as the head group. This preferential binding is indicative that the 2-isocyano is more electron donating than the 6-isocyano azulene moiety.[1, 5, 10] Additionally, to control the adsorption for SAM 7 on gold, that is the head group, a chromium carbonyl fragment [-$Cr(CO)_5$] was used to cap either the -NC end at positions 2 or 6 as seen in Figure 1.7**.** (SAM 11 and SAM 12). The FTIR results in Table 1.1 support SAM 11 and SAM 12 have controlled binding of the isocyanide via 2 and 6 positions respectively. In the CH_2Cl_2 solution of the free C–N form of SAM 11, a broad *v(CN)* band at 2123 cm^{-1} was assigned to a capped and free isocyanide. Consequently, two *v(CN)* bands observed for the SAMs at 2120 cm^{-1} characteristic of the capped isocyanide, and a shorter wavelength at 2171 cm^{-1} characteristic of the formation of the monolayer on the gold film were recorded.[1] The CH_2Cl_2 solution of the free C–N form of SAM 12 features two distinct *v(CN)* at 2115 cm^{-1} and 2135 cm^{-1} indicative of a capped and free isocyanide at positions 6 and 2 respectively. The capped isocyanide environment, upon coordination to form SAM 12, did not change. Instead, the 2115 cm^{-1} showed up at a shorter wavelength (2174 cm^{-1}) indicative of the SAM formation.[1] The $Cr(CO)_5$ fragment aided concluding remarks about the orientation and

binding mode of the compounds due to additional valuable spectroscopic information derived from the FTIR spectra are described in detail in chapter 3.

The extension of SAM 6 to build molecular wires using diisocyanoazulene linkers were envisioned by designing biazulene derivatives in the Barybin and Berrie labs. Charge transports study on isocyanobiazulenyl frameworks for the design of molecular wires featuring a 2,2´-, 2,6-, and a 6,6´- connectivies of the azulenic moieties as seen in Figure 1.8 were studied in our lab. The individual azulenic units are conjugated with one another to different extents in the three possible connectivities. Rotation around the interplanar angles has been calculated to be *ca.* 0°, 30° and 50° for the 2,2´, 2,6, and 6,6´ biazulenes respectively.[48-49] As the magnitude of the interplanar angle increases, delocalization of π-electrons along the whole biazulene system decreases due to the decrease in the π-orbital overlap between the azulenyl units and this may change the charge transport ability of these biazulenes.[48-49] The different connections of the linear biazulenyl derivatives were synthesized and the SAMs made have been analyzed using FTIR and ellipsometry (see Table 1.2).

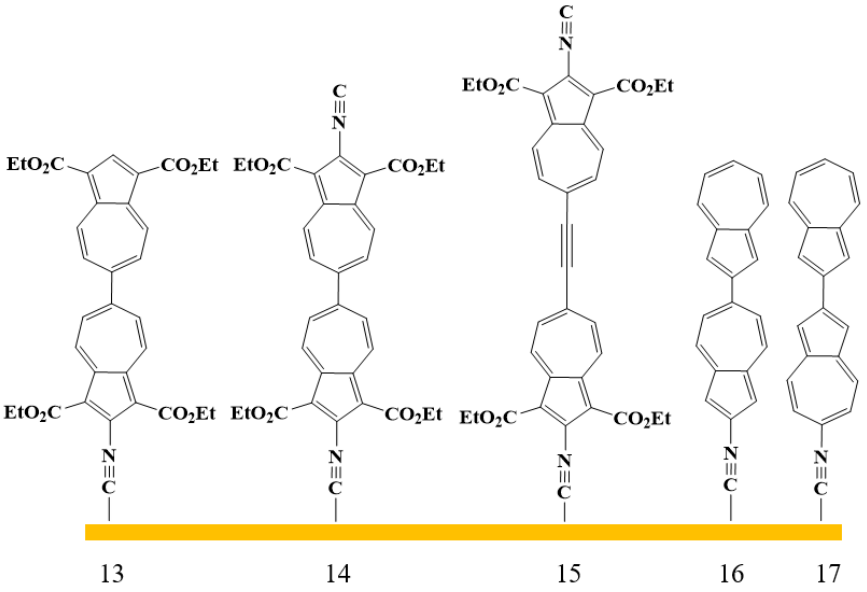

Figure 1.8. A variety of biazulenic derivatives featuring isocyano junction groups coordinated to gold thin film. The numbers below directly represents the above SAM.

The free isocyanide stretching frequencies ($\nu_{(CN)}$) of SAM 13 and SAM 14, before the monolayer formation, in CH_2Cl_2 solution occurred at 2127 cm^{-1} with the difference being the peak sharpness (see Figure 1.9). The diisocyanide as previously described by Dr. Brad Neal was broader in the solution of SAM 14,[7] which is indicative of two isocyanides present in the molecule as compared to the sharp *v(CN)* observed in the CH_2Cl_2 solution of SAM 13 described in this work in appendix 2. Not surprisingly, two *v(CN)* at 2119 cm^{-1} and 2170 cm^{-1} were observed for SAMs 14 on the grazing incidence reflection FTIR [7] while only one band at 2177 cm^{-1} occurred for SAM 13. As seen in Figure 1.9, there are two different isocyanide environments for SAM 14, a red-shifted *v(CN)* band at 2119 cm^{-1} and a blue-shifted *v(CN)* band at 2177cm^{-1}. The blue shift experienced upon coordination when the carbon lone pair donates to the gold substrate induces a partially positive charge [50] within the π-system which consequently weakens the other free -CN bond leading to the red-shifted band.[7] The broad IR band observed was attributed to some

inhomogenous environments of the surface adsorption sites due to defects in the gold film used.[7] In SAM 13, a smaller distribution of environment for the isocyanide stretching frequency seen at 2177 cm^{-1} is present. The short wavelengths observed in both spectra is indicative of the carbon lone pair on the isocyanide donate to the gold film. No oxidation of the SAMs was observed for both samples and the observed thicknesses, as seen in Table 1.2, measured at multiple spots supports the molecular monolayer SAM standing in an upright orientation. The synthesis of the molecule used in SAM formation 13 and 14 was by Dr. Toshinori Nakakita and Dr. Tiffany Maher of the Barybin and Berrie groups respectively.

1) SAM 13

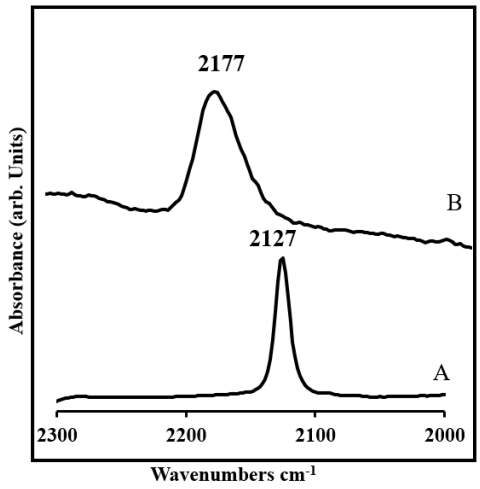

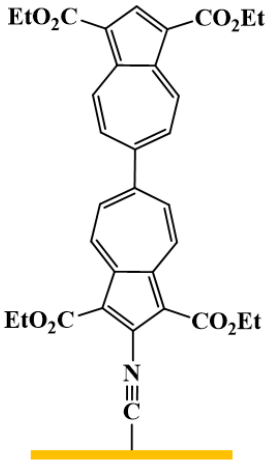

2) SAM 14

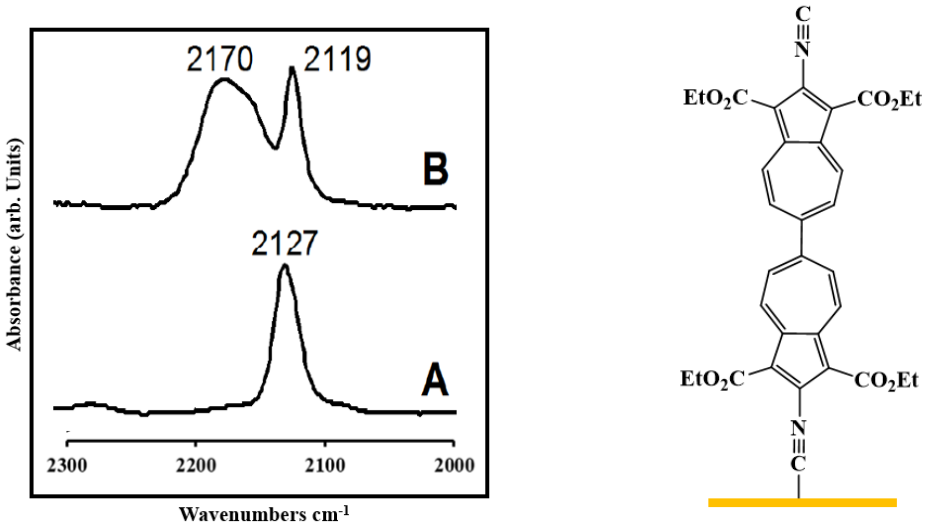

Figure 1.9. Schematic drawing showing upright orientation of SAM 13 and 14 and the FTIR data representing the ν(CN) regions of (A) in CH_2Cl_2 solution and (B) on gold(111) film for SAM 13 and 14 [7].

The synthesis of the compound used to form SAM 14 was by Dr. David McGinnis in the Barybin lab. SAM 15, as described by Dr. Brad Neal, featured an acetylene spacer C≡C, two isocyanides environment could coordinate to the gold.[51] The free stretching frequency showed a *ν(CN)* of 2119 cm^{-1} attributed to the isocyanides and an IR forbidden band with a very weak intensity assigned to the C≡C. Upon formation of SAM 15, a blue-shifted *ν(CN)* of 2177 cm^{-1} from the 2119 cm^{-1} was observed indicative of the gold accepting the carbon lone pair on the isocyanide. The ellipsometry measurements as seen in Table 1.2 supports an upright orientation of the monolayer formed.

All the SAMs described in this section so far has been made with a concentration of 2 mM of the corresponding azulene except SAM 16 and SAM 17. While SAM 16, as illustrated by Dr. Brad Neal, was created using 8 mM concentration, SAM 17 was made at 0.02 mM concentrations to obtain a successful monolayer. Though a shorter thickness was observed (see Table 1.2) in SAM

16 which were probably due to the packing density being low, the FTIR supported the coordination was through the isocyanide, indicating η^1 binding mode. For SAM 17, an upright orientation of the monolayer was observed though several debates on the monolayer formation occured. The descriptions by previous members of the group, Dr. Tiffany Maher and Dr. Brad Neal, as found by the ellipsometry data, suggested that the monolayer study of SAM 17 was not trivial.[51-52] The measured thicknesses by ellipsometry were far off the calculated thicknesses. While the FTIR data got was reproducible, the thicknesses were not. Dr. Brad and Dr. Tiffany suggested in their previous work that the absorbance employed of this molecule seen at 632 nm may have played a role in the observed result since the HeNe laser in the ellipsometer used in the lab has a wavelength at the similar region the molecule absorbs at.[51-52] The RAIR and ellipsometric result of the monolayer for SAM 17 done in this work is in Appendix 3. Dr. Mason Hart synthesized the compound used in this work for SAM 17 formation. The compound was soluble in almost no solvent which could have been affecting the SAM formation. It was seen that the use of 0.02 mM concentration of the molecule in distilled THF, made in the absence of air, gave average thicknesses of 18.3 ± 1.2 Å. The estimated thickness that would correspond to an upright binding mode was 17 Å assuming an Au–C bond distance of 2.04 Å. The solubility of the compound may affect the driving force for adsorption on the gold film. The solubility of the compound plays a vital role in determining the thickness of the film when bound to gold surface. At higher concentrations, inconsistent thicknesses with the accepted thickness values were regularly seen. It is evident that the method used in monolayer formation is vital. The solution IR and surface IR of SAM 17 showed *v(CN)* bands at 2113 cm^{-1} and a 2173 cm^{-1} respectively which is indicative that the stretching frequency of the compound increased by 60 cm^{-1}. The observed increase is due to the donation of the lone pair on carbon of the isocyanide to the Au leads to higher vibration energy.

Table 1.2. Free (CH_2Cl_2 solutions) and bound (SAM on gold) Infrared stretching frequencies of isocyano groups on isocyanide biazulenic derivatives and the ellipsometry thicknesses.

	SAM on gold, *ν(CN)* (cm^{-1})	CH_2Cl_2 solution, *ν(CN)* (cm^{-1})	Ellipsometry thickness (Å)	Expected thickness (Å)	Ref./*viz.*
13	2177	2127	17.4 ± 0.8	17.0	Appendix 2
14	2170, 2119	2127	20.5 ± 2.4	19.1	7
15	2177, 2121	2189, 2119	26.9 ± 1	23.0	50
16	2169	2120	13	17.0	16
17	2173	2113[a]	18.3 ±1.2	17.0	Appendix 3

The ellipsometry is a powerful technique used in SAM thickness characterization, and it is a nondestructive optical technique that has been employed to characterize these SAMs in the Berrie lab successfully. The expected thicknesses, if the monolayer is standing perfectly upright without any physisorptions, is calculated from the crystallography or the ChemDraw. Except stated otherwise, a 2.00 Å were added to the calculated thicknesses to account for the Au–C coordinate bond formed during the monolayer.[29] For mercaptoazulene derivatives, a 2.45 Å was added to the computed thicknesses instead, accounting for the formation of an Au–S bond.[54] Unlike in Au–C coordinates formed in isocyanide azulenic and biazulenic derivative SAMs, the Au–S formed in the thiol azulenic and biazulenic derivative SAMs characterized using the FTIR does not have detectable spectroscopic signatures to support the perceived interpretation of the monolayer.[14] Installation of a spectroscopic reporter on the thiol azulenic and biazulenic derivatives for SAM formation strongly supports the concluding remarks on the upright orientation. Perhaps installing

isocyanide that is excellent spectroscopic reporters on the mercaptoazulene SAMs will further aid these conclusions. Moreso, a mercaptoisocyanoazulene SAM will involve both electron donating and withdrawing groups which may be designed as a donor-bridge-acceptor. The alignment of the isocyano and mercapto junction groups to the linear azulenic framework – a new designs for molecular electronic applications, will be discussed in later chapters.

The application of azulene derivatives self-assembled on gold substrates provides useful tools for molecular electronics. The design, synthesis, and characterization of the azulenic SAMs on gold substrates can be studied using techniques like ellipsometry, spectroscopy, and microscopy to probe interesting properties like the packing, orientation, stability, conductivity, and topography. As outlined above, the packing and orientation of some azulenic SAMs have been studied in our lab. My work aims to further understand monolayer formation useful for molecular electronics. Chapter 2 introduces the techniques employed in this work. Azulene derivatives SAMs featuring the cyano and isocyano functional groups were employed in this chapter to describe the techniques. These techniques include ellipsometry, reflective absorption infrared spectroscopy, and scanning probe microscopy. Also, the chapter describes the preparation and type of gold substrates employed throughout this work. In chapter 3, linear azulenic linker asymmetrically anchored using isocyano and mercapto junction groups were described. The SAMs were made and proposed as new systems with high potential for molecular conductivity. An extension of the azulene systems described in chapter 3 by connection of two azulenes at the 6 positions was described in chapter 4 as a fulfillment of the complete model for molecular rectification. Chapter 5 describes the microscopy study of azulene derivative monolayers to understanding the topography and periodicity of the monolayers and how they differ from the gold substrates to which they are attached.

I.5. References

1. Dubose, D. L.; Robinson, R. E.; Holovics, T. C.; Moody, D. R.; Weintrob, E. C.; Berrie, C. L.; Barybin, M. V., Interaction of Mono- and Diisocyanoazulenes with Gold Surfaces: First Examples of Self-assembled Monolayer Films Involving Azulenic Scaffolds. *Langmuir : The ACS Journal of Surfaces and Colloids* **2006**, *22*, 4599-4606.
2. Fuentes, N.; Martn-lasanta, A.; Lvarez De Cienfuegos, L.; Ribagorda, M.; Parra, A.; Cuerva, J. M., Organic- Based Molecular Switches for Molecular Electronics. *Nanoscale* **2011**, *3*, 4003-4014.
3. Mark, A. R.; James, M. T., Computing with Molecules. *Scientific American* **2000**, *282*, 86-93.
4. Czerniak, M., What Lies Beneath? 50 years of Enabling Moore's Law. *Solid State Technology* **2015**, *58*, 25-28.
5. Robinson, R.; Holovics, T. C.; Deplazes, S.; Powell, D.; Lushington, G.; Thompson, W.; Barybin, M., Five Possible Isocyanoazulenes and Electron- Rich Complexes Thereof: A Quantitative Organometallic Approach for Probing Electronic Inhomogeneity of the Azulenic Framework. *Organometallics* **2005**, *24*, 2386-2397.
6. Barybin, M.; Chisholm, M.; Dalal, N.; Holovics, T.; Patmore, N.; Robinson, R.; Zipse, D., Long-range Electronic Coupling of MM Quadruple Bonds (M = Mo or W) via a 2,6-Azulenedicarboxylate Bridge. *Journal of the American Chemical Society* **2005**, *127*, 15182-15190.
7. Maher, T.; Spaeth, A. D.; Neal, B. M.; Berrie, C.; Thompson, W.; Day, V.; Barybin, M., Linear 6,6 '- Biazulenyl Framework Featuring Isocyanide Termini: Synthesis, Structure, Redox Behavior, Complexation, and Self- Assembly on Au(111). *Journal of the American Chemical Society* **2010**, *132*, 15924-15926.
8. Applegate, J. C.; Okeowo, M. K.; Erickson, N. R.; Neal, B. M.; Berrie, C. L.; Gerasimchuk, N. N.; Barybin, M. V., First π-Linker Featuring Mercapto and Isocyano Anchoring Groups within the same Molecule: Synthesis, Heterobimetallic Complexation and Self-assembly on Au(111). *Chemical Science* **2016**, *7*, 1422-1429.
9. Treboux, G.; Lapstun, P.; Silverbrook, K., Asymmetric I / V Characteristics in Nonalternant Carbon Networks. *The Journal of Physical Chemistry B* **1998**, *102*, 8978-8980.
10. Holovics, T. C.; Robinson, R. E.; Weintrob, E. C.; Toriyama, M.; Lushington, G. H.; Barybin, M. V., The 2,6- Diisocyanoazulene Motif: Synthesis and Efficient Mono- and Heterobimetallic Complexation with Controlled Orientation of the Azulenic Dipole. *Journal of the American Chemical Society* **2006**, *128*, 2300-2309.
11. Alberding, B.; Barybin, M.; Chisholm, M.; Gustafson, T.; Reed, C. R.; Robinson, R.; Patmore, N.; Singh, N.; Turro, C., Molecular, Electronic Structure and Spectroscopic Properties of MM Quadruply Bonded Units Supported by Trans- 6- carboethoxy- 2- carboxylatoazulene Ligands. *Dalton Transactions* **2010**, *39*, 1979-1984.
12. Barybin, M. V., Nonbenzenoid Aromatic Isocyanides: New Coordination Building Blocks for Organometallic and Surface Chemistry. *Coordination Chemistry Reviews* **2010**, *254*, 1240-1252.
13. Barybin, M. V., Book Review of Functional Supramolecular Architectures: For Organic Electronics and Nanotechnology, Vols. 1– 2. Functional Supramolecular Architectures: For

Organic Electronics and Nanotechnology, Vols. 1− 2 . WILEY-VCH (Book review). **2011**, 133, 8774-8774.
14. Neal, B. M.; Vorushilov, A.; Delarosa, A.; Robinson, R.; Berrie, C.; Barybin, M., Ancillary nitrile substituents as convenient IR spectroscopic reporters for self- assembly of mercapto- and isocyanoazulenes on Au(111). *Chemical Communications* **2011**, *47*, 10803-10805.
15. Nuzzo, R. G.; Allara, D. L., Adsorption of Bifunctional Organic Disulfides on Gold Surfaces. *Journal of the American Chemical Society* **1983**, *105*, 4481-4483.
16. Nuzzo, R. G.; Dubois, L. H.; Allara, D. L., Fundamental Studies of Microscopic Wetting on Organic Surfaces. 1. Formation and Structural Characterization of a Self-Consistent Series of Polyfunctional Organic Monolayers. *Journal of the American Chemical Society* **1990**, *112*, 558-569.
17. Nuzzo, R. G.; Fusco, F. A.; Allara, D. L., Spontaneously Organized Molecular Assemblies. 3. Preparation and Properties of Solution Adsorbed Monolayers of Organic Disulfides on Gold Surfaces. *Journal of the American Chemical Society* **1987**, *109*, 2358-2368.
18. Love, J.; Estroff, L.; Kriebel, J.; Nuzzo, R. G.; Whitesides, G., Self-Assembled Monolayers of Thiolates on Metals as a Form of Nanotechnology. *Chemical Reviews* **2005**, *105*, 1103-1169.
19. Whitesides, G. M.; Grzybowski, B., Self-Assembly at all Scales. *Science* **2002**, *295*, 2418-2421.
20. Ulman, A., Formation and Structure of Self-Assembled Monolayers. *Chemical Reviews* **1996**, *96*, 1533-1554.
21. Tachiban, M.; Yoshizawa, K.; Ogawa, A.; Fujimoto, H.; Hoffman, R., Sulfur- Gold Orbital Interactions, which Determine the Structure of Alkanethiolate/ Au (111) Self- Assembled Monolayer Systems. *Journal of Physical Chemistry B* **2002**, *106*, 12727-12736.
22. Dubois, L. H.; Nuzzo, R. G., Synthesis, Structure, and Properties of Model Organic Surfaces. *Annual Review of Physical Chemistry* **1992**, *43*, 437-463.
23. Nuzzo, R. G.; Zegarski, B. R.; Dubois, L. H., Fundamental Studies of the Chemisorption of Organosulfur Compounds on Gold(111). Implications for Molecular Self-assembly on Gold Surfaces. *Journal of the American Chemical Society* **1987**, *109*, 733-740.
24. Porter, M. D.; Bright, T. B.; Allara, D. L.; Chidsey, C. E. D., Spontaneously Organized Molecular Assemblies. 4. Structural Characterization of N-Alkyl Thiol Monolayers on Gold by Optical Ellipsometry, Infrared Spectroscopy, and Electrochemistry. *Journal of the American Chemical Society* **1987**, *109*, 3559-3568.
25. Jones, J. A.; Qin, L. A.; Meyerson, H.; Kwon, I. K.; Matsuda, T.; Anderson, J. M., Instability of Self-assembled Monolayers as a Model Material System for Macrophage/ FBGC Cellular Behavior. *Journal of Biomedical Materials Research Part A* **2008**, *86*, 261-268.
26. Venables, J., *Introduction to Surface and Thin Film Processes*. Cambridge ; New York : Cambridge University Press, Cambridge ; New York, **2000**.
27. Landolt, D.; Schlesinger, M.; Paunovic, M., *Modern Electroplating*. Wiley, New York, The Electrochemical Society Inc, Pennington, NJ, **2001**.
28. Hou, Z.; Abbott, N. L.; Stroeve, P., Electroless Gold as a Substrate for Self-Assembled Monolayers. *Langmuir* **1998**, *14*, 3287-3297.
29. Lazar, M.; Angelici, R. J., Isocyanide Binding Modes on Metal Surfaces and in Metal Complexes. In *Modern Surface Organometallic Chemistry*, Basset, J. M.; Psaro, R.; Roberto, D.; Ugo, R., Eds. Weinheim: Wiley-VCH, **2009**, 513-556.

30. DeBono, R. F.; Loucks, G. D.; Manna, D. D.; Krull, U. J., Self-assembly of Short and Long- Chain N - Alkyl Thiols onto Gold Surfaces: A Real-time Study Using Surface Plasmon Resonance Techniques. *Canadian Journal of Chemistry* **1996**, *74*, 677-688.
31. Tamada, K.; Hara, M.; Sasabe, H.; Knoll, W., Surface Phase Behavior of N- Alkanethiol Self-Assembled Monolayers Adsorbed on Au(111): An Atomic Force Microscope Study. *Langmuir* **1997**, *13*, 1558-1566.
32. Wang, Y.; Solano Canchaya, J. G.; Dong, W.; Alcamí, M.; Busnengo, H. F.; Martín, F., Chain-Length and Temperature Dependence of Self-Assembled Monolayers of Alkylthiolates on Au(111) and Ag(111) Surfaces. *The Journal of Physical Chemistry A* **2014**, *118*, 4138-4146.
33. Han, P.; Kurland, A.; Giordano, A.; Nanayakkara, S.; Blake, M. M.; Pochas, C. M.; Weiss, P. S., Heads and Tails: Simultaneous Exposed and Buried Interface Imaging of Monolayers. *ACS Nano* **2009**, *3*, 3115-3121.
34. Kang, H.; Park, T.; Choi, I.; Lee, Y.; Ito, E.; Hara, M.; Noh, J., Formation of Large Ordered Domains in Benzenethiol Self-assembled Monolayers on Au(111) Observed by Scanning Tunneling Microscopy. *Ultramicroscopy* **2009**, *109*, 1011-1014.
35. Carro, P.; Carro, P., A Novel Model for the ($\sqrt{3} \times \sqrt{3}$)R30° Alkanethiolate–Au(111) Phase based on Alkanethiolate–Au Adatom Complexes. *Physical chemistry chemical physics : PCCP* **2014**, *16*, 19017-19023.
36. Kang, J.; Ulman, A.; Liao, S.; Jordan, R.; Yang, G.; Liu, G., Self-Assembled Rigid Monolayers of 4 '- Substituted- 4- Mercaptobiphenyls on Gold and Silver Surfaces. *Langmuir* **2001**, *17*, 95-106.
37. Gottschalck, J.; Hammer, B., A Density Functional Theory Study of the Adsorption of Sulfur, Mercapto, And Methylthiolate on Au(111). *The Journal of chemical physics* **2002**, *116*, 784-790.
38. Mallick, G., *Scanning tunneling microscopic characterization of an engineered organic molecule*. Aberdeen Proving Ground, MD : Army Research Laboratory, Aberdeen Proving Ground, MD, *Army Research Laboratory* **2011**.
39. Noh, J.; Ito, E.; Hara, M., Self- assembled monolayers of benzenethiol and benzenemethanethiol on Au(1 1 1): Influence of an alkyl spacer on the structure and thermal desorption behavior. *Journal of Colloid And Interface Science* **2010**, *342*, 513-517.
40. Tao, Y.; Wu, C.; Eu, J.; Lin, W., Structure Evolution of Aromatic- Derivatized Thiol Monolayers on Evaporated Gold. *Langmuir* **1997**, *13*, 4018-4023.
41. Frey, S.; Stadler, V.; Heister, K.; Eck, W.; Zharnikov, M.; Grunze, M.; Zeysing, B.; Terfort, A., Structure of Thioaromatic Self-Assembled Monolayers on Gold and Silver. *Langmuir* **2001**, *17*, 2408-2415.
42. Käfer, D.; Witte, G.; Cyganik, P.; Terfort, A.; Wöll, C., A Comprehensive Study of Self-Assembled Monolayers of Anthracenethiol on Gold: Solvent Effects, Structure, and Stability. *Journal of the American Chemical Society* **2006**, *128*, 1723-1732.
43. Carron, K. T.; Hurley, L. G., Axial and Azimuthal Angle Determination with Surface-Enhanced Raman Spectroscopy: Thiophenol on Copper, Silver, and Gold Metal Surfaces. *The Journal of Physical Chemistry* **1991**, *95*, 9979-9984.
44. Azzam, W.; Wehner, B.; Fischer, R.; Terfort, A.; Woll, C., Bonding and Orientation in Self-Assembled Monolayers of Oligophenyldithiols on Au Substrates. *Langmuir* **2002**, *18*, 7766-7769.

45. Jiang, P.; Nion, A.; Marchenko, A.; Piot, L.; Fichou, D., Rotational Polymorphism in 2-naphthalenethiol SAMs on Au(111). *Journal of the American Chemical Society* **2006**, *128*, 12390-12391.
46. Maher, T. R.; Spaeth, A. D.; Neal, B. M.; Berrie, C. L.; Thompson, W. H.; Day, V. W.; Barybin, M. V., Linear 6,6′-Biazulenyl Framework Featuring Isocyanide Termini: Synthesis, Structure, Redox Behavior, Complexation, and Self-Assembly on Au(111). *Journal of the American Chemical Society* **2010**, *132*, 15924-15926.
47. Dutta, S.; Lakshmi, S.; Pati, S., Comparative Study of Electron Conduction in Azulene and Naphthalene. *Bulletin of Materials Science* **2008**, *31*, 353-358.
48. Barybin, M. V.; Thompson, W. H., *Unpublished Work*.
49. Maher, T. R.; Spaeth, A. D.; Neal, B. M.; Berrie, C. L.; Thompson, W. H.; Day, V. W.; Barybin, M. V., Linear 6,6'-Biazulenyl Framework Featuring Isocyanide Termini: Synthesis, Structure, Redox Behavior, Complexation, and Self-Assembly on Au(111). *Journal of the American Chemical Society* **2010**, *132*, 15924-15926.
50. Hong, S.; Reifenberger, R.; Tian, W.; Datta, S.; Henderson, J. I.; Kubiak, C. P., Molecular Conductance Spectroscopy of Conjugated, Phenyl- Based Molecules on Au(111): The Effect of End Groups on Molecular Conduction. *Superlattices and Microstructures* **2000**, *28*, 289-303.
51. Neal, B. Self-assembly of Azulenic Monolayer Films on Metallic Gold Surfaces. Dissertation Abstracts International, University of Kansas, ProQuest Dissertations Publishing, **2012**.
52. Maher, T. Design of Novel Electron-rich Organometallic Frameworks involving Metal-Isocyanide Junctions. Dissertation Abstracts International, University of Kansas, ProQuest Dissertations Publishing, **2009**.
53. Neal, B. M.; Vorushilov, A.; Delarosa, A.; Robinson, R.; Berrie, C. L.; Barybin, M. V., Ancillary Nitrile Substituents as Convenient IR Spectroscopic Reporters for Self-assembly of Mercapto- and Isocyanoazulenes on Au(111). *Chemical Communications* **2011**, *47*, 10803-10805.

54. Cossaro, A.; Mazzarello, R.; Rousseau, R.; Casalis, L.; Verdini, A.; Kohlmeyer, A.; Floreano, L.; Scandolo, S.; Morgante, A.; Klein, M. L.; Scoles, G., X-ray Diffraction and Computation Yield the Structure of Alkanethiols on Gold(111). *Science* **2008**, *321*, 943-946.

Chapter II:

Azulenic SAM formation and analytical methods used in the characterization of SAMs on Au (111) films

II.1. Overview and the highlights of chapter II

To elucidate the packing, orientation, periodicity, and stability of linearly functionalized azulene derivatives self-assembled on Au (111) films, characterization methods including optical ellipsometry, reflection-absorption infrared (RAIR) spectroscopy, and scanning probe microscopy (SPM) are used throughout this project. Information on the molecular packing, binding mode, molecular orientation, and stability are deduced from ellipsometry and RAIR studies. Resolved atomic- and molecular-scale images of azulenic SAMs from SPM experiments aid discernment on the packing geometry, molecular packing, stability, and periodicity of the molecules relative to the gold substrates.

Azulene may be considered a molecular diode due to its permanent dipole moment (*ca.* 1 Debye) aligned along the molecular axis. The origin of this hydrocarbon's polar nature stems from an intramolecular charge transfer between the fused 5 and 7 membered rings.[1-6] This property makes azulene and its derivatives attractive in the design of materials for molecular electronics applications. One of the research themes in the Barybin and Berrie laboratories encompasses the design, synthesis, and assessment of physicochemical characteristics of π-conducting azulenic molecular linkers equipped with junction groups the 2 and 6 positions of the azulenic scaffold (i.e., along the molecular axis). The most studied anchoring moieties connecting the azulene derivatives to the gold substrates are isocyanides and thiolate groups.[7-8] Typically, our key initial analyses of azulenic SAMs involve RAIR spectroscopy and ellipsometry. The isocyanoazulenes, as discussed in chapter one, adsorbed on gold give rise to characteristic ν(CN) bands in their RAIR spectra. The thiolate groups are very useful anchoring groups due to stable Au-S interactions,[9-12] but the thiolate junction unit does not provide an easily recognizable and interpretable vibrational signature. Incorporating substituent(s) at the azulenic core that would offer distinctive IR characteristics,

therefore, becomes imperative for facilitating qualitative analysis of the azulenyl thiolate SAMs by RAIR spectroscopy. Nitrile groups (cyano groups) can serve as a particularly convenient remote spectroscopic handle in the RAIR analysis of azulenyl thiolate derivatives adsorbed on gold surfaces.[13] Moreover, it has been recognized in theoretical studies that the nitrile moiety is well-suited to fulfill the role of the electron-withdrawing junction group in the design of asymmetrically anchored molecular rectifyers.[14] As discussed in chapter one, interactions between tail groups within monolayers affects molecular packing in the SAMs. The dipole-dipole interactions of the ancillary cyano substituents may influence molecular packing which is critical to probe for fully understanding the structure-property relationships function of new materials with potential applications in organic electronics. Herein, nitrile functionalized isocyanoazulene SAMs of 6-cyano-1,3-diethoxycarbonyl-2-isocyanoazulene **(1),** 2-cyano-6-isocyanoazulene **(2)**, and 2-cyano-4-isocyanoazulene **(3)** molecules on gold substrates are probed using ellipsometry and RAIR. The techniques for investigating the systems are discussed in detail. The assumption is that for isocyano/cyano-functionalized azulenic SAMs, the cyano groups would have much lower affinity to bind to the Au (111) surface than the isocyanide groups and therefore, the cyanides would be the cyano tail groups of the SAM not interacting with the metal surface. Therefore, the isocyanides would serve as the head groups providing junction between the metal surface and the azulenic scaffold. Interpreted results, for instance orientation, binding, stability, or molecular packing of both the head and tail groups may reveal structural and mechanistic details for designing single molecular junctions.

II.2. Gold substrates and preparation of atomically flat gold substrates

Gold substrates remain among the most studied material in surface chemistry because of its oxidative inertness.[15-16] Gold substrates are commonly used in monolayer formation of thiolate-head group molecules, for biological and technical applications, due to the stable gold-sulfur interaction formed.[9-12] Also, gold substrates are widely employed in many other types of monolayers for molecular electronics.[12, 17-18] Due to gold's conductive properties, gold substrates are used as an electrochemically active surface to analyze the behaviors of chemical or biological samples.[12, 18] Hence, in conducting electrochemical experiments, the quality of the active surface is essential as it may influence the results obtained. As such, the preparation of gold substrates is critical to avoid contaminants that may skew the conductive properties as well as the binding kinetics of the monolayer substrates. The gold substrates assume a face cubic crystal structure (fcc) with the most stable and adopted face being the (111) terrace.[12, 18] The substrate employed throughout this work is the Au (111) substrate. This Au (111) substrate is typical for a distinct close packing plane of gold's crystalline lattice as described by Miller indices seen in Figure 2.1b.[18]

a)

b)

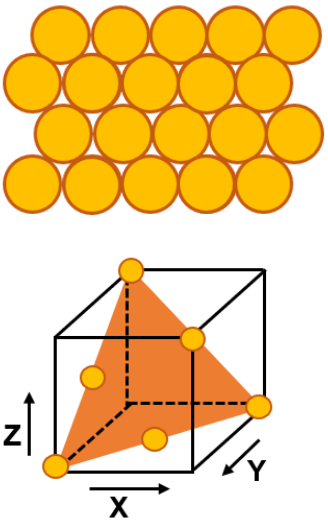

Figure 2.1. a) Vapor deposition Chamber (Auto 306) employed. b) The top image is the closed pack density of the 111 lattice diagram in an fcc crystal structure. Illustrated in the bottom picture is the cutout 111 face shown on the x-, y-, and z- coordinates of the unit cell.[12]

Vapor deposition of gold under high vacuum, critical for high-quality substrates, was used in the preparation of the Au (111) substrates There are two types of gold substrates used in this work: the commercially available gold-coated silicon and the house-gold (gold-coated mica). The gold substrates were prepared by either deposition directly on freshly cleaved mica or on silicon substrates coated with a titanium adhesion layer underneath the gold. The thickness of the gold film depends on the coating conditions. While the gold-coated mica substrate with a thickness of about 50 - 100 nm was prepared in the Berrie Lab using Edwards Rotary Evaporator (Auto 306), the gold-coated silicon substrates purchased from Platypus Technologies had a thickness of 100 nm.

Thorough understanding of the slightest changes that may occur at the molecular level is essential for advanced material technologies. Therefore, it is highly relevant to study the molecular packing, orientation, packing geometry, and periodicity of SAMs for further application processes. In other to study the packing and the periodicity of SAMs using SPM at a nanoscale level on Au (111), atomically flat gold-coated mica substrates were employed. The quality and cleanliness of the sample substrate used in this study are highly critical for excellent measurements, reproducible results, and data quality. The gold-coated mica made in the Berrie Lab was very cheap compared to commercially available gold-coated mica. The gold-coated mica substrates were prepared in the lab using the Auto 306 instrument at pressures as low as 1.3×10^{-7} torr while the chamber was heated up to temperatures of about 200 – 300 $^{\circ}$C. A diffusion pump and a rough pump were used to maintain vacuum condition while the traps above the pumps were kept at reasonable temperature conditions using liquid nitrogen and a water-cooling system plumbed to the evaporator. The cooling of these traps helps prevent pump oil from flowing into the vacuum chamber. With very high temperature in the chamber and low pressure, current is run through the gold wire for it to heat up and vaporize onto the freshly cleaved mica in the chamber until the desired thickness is obtained. The deposition rate (1-3 nm/sec) and desired thickness are monitored and measured by a quartz crystal microbalance (QCM). The QCM works as a sensor, accurately monitoring the small variations in mass per unit area, by measuring the frequency of the sensitive quartz crystal resonator. The gold substrates made were annealed for an hour in the chamber and immediately stored in a desiccator. Additional treatment to improve the substrate quality is usually done by flame annealing using hydrogen flame for homogeneity. The annealing method is a crucial step in achieving qualitative large Au (111) terraces which should result in atomically flat gold substrates. Before the annealing step, the substrate was rinsed with large volume of milli-Q water and dried

with a nitrogen gas stream. The annealing of the substrate was done by using a hydrogen flame torch which was held at *ca.* 30 degrees angle with respect to the substrate and gently sweeping the 4 cm long flame torch back and forth at *ca.* 1 Hz across the gold substrate. The 4 cm long flame touch was placed 3 cm away from the substrate during the annealing process which lasted for about 30-50 secs.[19] Figure 2.2.b shows the Atomic Force Microscope (AFM) image of a freshly annealed gold-coated mica film made in this work. The cross-section analysis shows that the gold-coated mica, for a randomly selected grain, was *ca.* 150 nm and this is bigger and flatter than the observed 50 nm grain size of gold-coated silicon purchased from Platypus Technologies (Figure 2.2 a). The atomically resolved image of the gold-coated mica in Figure 2.2d is typical for an annealed gold film. The z scale rangeof the images in Figure 2.2a indicates flatness of the substrate.

The commercially available gold-coated silicon substrates from Platypus Technologies were prepared using a similar process except a titanium adhesion layer was utilized. Titanium adhesion layer was first uniformly deposited on the silicon before the gold deposition for proper formation of the substrates. Although gold-coated mica substrates formed flatter and wider grains than the gold-coated silicon substrate, optical interference from the thin mica substrate below the gold-coated mica films causes difficulties in measuring monolayer thickness under the optical ellipsometer. Therefore, it is necessary to use the gold-coated silicon substrates for measuring the monolayer thickness on an optical ellipsometer, even though the gold-coated silicon may have smaller grain sizes.

a)

b)

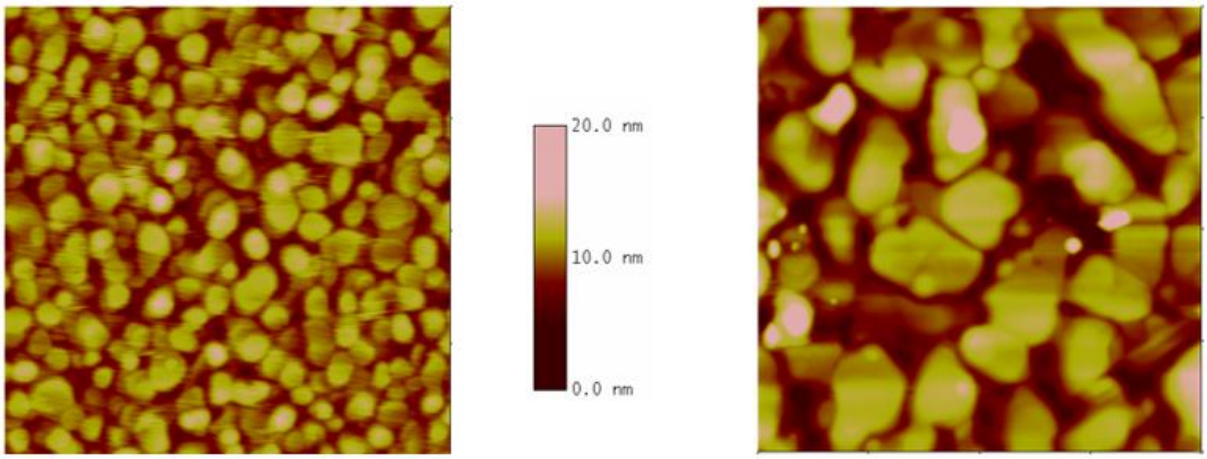

c)

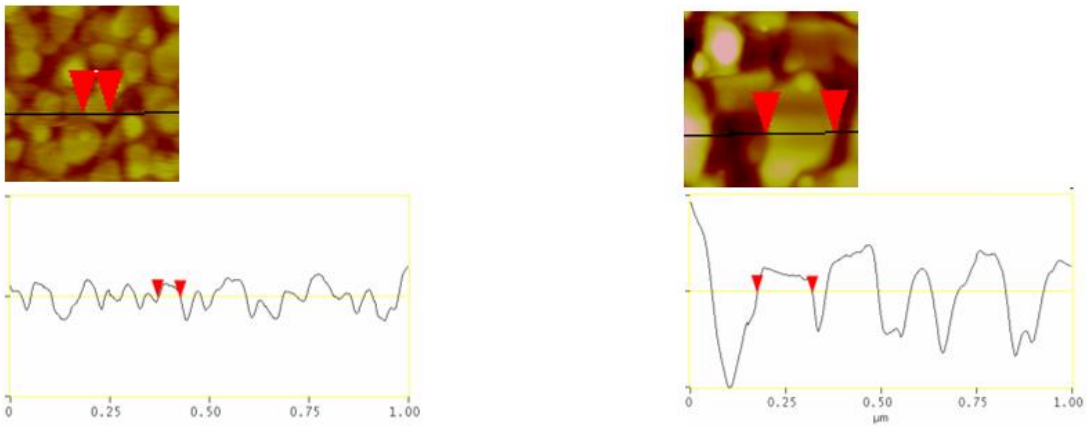

d)

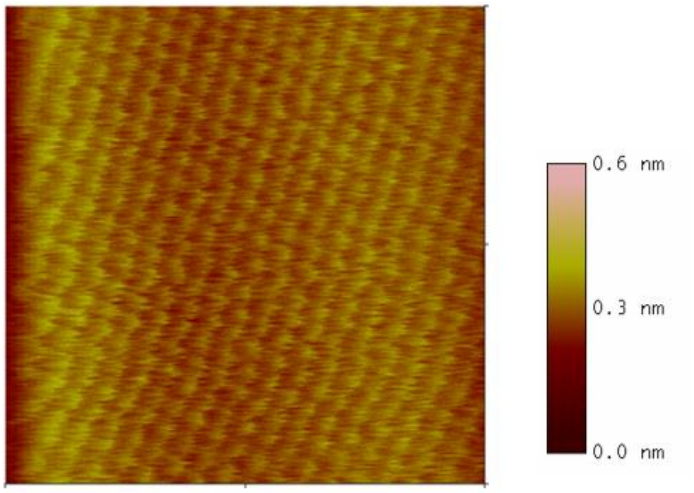

Figure 2.2. AFM images of a) commercial gold-coated silicon substrate and b) gold-coated mica made in the Berrie Lab. Scan size - 1000 nm x 1000 nm at z scale range20 nm, Probe tip - DNPs, applied set point - 1.892 V c) The width of the grain size measured for the top images. The width of a) highlighted with the red arrows is 50 nm and b) is 150 nm. d) Atomically resolved image of the annealed gold-coated mica. Set point - 0.3393 V spaced by 0.32 nm. All images were collected in ambient conditions.

II.3. Cyano and isocyano substituted azulenic derivatives on Au (111) Substrate

The studies discussed herein are cyano functionalized isocyanoazulene derivatives coordinated on Au (111) substrates. This interesting cyano substitution may aid molecular packing due to the dipole-dipole interaction of the tail ends. Also, the cyano groups may provide useful complementary vibrational data that facilitates physicochemical interpretation of azulenic film self-assembly. To understand the structural formation and molecular arrangement of nitrile substituted isocyanoazulene derivatives in molecular films, the rest of this chapter describes the

analysis of these SAMs using the optical ellipsometry and Fourier transform infrared spectroscopy. Perhaps, understanding the stability and influence of cyano groups on the azulenic SAMs, as well as influence of cyano groups on conductance characteristics for organoelectronics is necessary.

II.4. Introduction

The electronic properties of azulene make it attractive for applications in nanoelectronics. The bluish non-benzenoid aromatic hydrocarbon, azulene, has a dipole moment of *ca.* 1.1 Debye. The azulenic scaffold, due to the dipole moment, can in principle behave as molecular-diode with/without incorporating any substituents along its molecular axis which makes it a useful tool in organoelectronics.[11, 20-22] Hence, the influence of donor/acceptor substituents on azulene with focus on charge transport properties, when bound to a conductive substrate, will be interesting to investigate. Suitably, understanding the charge transport property of the azulenic derivative SAM is achievable by varying the substituents along the azulenic molecular axis.[11, 21-23] The nature of the substituent group may affect the electronic properties of the azulene in different ways, by either widening or shrinking its frontier energy gap. The frontier energy gap (HOMO-LUMO gap) can be adjusted based on electron donating or withdrawing groups incorporated on the azulene.[1, 4, 20, 24-25] Electron withdrawing groups (EWG) at the 2, 4, or 6 positions carbon atoms stabilize the LUMO energy, but EWG at the 1, 3, 5, or 7 positions destabilizes just the HOMO energy level.[2-6] This observation affirms the complementary orbital density distribution of azulene's frontier orbitals as seen in Figure 2.3. The most studied junction groups used in assembling azulene derivatives on a conductive substrate like gold substrate are the isocyano and mercapto-anchoring groups.[1, 4, 20, 24-25] Analyses of the monolayer properties such as molecular packing, coverage, stability, orientation, anchoring groups, and defects are highly crucial towards understanding conductivity and charge transport properties of the SAM films. These analyses in this work involve

the use of optical ellipsometry, reflective absorption infrared spectroscopy (RAIR), and scanning probe microscopy (SPM).

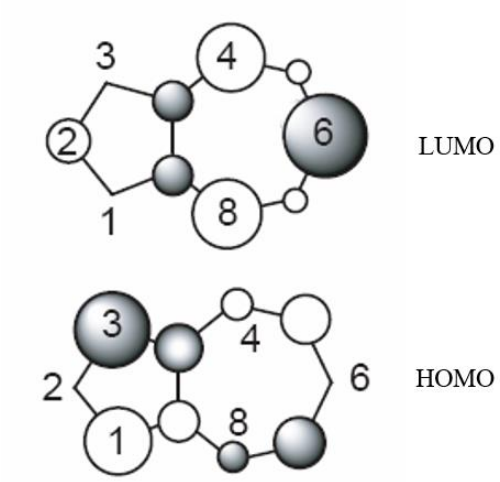

Figure 2.3. An Illustration of Azulene's frontier orbital density distribution.[5]

Several studies of isocyanoazulenes SAM in our work involves the use of isocyanide as junction group to the gold substrate which influences the dipole property of the parent azulene. The dipole moment of five different isocyanoazulenes calculated in our previous work (Robinson *et al.*) showed that 2-isocyanoazulene has the highest dipole moment (5.40 Debye) while 6-isocyanoazulene has the lowest dipole moment (3.14 Debye) as influenced by the position of the isocyano substituent on the aulenic framework.[5] Therefore, the interest to probe the electronic behavior of SAM with isocyanide junction groups at the positions 2, 6 or both positions arise as the electronic environment is changed. Two possible bonding interactions of organic isocyanide with a metal atom or ion are known, a σ bond in which the isocyanide donates its electron pair to the metal and a π-backbonding in which the metal donates to the isocyanide empty π*-orbital as seen in Figure 2.4.[26] The isocyanide junction group experiences an increase in bond strength upon

SAM formation on the gold substrates.[1-6] This increase in bond strength is indicative of the σ-bonding via donation of the isocyanides carbon atom's lone pair to the gold substrate.[1-6] The donated lone pair occupied antibonding energy with respect to the C≡N bond and became more energetically stable upon donation to the gold substrate. The SAM formation that occurs via coordination of isocyanide to gold (Au-CNAz) reveals no π-backbonding from the gold substrate to the junction group due to the observed blue shift in the ν(C≡N). Therefore, the coordination solely occurs via σ-bonding.

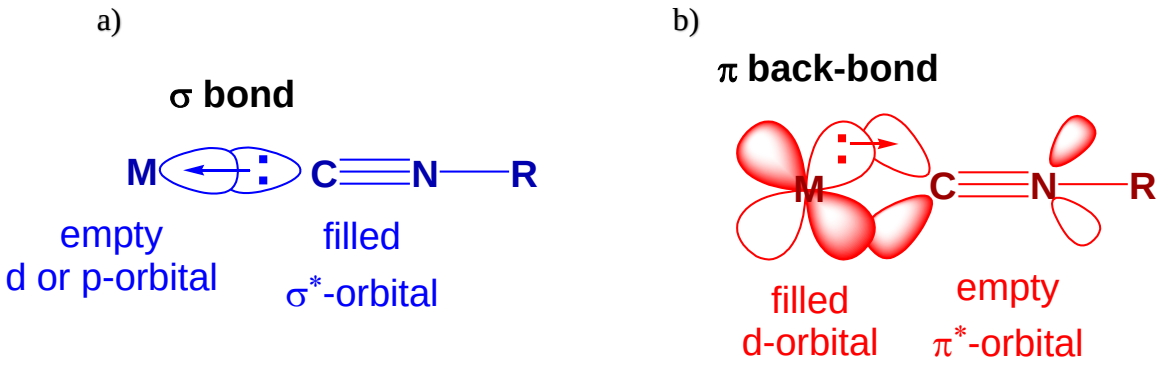

Figure 2.4. a) The isocyanide's lone pair forms σ-bond with an empty orbital in the metal, b) π-back bond from a filled metal d-orbital of π-symmetry to an empty π* orbital of the isocyanide.[26]

The thiol-headgroup azulene is also a common junction group used in our study. When the thiolate azulene derivatives are coordinated to the conductive gold substrate, an Au-S bond is formed. The SAM formation is confirmed using accessible analytical techniques, that is, ellipsometry and RAIR spectroscopy. The vibrational bands from thiolate-headgroup azulene SAMs are not spectroscopically interpretable using the RAIR spectroscopy due to the ν(Au–S) band (*ca.* 400 cm^{-1}) is unobservable in the IR window available on our spectrophotometer (4000 cm^{-1}- 600 cm^{-1}). This limitation in our spectroscopic technique can be circumvented by the use of substituent groups that have observable IR bands on the RAIR employed in this work and taking

advantage of the RAIR selection rule to interpret the relative intensities of the peaks in the spectrum for information on orientation. Cyano groups have stretching frequencies in an observable IR region, (2200 cm^{-1} – 2300 cm^{-1}), therefore, incoporating cyano substituent to the azulene would facilitate qualitative analysis of the monolayer.

The possible interactions between terminal ends of SAMs can affect molecular packing. Cyano-terminated alkyl thiols have been studied using different techniques to understand their influence on the monolayer formation.[28-29] The monolayers of cyano-terminated alkylthiolates were compared to similar molecules of non-substituted alkylthiolates adsorbed on gold and silver films. Zharnioff *et al.* suggested that strongly interacting nitrile entities may influence the packing, orientation, and structure of the alkylthiol films.[29] The non-substituted benzenethiol monolayer films and cyano-substituted benzenethiol monolayer films adsorbed on gold surface were studied, well-ordered and densely packed SAMs were observed more in the cyano substituted than the non-substituted monolayers.[29-30] In the cyano-substituted alkylthiol monolayer, only disordered monolayers and rearrangements were observed due to strong electrostatic interactions from the polar -CN moieties. The π-π interaction in the benzenethiol monolayer, as well as the cyano group, aided the formation of the well-ordered monolayer than in the alkylthiol SAMs. The presence of the nitrile group leads to significant increase in the density packing of the film as compared to the analogous non-substituted SAMs.[30] Therefore, understanding the packing density in the azulene derivative SAMs may be an interesting study which may be useful for systems like the mercaptoazulene SAMs films. Also, the cyano moiety have been employed to study charge transfer dynamics through the azulenic molecular backbone and head group substrates using Auger electron spectroscopy.[27] In addition, electron withdrawing cyano groups have been suggested in

theoretical studies as junction group in the design of asymmetrically anchored molecular rectifiers.[14]

Extensive study has been done to elucidate the packing and orientation of mercaptoazulene monolayer adsorbed on gold substrate in our lab. The measurements from the ellipsometer has provided us with information about the molecular orientation. On the other hand, mercaptoazulene SAMs' orientation and binding properties are better interpreted with the RAIR spectroscopy when substituent groups that can serve as a suitable spectroscopic marker are attached to determine molecular orientation unambiguously. The RAIR is governed by a selection rule that vibrational modes perpendicular to the gold substrate are enhanced on the RAIR. The selection rule helps interpret the orientation of the monolayer on the gold substrate. The molecular orientations in the isocyano-headgroup monolayer are deducible using both the FTIR and the Ellipsometer. Additional techniques mentioned above may provide insight into monolayer packing and orientation. In this work, FTIR and ellipsometry are employed.

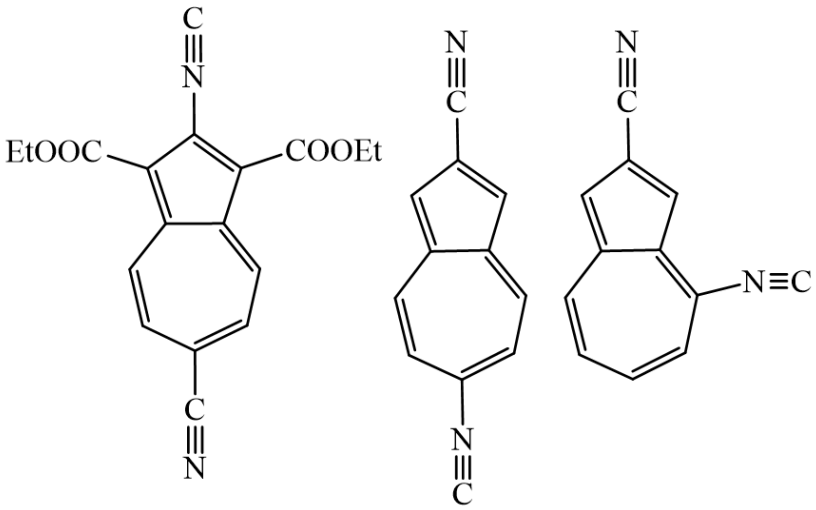

Figure 2.5. cyano substituted isocyanide molecules employed in SAM formation

II.5. Experimental section

II.5.1. General procedures and starting materials

All compounds used in the preparation of the molecular films were synthesized in the Barybin Lab by Jason Applegate, Nathan Erickson, and Zack Wood. Au (111) films used in SAM formation were either purchased from Platypus Technologies or made in the Berrie Lab as described in Section 1.2.

For ellipsometry and RAIR spectroscopic analyses, commercial gold-coated silicon substrates from Platypus Technologies were employed in SAMs formation. Unless stated otherwise, the gold substrates used were cut to a 1 x 1 cm^2 size, washed by soaking in chloroform, acetone, and 200- proof ethanol for two hours in each solvent, and rinsed with a large volume of ethanol before drying with nitrogen gas. The optical ellipsometric physical constants of the dried gold substrates were recorded at a minimum of five different spots on each substrate. The gold substrates were placed in a 2 mM solution of the azulene of interest in distilled dichloromethane for *ca.* 24 hours for molecules to fully self-assemble on a gold substrate. The experiment was performed without any protection from air or ambient laboratory lighting. Analytical methods for characterizing the SAMs as well as results and discussions on the SAMs herein are detailed in section 1.5.

The molecules studied herein are depicted in Figure 2.5. The first molecule has a cyano tail group at the 6 position of the azulene and is expected to coordinate via the isocyanide-headgroup at the 2 position of the azulene framework while the second molecule has the tail and head groupss switched in this case. The main difference is the switch in the azulene molecular axis with respect to the attached substituents though both molecules are expected to orient in an upright fashion

when coordinated to the gold substrate. The third molecule, however, features the azulene oriented partially parallel to the gold substrate. Therefore the RAIR result may give important information about the molecular orientation. The cyano group is substituted on the position 2 while the isocyanide-headgroup on the position 4 is expected to bind to the gold substrate. The packing especially the third molecule may be influenced differently due to the orientation and position of the cyano group.

II.5.2. SAM formation of 6-cyano-1,3-diethoxycarbonyl-2-isocyanoazulene on Au (111) film (1)

The gold substrates were first cleaned with hot Piranha solution (**Warning**: extreme care should be employed when using the solution due to violent reaction of the oxidant with organic substances). The gold substrates were subjected to further cleaning using the described cleaning method in general procedures and starting materials. The ellipsometric physical constants *n* and *k* of the cleaned gold substrates were measured at five different spots on the substrates before immersing the gold substrates into a 2 mM solution of 6-cyano-1,3-diethoxycarbonyl-2-isocyanoazulene in distilled dichloromethane CH_2Cl_2 for *ca.* 24 hours to make SAMs-coated gold substrates. Analyses using ellipsometer and the grazing incidence reflection absorption infrared (RAIR) spectrophotometer were done to investigate the molecular orientation, packing, and binding of the SAM. Prior to any analysis, the SAM-coated substrates were rinsed thoroughly with distilled CH_2Cl_2 to remove any loosely bound or physisorbed molecules, and the substrates were dried in a flow of N_2 gas. The SAMs of **1** were made in an inert, glovebox environment due to the stability of the SAM films. Analyses of **1** were taken immediately after SAMs formation.

II.5.3. SAM formation of 2-cyano-6-isocyanoazulene on Au (111) film (2)

The gold samples were cleaned as described in the section on general procedures and starting materials. The cleaned bare gold substrates were dried thoroughly under a nitrogen stream and their ellipsometric optical constants *n* and *k* were measured at five separate spots on the substrates. The freshly cleaned substrates were placed into a 2 mM solution of 2-cyano-6-isocyanoazulene in chloroform $CHCl_3$ for *ca.* 24 hours to afford the SAM formation of the compound. Investigation of the molecular orientation, packing, and binding of the SAM was analyzed using ellipsometry and a grazing incidence reflection absorption infrared (RAIR) spectrophotometry. Prior to any analysis, the SAM-coated substrates were rinsed thoroughly with $CHCl_3$ and dried in a flow of N_2 gas to remove loosely bound molecules. There were no precautions to exclude air or ambient laboratory lighting exercised during these SAM preparations.

II.5.4. SAM formation of 2-cyano-4-isocyanoazulene on Au (111) film (3)

The ellipsometric physical constants *n* and *k* of the thoroughly cleaned, dried bare gold substrates were measured at five different spots on the substrates. The gold substrates were cleaned using the methods described in general procedures and starting materials. SAM films of these compounds were formed by placing the freshly cleaned *ca.* 1×1 cm^2 gold substrate into a 0.02 mM solution of 2-cyano-4-isocyanoazulene in $CHCl_3$ for ca. 24 hrs. Analysis using ellipsometer and the grazing incidence reflection absorption infrared (RAIR) spectrophotometer was done to investigate the molecular orientation, packing, and binding of SAM. Before any analysis, the SAM-coated substrates were rinsed thoroughly with $CHCl_3$ and dried in a flow of N_2 gas. There were no precautions to exclude air or ambient laboratory lighting exercised during these SAM preparation experiments.

II.6. Method of Analysis

II.6.1. Optical Ellipsometry

Ellipsometry is primarily used to determine optical constants and structural characteristics information such as film thicknesses and density distribution. This technique affords the investigation of optical properties and physical structure of thin film by measuring the polarization change as light reflects through the material structure.[31] The technique does not directly measure the thickness or the optical properties of the film, instead the technique measures the change in polarization of the light. The polarization change is represented by two parameters, the amplitude ratio Ψ and the phase change Δ, which determines the differential change in amplitude and phase thereby measuring the degree of elliptical polarization.[32] This provides information about the optical constants of the bare gold substrate. The optical constants include the refractive index *n* and the extinction coefficient *k* and are used in the determination of the thickness of the film. This work uses the single-wavelength ellipsometry method to determine the thickness of self-assembled monolayer (SAM) of organic films. The technique is non-destructive and has been used extensively over the years.[12, 31-34]

Ellipsometer consists of a light source, a polarizer, compensator, sample, analyzer, and detector as shown in Figure 2.6.[34] The rotation of the polarizer, compensator, and analyzer during the analyses majorly provide information on the optical properties of the thin film or sample substrate.[33] The light source employed throughout this work is a HeNe laser which passes through the polarizer and a compensator before getting to the substrate as elliptically polarized light. A change in polarization occurs as the light passes through the film and enters an analyzer which is rotated until a null or minimum signal is detected, aiding the required measurements.[34] The optical constant of the gold film is vital for analyses of the monolayer thickness using ellipsometry.

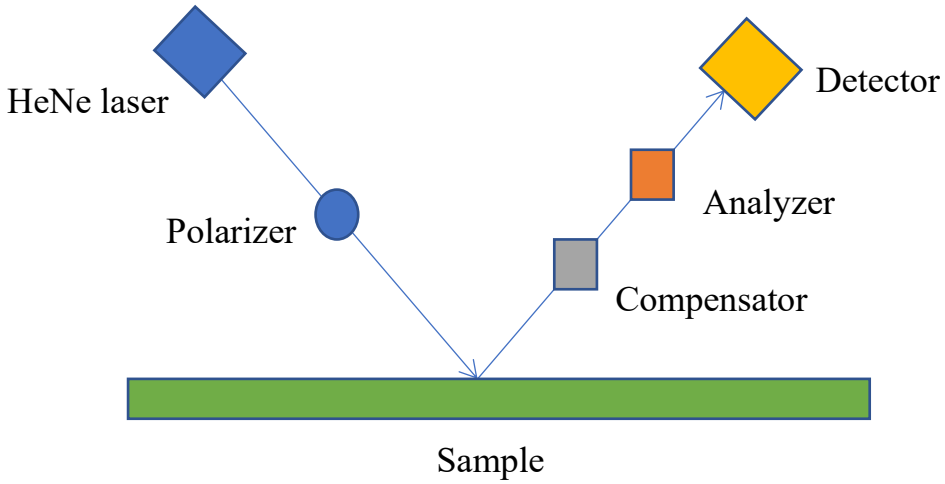

Figure 2.6. Schematic representation of an ellipsometric experiment.

II.6.1.1. Method

The Ellipsometer was first calibrated using a freshly cleaned silicon wafer control sample. The silicon wafer was cleaned by first wiping the wafer with a soap solution using a Kimtech wipe, rinsed with deionized water, dried with nitrogen stream before washing with 50:50 ethyl ether and methanol followed by drying with a nitrogen stream.[34]

The film thickness values were determined using an Auto EL III fixed wavelength ellipsometer (Rudolph Research). All measurements conducted was with a HeNe laser at a wavelength of 632.8 nm and an incident angle of 70° to the surface normal. The optical constants *n* and *k* were obtained for each sample individually by measuring these parameters for the corresponding freshly cleaned bare gold substrates at a minimum of 5 different spots before the SAM formation as seen in Table 2.1. These optical constants were used as input in determining thicknesses of the adsorbed thin layers of 6-cyano-1,3-diethoxycarbonyl-2-isocyanoazulene (**1**), 2-cyano-6-isocyanoazulene (**2**), and 2-cyano-4-isocyanoazulene (**3**). A refractive index of 1.45 was assumed for all organic thin films described herein.[35-37] For each SAM sample, the reported

thickness value constitutes an average of those derived from ellipsometric measurements at five different spots of the SAM substrate.

II.6.1.2. Result and Discussion

The resulting thicknesses from the ellipsometry measurements ($D_{obs.}$) are found in Table 2.1 and are compared to the theoretical/calculated thicknesses ($D_{calc.}$). The theoretical thicknesses for a monolayer assuming a completely upright orientation without any physisorption were calculated using the MM2-optimized model in ChemBio3D Ultra 15.1. The expected result from the SAM formation was that **1, 2,** and **3** will coordinate to the gold film via the formation of an Au–C bond. The addition of the Au–C coordination bond length of 2.04 Å to the results calculated from ChemBio3D gave the overall theoretical thickness values of the monolayer.

Table 2.1. Ellipsometry data showing the averaged *n* and *k* values of the bare substrates, observed thicknesses, and calculated thicknesses for SAMs of **1**, **2,** and **3**, respectively.

	Compounds	***n***	***k***	$D_{obs.}$ ***(Å)***	$D_{calc.}$***(Å)***
1	6-cyano-1,3-diethoxycarbonyl-2-isocyanoazulene	0.147	3.459	9.2 ± 0.8	11.9
2	2-cyano-6-isocyanoazulene	0.174	3.508	10.7 ± 0.3	11.9
3	2-cyano-4-isocyanoazulene	0.152	3.455	8.6 ± 0.2	8.5

The reported *n* and *k* values for the specific gold films used in these experiments (as seen in Table 2.1) were used as input in the modeling to obtain the corresponding observed thicknesses (D_{obs}). The observed thickness of **1** (9.2 ± 0.8 Å) is comparable to the calculated thickness (11.9 Å) signifying formation of an upright monolayer. Similarly, D_{obs} in **2** were closely related to $D_{calc.}$

indicative of the creation of a monolayer. Although the D_{obs} in **1** is somewhat shorter than the $D_{calc.}$ for completely upright coordination of **1**, probably due to less packing monolayer of **1** than **2,** the results are comparable. The less packed monolayer is as a result of the bulky substituent diethoxycarbonyl, in the 1 and 3 positions in **1**. These bulky groups can affect the intermolecular interactions of the monolayer, simultaneously changing the density packing of the monolayer. In **1** and **2**, $D_{calc.}$ is in reasonable agreement with $D_{obs.}$, signifying an upright orientation of the monolayer and the formation of an Au–C bond accounted for in the D_{calc}. Since the assumption is that the coordination to the gold substrate is via the isocyanide group, accounting for an Au–C bond of 2.04 Å was done. Confirmation of the observed interpretation is further supported by the RAIR spectroscopic data.

In **3**, the $D_{calc.}$ is 8.5 Å for a monolayer formed via the creation of the Au–C bond. The $D_{obs.}$ and $D_{calc.}$ agree with the assumption that the isocyanide at the position 4 of the azulene coordinates to the gold film. The coordination of this molecule to the surface will be further confirmed using the FTIR. The cyano substituent may serve as an additional spectroscopic characterization of these molecules.

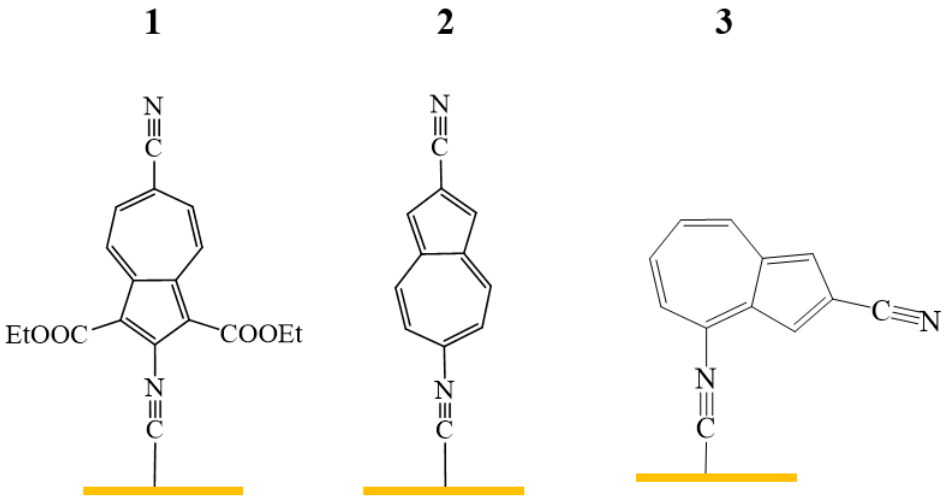

Figure 2.7. Illustration for the SAM formation of **1, 2,** and **3** linearly coordinated on the gold substrate via the isocyanide junction group.

II.6.2. Fourier-Transform Infrared Spectroscopy

Fourier Transform Infrared Spectroscopy FTIR, which measures the absorption of infrared radiation resulting in vibrations of ensembles of chemical bonds present in a molecule.[33] Infrared radiation directed at a sample is absorbed due to the vibrations of chemical bonds present in the molecule. The IR spectrum gives information on molecular components and structures present in a sample.[33] Infrared spectrum can be collected using different methods depending on the sample's properties and the information required. For analyses of materials deposited on a surface, the FTIR method could be absorption, attenuated total reflectance, diffuse reflectance, or reflection absorption spectroscopy.

For SAMs on reflective substrates like gold, reflection absorption infrared (RAIR) spectroscopy is usually employed. This method is also called the grazing incidence reflection absorption FTIR.[33, 38] The area of the substrates analyzed is relatively large, increasing the signal for direct measurements of a bulk average of the substrate. RAIR follows a selection rule which polarization of the incident radiation and molecular orientation are essential for IR spectrum collected. The polarizer is useful in the enhancement of sensitivity in the grazing angle measurements as it monitors molecular orientation in the film. The selection rule as described in Figure 2.8 shows two orientations, a parallel and a perpendicular polarization with respect to the substrate, for the changing instantenous dipole moments in the molecules. Only the vertical polarization enhances the dipoles on the substrate and, therefore, is IR-active. The parallel dipoles are reduced and may not be detected on the metallic substrate, hence IR-inactive.

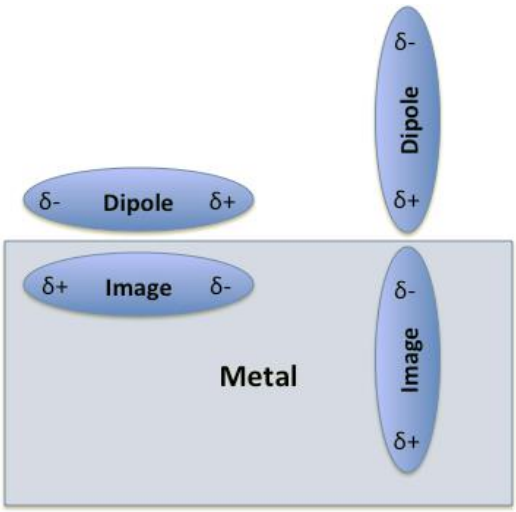

Figure 2.8. Illustration showing RAIR selection rule, describing the parallel and perpendicular dipole observed on a reflective substrate with reduced and enhanced dipoles, respectively.

Cyano groups have been employed as substituents at the azulenic framework due to the vibration frequencies of the cyano group are observable on the RAIR spectrum. For comparisons, monolayers of 1,3-dicyano-2-azulenylthiolate and 1,3-dicyano-2-isocyanoazulene on gold films

made by Dr. Brad Neal, a previous member of the group, were studied using both ellipsometry and RAIR spectroscopy.[1] The presence of the cyano groups helps to qualitatively interprete the results obtained from the RAIR as seen in Figure 2.9.

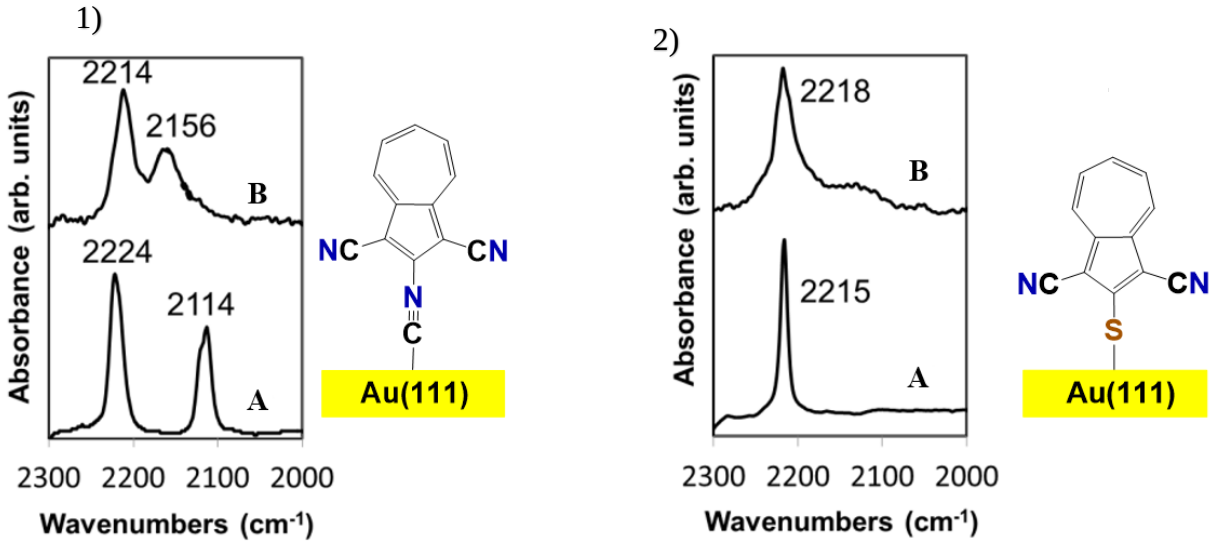

Figure 2.9. Left: (1A) FTIR spectrum of 1,3-dicyano-2-isocyanoazulene dissolved in $CHCl_3$ and (1B) RAIR spectrum of 1,3-dicyano-2-isocyanoazulene adsorbed on Au (111). Right: (2A) FTIR spectrum of 1,3-dicyano-2-mercaptoazulene dissolved in THF and (2B) RAIR spectrum of 1,3-dicyano-2-azulenylthiolate adsorbed on Au (111). The images beside each spectrum represent how the molecules orient on the surface upon adsorption via the isocyanide or thiolate junction groups.[1]

Incorporating the nitrile reporters into the 2-mercapto- and 2-isocyanoazulene scaffolds helped to facilitate probing the self-assembly of the corresponding azulenic SAM films.Figure 2.9 shows the IR spectra of **1** and **2** in the solution phase (1a (in $CHCl_3$) and 2a (in THF)) and bound to the gold surface.In the recorded data in Figure 2.9(2), only one band is present in 2a and 2b spectra which is indicative of a cyano stretching frequency ν(N≡CR). The energy of the IR band attributed to ν(N≡CR) in 2a and 2b remains the same since the cyano group environment is unchanged. Therefore, coordination of the molecule to the gold film is via the thiolate-headgroup present within the molecule. But in the case of Figure 2.9(1), two distinct bands attributed to cyano

ν(N≡CR) and isocyanide ν(C≡NR) stretching frequencies are observed in solution FTIR (1a) and RAIR (1b).

In the solution IR (Figure 2.9 (1a)) for molecules in **1**, the band at 2224 cm^{-1} is indicative of a ν(N≡CR) and compared to RAIR in Figure 2.9 (1b), the ν(N≡CR) band occurs at higher wavenumber due to the electron withdrawing ability of the isocyanide on the position 2 of the molecule. Donation of the isocyano carbon lone pair to the gold substrates strengthens the isocyano bond, leading to the blue shift of the isocyanide ν(C≡NR) band by 42 cm^{-1} upon coordination.[1] The isocyanide ν(C≡NR) band at 2114 cm^{-1} corresponding to the uncomplexed isocyanide group in the solution IR spectrum moved to 2156 cm^{-1} upon adsorption of the molecule to the gold surface while the cyano ν(N≡CR) band observed at 2224 cm^{-1} in the solution IR spectrum undergoes a red shift upon SAM formation. The IR data described above suggest that both **1** and **2** are coordinated to the gold surface in an upright orientation. This conclusion is consistent with the ellipsometric thickness measurements obtained for the SAMs of **1** and **2**.[1]

II.6.2.1. Method

The grazing incidence Reflection Absorption Fourier Transform Infrared (RAIR) spectra for the SAMs of 6-cyano-1,3-diethoxycarbonyl-2-isocyanoazulene **(1)**, 2-cyano-6-isocyanoazulene (**2)**, and 2-cyano-4-isocyanoazulene **(3)** on gold were collected using a Thermo Nicolet Nexus 670 FTIR spectrometer with a VeeMax grazing angle accessory set at an angle of 70°. A background spectrum was obtained using a freshly cleaned bare gold substrate before acquiring the spectrum of each sample. The bare gold used for calibration was cleaned using the same cleaning method of SAM preparation. Ten thousand or one thousand scans from 600 to 4000 cm^{-1} at 2 cm^{-1} resolution were obtained for each background/sample combination. The MCT

detector of Thermo Nicolet Nexus 670 was constantly cooled with liquid nitrogen, and the instrument was connected to an air purifying system to purge out CO_2 and H_2O continually.

Solution phase (in $CHCl_3$) FTIR spectra were recorded for samples enclosed in 0.2 mm NaCl cells using Thermo Nicolet Nexus 670 FTIR spectrometer A background spectrum of the $CHCl_3$ solvent was recorded prior to each sample run.

II.6.2.2. Result and Discussion

Freshly prepared **1, 2,** and **3** SAMs were analyzed using RAIR spectroscopy. The spectra suggest that all molecules adsorbed on the Au surface are oriented vertically, particularly for **1** and **2**, and no free (i.e., unbound) molecules are incorporated in the films. Two IR bands are present in the solution IR and in the RAIR spectra of **1**. In the solution IR, the weak band at 2225 cm^{-1} is indicative of a cyano stretching frequency while 2123 cm^{-1} represents the isocyanide stretching frequency on the position 2 of the azulene molecule. After the monolayer formation, one thousand scans of **1** were collected using the RAIR instrument (Figure 2.10 (2b)). The coordination of **1** to the gold substrate resulted in isocyanide ν(C≡NR) blue shift to 2173 cm^{-1} due to the formation of the Au–C bond. The shift of the isocyanide band to a higher energy is indicative of the donation of the isocyanide carbon's lone pair, which is antibonding with respect to the C≡N bond, to the gold film. The cyano on the other hand experiences little or no change from the solution to the RAIR spectrum, therefore, the gold substrates predominantly withdraw electron densities from the isocyano junction group and less conjugation between the π-system of the cyano moiety and the azulene backbone is present. The broadness of the isocyanide ν(C≡NR) band at 2173 cm^{-1} in the RAIR spectrum of **1** may be due to inhomogeneity in the adsorption sites on the gold substrates and it almost buries the weak cyano peak. Although the peak intensity of the cyano band in the RAIR spectrum is small, the peak is observed based on the selection rule. The cyano peak intensity

in both the solution IR and the RAIR is small but the relative peak intensity of the cyano group with respect to the isocyanide group in both the solution IR and the RAIR are similar. The relative peak intensities are similar though the RAIR cyano peak is broader which may be due to inhomogeneity in the gold substrates. However, in a similar analogous system with thiolate junction group as seen in Figure 2.11(b), the RAIR for SAMs of 6-cyano-2-mercaptoazulene shows only one intense peak at 2213 cm^{-1} attributed to the cyano ν(N≡CR) band. As mentioned earlier, the Au–S peak around 400 cm^{-1} is not observable in the IR window available on our spectrophotometer.

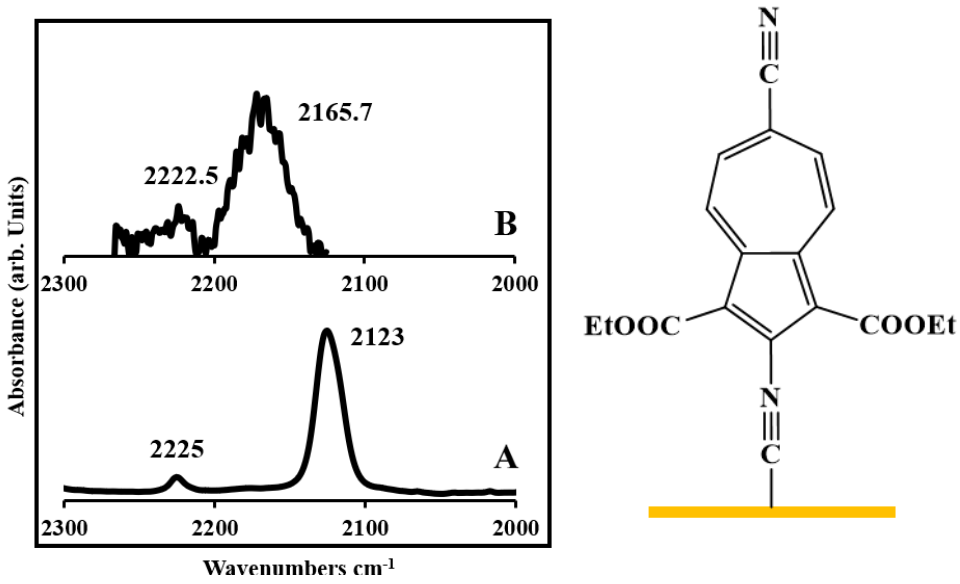

Figure 2.10. Solution IR (A) and RAIR (B) spectra of 1,3-ethoxycarbonyl-6-cyano-2-isocyanoazulene (**1**) and an illustration showing the upright orientation of the molecule coordinated via the isocyanide junction group.

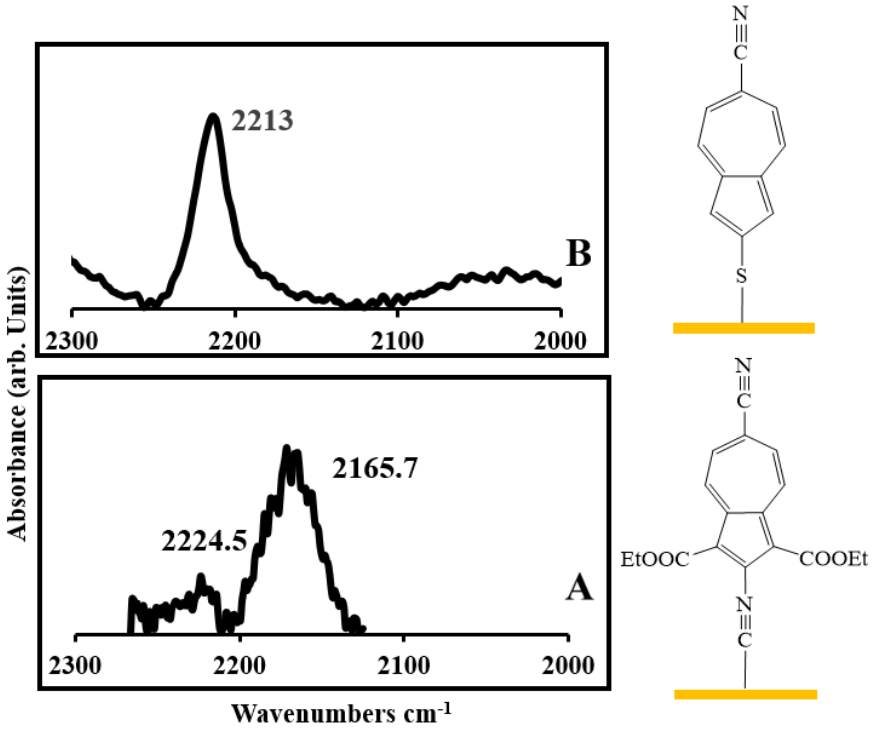

Figure 2.11. RAIR spectra of (A) **1** and (B) 6-cyano-2-azulenylthiolate and the illustrations showing the upright orientation of the molecules coordinated via the isocyanide and thiolate junction groups.

SAMs **2**, an analogue of **1**, featuring the inverse orientation of the attached groups in the molecule with no substitutions at the 1 and 3 positions, were analyzed using the RAIR. One thousand scans were collected for the RAIR spectrum. In the solution IR, two IR bands as seen in Figure 2.12a at 2113 cm^{-1} and 2227 cm^{-1} were observed for the isocyano ν(C≡NR) and cyano ν(N≡CR) stretching vibrations respectively. Both bands experienced shifts in energy upon coordination of **2** to the gold substrates (see Figure 2.12b). The isocyano ν(C≡NR) band shifted to higher energy indicating the donation of the isocyano carbon's lone pair to the gold substrate while the cyano ν(N≡CR) band shifted to lower energy due to the reduction in electron density of the

cyano group exerted by coordination of the isocyano group to the gold substrate. Due to the coordination of the isocyano junction to the gold substrate and conjugation between the π-system of the cyano moiety and the azulene backbone, π-electron density in the cyano group reduces causing a redshift of the band by 4 cm^{-1}. The RAIR result support the ellipsometric thickness of **2** which signifies that a layer is self-assembled in an upright orientation on the gold film. Both the isocyano ν(C≡NR) and cyano ν(N≡CR) band in the RAIR spectrum are broader; this may be due to the inhomogeneity in the adsorption sites on the gold substrates. The result did not signify any oxidization of either the cyano and isocyano groups which would give characteristic stretching band at 2250 cm^{-1} - 2275 cm^{-1}.

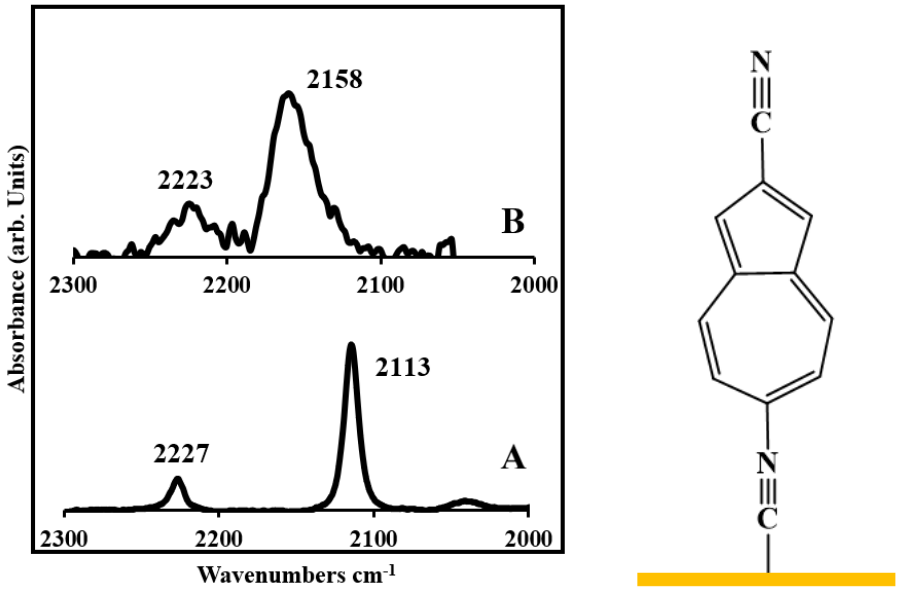

Figure 2.12. Solution IR (A) and RAIR (B) spectra of 2-cyano-6-isocyanoazulene (**2**) and an illustration showing the upright orientation of the molecule coordinated via the isocyanide junction group.

Similarly, in **3**, two major bands for the isocyano ν(C≡NR) and cyano ν(N≡CR) at 2119 cm^{-1} and 2228 cm^{-1} respectively were observed (see Figure 2.13). The shifts of these bands in the RAIR spectrum compated to the solution spectrum of **3** are indicative of the coordination of the molecule to the gold substrate. The coordination of **3** occurs via the isocyanide junction group where the lone pair of the carbon with respect to the C≡N, which is somewhat antibonding, is donated to the gold substrate resulting in the isocyano oscillator shift to 2162 cm^{-1}. Consequently, the cyano ν(N≡CR) band at 2228 cm^{-1} experienced a red shift due to the reduction of the π-electron density on the cyano group. The difference between the solution IR and the RAIR cyano bands is about 7cm^{-1}. Two possibilities are proposed for the weak band seen on the major contributing band at 2221 cm^{-1} for the ν(N≡CR) in the RAIR spectrum. The first possibility is that physisorbed loosely bound molecules intercalated between the SAMs appear in the spectrum. The isocyano ν(C≡NR) band is very broad, which may be due to inhomogeneity of the gold substrate and might lead to the other possibility. The cyano does not form a strong covalent bond with the gold substrate but might weakly interact with the inhomogenous gold substrate. There might be interactions of the cyano group with an adatom or other clusters in the gold surface, therefore, the second possibilty for the peak.

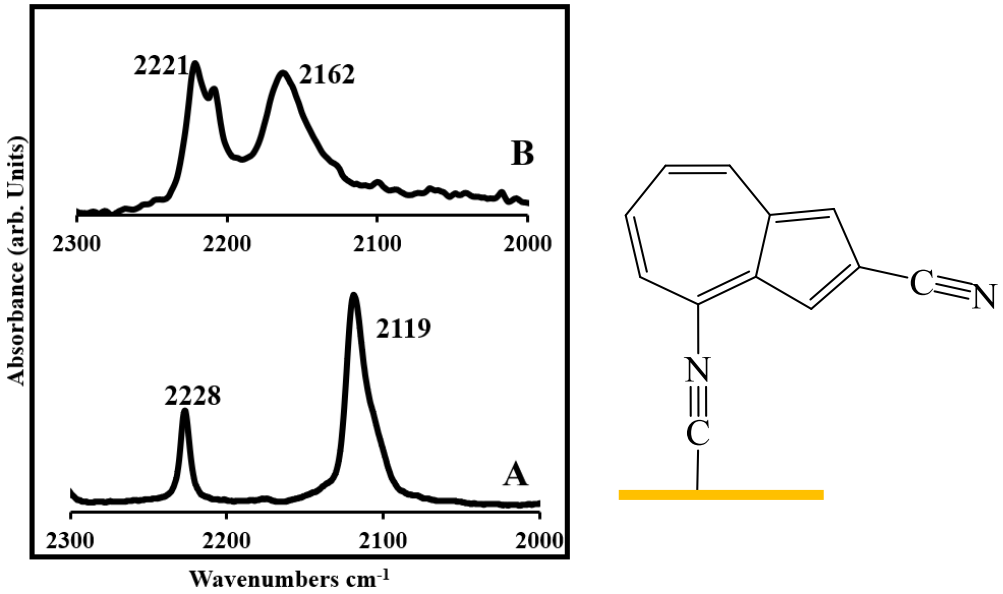

Figure 2.13. Solution IR (A) and RAIR (B) spectra of 2-cyano-4-isocyanoazulene **(3)** and an illustration showing the upright orientation of the molecule coordinated via the isocyanide junction group.

II.7. Conclusions and Outlook

Substituents with distinct IR signatures such as cyano groups provide useful complementary vibrational data to facilitate physicochemical interpretation of azulenic film self-assembly. Self-assembled monolayer SAM of new azulene derivatives featuring cyano-substituted isocyanoazulene adsorbed on Au (111) has been described in this chapter. Ellipsometry ad RAIR were employed in the analyses of the SAMs. The varied isocyano junction group on the azulenic framework significantly controlled the binding orientation of azulene molecules adsorbed on the gold film. The azulene motif in **1** and **2** orients vertically with respect to the gold surface and solely binds to the gold surface via the isocyanide junction group, forming an Au-C bond. The azulene motif in **3** orients almost parallel with respect to the gold surface, binding through the isocyanide group as well. The cyano group has a tendency to weakly interact with the gold surface depending

on its proximity from the surface. The cyano group have a much lower affinity to interact with the gold surface but serve as remote spectroscopic handles. The remote cyano vibrational reporters are sensitive to electronic perturbations exerted by the coordination of the isocyanoazulenic motif to the gold surface.

The use of other remote vibrational reporters that may serve as spectroscopic reporters to facilitate physicochemical interpretation of azulenic SAM films may be useful to expand our tools. The tail end of the azulene SAMs complexed to a zero-valent chromium center of the $Cr(CO)_5$ motif, due to the vibrations from the carbonyl, will serve as a remarkable spectroscopic reporter and may be very interesting due to different possible vibration frequencies present in a C_{4v}-symmetric[(–CN) Cr(CO)5] moiety. This expansion of our system will be discussed in the next chapter. Further investigation of azulenic SAMs using Atomic Force Microscope (AFM) techniques may provide information on the packing geometry, molecular packing, and periodicity of the azulene molecules relative to the gold film. AFM studies will be discussed in detail in chapter V.

II.8. References

1. Neal, B. M.; Vorushilov, A.; Delarosa, A.; Robinson, R.; Berrie, C.; Barybin, M., Ancillary Nitrile Substituents as Convenient IR Spectroscopic Reporters for Self-assembly of Mercapto- and Isocyanoazulenes on Au(111). *Chemical Communications* **2011**, *47*, 10803-10805.
2. Barybin, M. V., Nonbenzenoid Aromatic Isocyanides: New Coordination Building Blocks for Organometallic and Surface Chemistry. *Coordination Chemistry Reviews* **2010**, *254*, 1240-1252.
3. Holovics, T. C.; Robinson, R. E.; Weintrob, E. C.; Toriyama, M.; Lushington, G. H.; Barybin, M. V., The 2,6- Diisocyanoazulene Motif: Synthesis and Efficient Mono- and Heterobimetallic Complexation with Controlled Orientation of the Azulenic Dipole. *Journal of the American Chemical Society* **2006**, *128*, 2300-2309.
4. Dubose, D. L.; Robinson, R. E.; Holovics, T. C.; Moody, D. R.; Weintrob, E. C.; Berrie, C. L.; Barybin, M. V., Interaction of Mono- and Diisocyanoazulenes with Gold Surfaces: First Examples of Self-assembled Monolayer Films Involving Azulenic Scaffolds. *Langmuir : The ACS Journal of Surfaces and Colloids* **2006**, *22*, 4599-4606.
5. Robinson, R.; Holovics, T. C.; Deplazes, S.; Powell, D.; Lushington, G.; Thompson, W.; Barybin, M., Five Possible Isocyanoazulenes and Electron- Rich Complexes Thereof: A Quantitative Organometallic Approach for Probing Electronic Inhomogeneity of the Azulenic Framework. *Organometallics* **2005**, *24*, 2386-2397.
6. Barybin, M.; Chisholm, M.; Dalal, N.; Holovics, T.; Patmore, N.; Robinson, R.; Zipse, D., Long-range Electronic Coupling of MM Quadruple Bonds (M = Mo or W) via a 2,6-Azulenedicarboxylate Bridge. *Journal of the American Chemical Society* **2005**, *127*, 15182-15190.
7. Barybin, M. V., Book Review of Functional Supramolecular Architectures: For Organic Electronics and Nanotechnology, Vols. 1– 2. . *Journal of the American Chemical Society* **2011**, *133*, 8774-8774.
8. M., L.; J., A. R., Modern Surface Organometallic Chemistry. *Wiley-VCH* **2009**, *Weinheim*, 513-556.
9. Dubois, L. H.; Nuzzo, R. G., Synthesis, Structure, and Properties of Model Organic Surfaces. *Annual Review of Physical Chemistry* **1992**, *43*, 437-463.
10. Nuzzo, R. G.; Zegarski, B. R.; Dubois, L. H., Fundamental Studies of the Chemisorption of Organosulfur Compounds on Gold(111). Implications for Molecular Self-assembly on Gold Surfaces. *Journal of the American Chemical Society* **1987**, *109*, 733-740.
11. Neal, B. M.; Vorushilov, A.; Delarosa, A.; Robinson, R.; Berrie, C.; Barybin, M., Ancillary nitrile substituents as convenient IR spectroscopic reporters for self- assembly of mercapto- and isocyanoazulenes on Au(111). *Chemical Communincations* **2011**, *47*, 10803-10805.
12. Attard, G., *Surfaces*. Oxford Science ; New York : Oxford University Press, Oxford ; New York, **1998**.
13. Zharnikov, M., High-Resolution X-Ray Photoelectron Spectroscopy in Studies of Self-Assembled Organic Monolayer. *Journal of Electron Spectroscopy and Related Phenomena* **2010**, *178–179*, 380-393.
14. Van Dyck, C.; Ratner, M. A., Molecular Rectifiers: A New Design Based on Asymmetric Anchoring Moieties. *Nano Letters* **2015**, *15*, 1577-1584.

15. Haruta, M.; Daté, M., Advances in the Catalysis of Au Nanoparticles. *Applied Catalysis A: General* **2001**, *222*, 427-437.
16. Hanke, F.; Björk, J., Structure and Local Reactivity of the Au(111) Surface Reconstruction. *Physical Review B* **2013**, *87*, 235422-235426.
17. Hong, S.; Reifenberger, R.; Tian, W.; Datta, S.; Henderson, J. I.; Kubiak, C. P., Molecular Conductance Spectroscopy of Conjugated, Phenyl- Based Molecules on Au(111): The Effect of End Groups on Molecular Conduction. *Superlattices and Microstructures* **2000**, *28*, 289-303.
18. Rabinovich, D., Advanced Inorganic Chemistry. *Journal of Chemical Education* **2000**, *77*, 311-311.
19. Supplies, S. Flame Annealing Kit. https://www.2spi.com/item/04664-ab/ (accessed 08/13/2014).
20. Maher, T.; Spaeth, A. D.; Neal, B. M.; Berrie, C. L.; Thompson, W.; Day, V.; Barybin, M. V., Linear 6,6 '- Biazulenyl Framework Featuring Isocyanide Termini: Synthesis, Structure, Redox Behavior, Complexation, and Self- Assembly on Au(111). *Journal of the American Chemical Society* **2010**, *132*, 15924-15926.
21. Maher, T. R.; Spaeth, A. D.; Neal, B. M.; Berrie, C. L.; Thompson, W. H.; Day, V. W.; Barybin, M. V., Linear 6,6′-Biazulenyl Framework Featuring Isocyanide Termini: Synthesis, Structure, Redox Behavior, Complexation, and Self-Assembly on Au(111). *Journal of the American Chemical Society* **2010**, *132*, 15924-15926.
22. Treboux, G.; Lapstun, P.; Silverbrook, K., Asymmetric I / V Characteristics in Nonalternant Carbon Networks. *The Journal of Physical Chemistry B* **1998**, *102*, 8978-8980.
23. Schwarz, F.; Koch, M.; Kastlunger, G.; Berke, H.; Stadler, R.; Venkatesan, K.; Loertscher, E., Charge Transport and Conductance Switching of Redox- active Azulene Derivatives. *Angewandte Chemie International Edition* **2016**, *55*, 11781-11786.
24. Applegate, J. C.; Okeowo, M. K.; Erickson, N. R.; Neal, B. M.; Berrie, C. L.; Gerasimchuk, N. N.; Barybin, M. V., First π-Linker Featuring Mercapto and Isocyano Anchoring Groups within the same Molecule: Synthesis, Heterobimetallic Complexation and Self-assembly on Au(111). *Chemical Science* **2016**, *7*, 1422-1429.
25. Alberding, B.; Barybin, M.; Chisholm, M.; Gustafson, T.; Reed, C. R.; Robinson, R.; Patmore, N.; Singh, N.; Turro, C., Molecular, Electronic Structure and Spectroscopic Properties of MM Quadruply Bonded Units Supported by Trans- 6- carboethoxy- 2- carboxylatoazulene Ligands. *Dalton Transactions* **2010**, *39*, 1979-1984.
26. Neal, B. Self-assembly of Azulenic Monolayer Films on Metallic Gold Surfaces. Dissertation Abstracts International, University of Kansas, ProQuest Dissertations Publishing, **2012**.
27. Wächter, T.; Scheetz, K. J.; Spaeth, A. D.; Barybin, M. V.; Zharnikov, M., Dynamics of Electron Transfer in Azulene- Based Self-Assembled Monolayers. *The Journal of Physical Chemistry C* **2017**, *121*, 13777-13785.
28. Meyerbröker, N.; Zharnikov, M., Modification of Nitrile-Terminated Biphenylthiol Self-Assembled Monolayers by Electron Irradiation and Related Applications. *Langmuir* **2012**, *28*, 9583-9592.
29. Frey, S.; Shaporenko, A.; Zharnikov, M.; Harder, P.; Allara, D. L., Self-assembled Monolayers of Nitrile-functionalized Alkanethiols on Gold and Silver Substrates. *Journal of Physical Chemistry B* **2003**, *107*, 7716-7725.
30. Ballav, N.; Schupbach, B.; Neppl, S.; Feulner, P.; Terfort, A.; Zharnikov, M., Biphenylnitrile-Based Self-Assembled Monolayers on Au(111): Spectroscopic Characterization

and Resonant Excitation of the Nitrile Tail Group. *The Journal of Physical Chemistry C* **2010**, *114*, 12719-12727.
31. Fujiwara, H., *Spectroscopic Ellipsometry : Principles and Applications*. Chichester, England ; Hoboken, NJ : John Wiley & Sons, Chichester, England ; Hoboken, NJ, **2007**; 369.
32. Tompkins, H. G.; McGahan, W. A., *Spectroscopic Ellipsometry and Reflectometry : A User's Guide*. New York : Wiley, New York, **1999**.
33. Vickerman, J. C.; Vickerman, J. C., *Surface Analysis : The Principal Techniques*. Chichester England ; New York : John Wiley, Chichester [England] ; New York, **1997**; 457.
34. Automatic Refractometer: Rudolph Research Analytical. *Laboratory Equipment* **2003**, *39*, 87.
35. Wasserman, S. R.; Whitesides, G. M.; Tidswell, I. M.; Ocko, B. M.; Pershan, P. S.; Axe, J. D., The Structure of Self-Assembled Monolayers of Alkylsiloxanes on Silicon: A Comparison of Results from Ellipsometry and Low-Angle X-Ray Reflectivity. *Journal of the American Chemical Society* **1989**, *111*, 5852-5861.
36. Le Grange, J. D.; Markham, J. L.; Kurkjian, C. R., Effects of Surface Hydration on the Deposition of Silane Monolayers on Silica. *Langmuir* **1993**, *9*, 1749-1753.
37. Clear, S. C.; Nealey, P. F., Lateral Force Microscopy Study of the Frictional Behavior of Self-Assembled Monolayers of Octadecyltrichlorosilane on Silicon/Silicon Dioxide Immersed in n-Alcohols. *Langmuir* **2001**, *17*, 720-732.
38. Soriaga, M. P., *Thin Films : Preparation, Characterization, Applications*. New York : Kluwer Academic/Plenum Publishers, New York, **2002**; 367.
39. Querebillo, C. J.; Terfort, A.; Allara, D. L.; Zharnikov, M., Static Conductance of Nitrile-Substituted Oligophenylene and Oligo(phenylene ethynylene) Self-Assembled Monolayers Studied by the Mercury-Drop Method. *The Journal of Physical Chemistry C* **2013**, *117*, 25556-25561.
40. Kao, P.; Neppl, S.; Feulner, P.; Allara, D. L.; Zharnikov, M., Charge Transfer Time in Alkanethiolate Self-Assembled Mono layers via Resonant Auger Electron Spectroscopy. *The Journal of Physical Chemistry C* **2010**, *114*, 13766-13773.
41. Chockalingam, M.; Darwish, N.; Le Saux, G.; Gooding, J., Importance of the Indium Tin Oxide Substrate on the Quality of Self- Assembled Monolayers Formed from Organophosphonic Acids. *Langmuir* **2011**, *27*, 2545-2552.

Chapter III:

SAMs of azulene scaffolds featuring mercapto and isocyano anchoring groups within the same molecule adsorbed on Au (111) substrates

Portions of this work have been published in:

Applegate, J. C.; Okeowo, M. K.; Erickson, N. R.; Neal, B. M.; Berrie, C. L.; Gerasimchuk, N. N.; Barybin, M. V., First π- linker featuring mercapto and isocyano anchoring groups within the same molecule: synthesis, heterobimetallic complexation and self-assembly on Au(111). *Chem. Sci.* **2016,** *7* (2), 1422-1429.

III.1. Linear azulenic linker asymmetrically anchored using isocyano and mercapto junction groups, a new paradigm for molecular rectification

Isocyanide and thiolate anchoring groups are commonly employed in molecular self-assembly on metal surfaces. This chapter focuses on the surface chemistry of linear azulenic linkers equipped with an isocyano (-N≡C) junction group at one terminus, and a mercapto (-SH) junction group at the other end, compared to the symmetric analogue where only isocyanide junction groups are attached to both ends of the azulenic bridge. In each case, the isocyano terminus is complexed to the zero-valent chromium center of the $Cr(CO)_5$ motif; whereas, the mercapto terminus serves to form the thiolate-gold junction upon self-assembly of the resulting organochromium scaffold on the Au(111) surface. Characterization of the above azulenic monolayer films using Reflection-Absorption Infrared (RAIR) spectroscopy and optical ellipsometry will be discussed in detail. The C_{4v}-symmetric[(–CN)$Cr(CO)_5$] moiety provided highly informative ν(C≡N) and ν(C≡O) infrared signatures indicating right-side up molecular orientation and "hollow-linear" coordination mode of the 2-isocyano-6-azulenylthiolate platform self-assembled on metallic gold. This chapter describes the design, formation, properties, and stability of self-assembled monolayers of isocyanoazulenylthiolate derivatives linearly terminated with the junction units, for molecular conductivity and, possibly, rectification applications.

III.2. Introduction

An area of considerable research interest is molecular electronics. In molecular electronic devices, charge transfer can be studied in terms of electron hopping or tunneling when a molecule is connected to electrodes at both ends, as depicted in Figure 3.1 below. Molecular rectifiers, molecular wires, molecular switches, and molecular transistors are types of molecular electronics components.[1] Molecular rectification, as proposed by Aviram and Ratner, can be exerted by a single donor-bridge-acceptor (DBA) molecule with a σ-sigma decoupling bridge.[1] The bridge is

known to induce high barriers during tunneling which significantly affect the electron transfer rate. More recently, π-conjugated molecules have been used to replace the bridge thereby leading to higher molecular conductance.[2-5] Azulene, due to its inherent dipole along the molecular axis that arises from charge separation between the electron-poor 7-membered ring and the electron rich 5-membered ring, may be viewed as a "molecular diode" and, therefore, is an appealing building block in the design of molecular electronics devices.[6-11, 12-14, 15]

The azulenic scaffold can be derivatized to enhance its dipole moment, which may lead to improved rectification depending on the nature of the junction groups and the positions of their attachment. One can study how the electronic property of the azulenic framework changes when electron donating or withdrawing substituent groups are aligned along the azulenic molecular axis. As previously mentioned, EWG and EDG are known to influence the energies of the frontier molecular orbitals of azulene by independently raising or lowering either the HOMO or LUMO energy when substituted at the odd or even positions, respectively. [6-11]

The use of donor-acceptor terminated molecular linkers to facilitate connection of the molecule to the metal and provide stable junctions is an important design feature to conductivity. The proposed method of rectification was improved to result in a D-π-A molecule, linked to a conductive metal.[1-5] Figure 3.1 describes the molecular electronic assembly connected to two electrodes at both ends through head and terminal groups. The measure of the conductivity along the π-conjugated linker may give insight into tunneling across the film. Mercapto (–SH) and isocyano (–NC) substituents are among particularly popular anchoring groups in coordination and surface chemistry for being known to provide stable junctions at metal/organic interfaces.[16-17] Literature shows that theoretical and experimental studies of isocyanides and mercaptans, as stable molecular electronic junctions, have been achieved.[18-34] Consequently, several symmetrically

junctioned dimercapto or diisocyano derivatives have been studied on gold substrates to probe their electron transport behavior.[29-34] Yet, there have been almost no studies of both isocyano and mercapto junction groups within the same molecule due to synthetic challenges.[35]

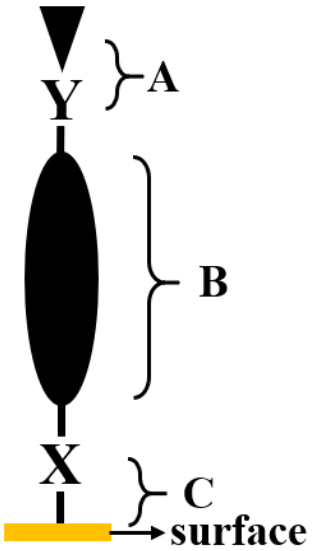

Figure 3.1. A scheme illustrating a conductive probe in molecular electronics through X and Y electrodes. The conductivity could be limited by charge transport from the probe tip and the Y electrode labeled as A, via the molecular linker labeled as B, or the X electrode and the surface labeled as C.

A recent theoretical study by Ratner *et al.* in 2015 concluded that asymmetrically junctioned π-linkers are attractive candidates for improving molecular rectification.[36] The design of potentially efficient molecular rectifiers involved two π-conjugated units asymmetrically anchored to metallic electrodes and separated by a saturated $(-CH_2-)_n$ decoupling bridge.[36] Their intriguing theoretical study suggested mercapto and cyano (–CN) junctions for accommodating the asymmetric anchoring on the premises that the –SH and –CN termini would facilitate

alignments of a linker's HOMO (Highest Occupied Molecular Orbital) and LUMO (Lowest Unoccupied Molecular Orbital), respectively, through Fermi level pinning.[36] However, from an experimental standpoint, the model presents severe drawbacks since the π-decoupling unit would significanlty dampen the extent of conductivity.

Very few organic linkers with asymmetrical junctioning have been experimentally studied [19] in the quest for efficient organoelectronic materials. More specifically, SAMs of species containing both free mercapto and isocyano functionalities in the same molecule are presently unknown, and such systems constitute a formidable synthetic challenge. In 2009, Yu *et al*. described a molecule terminated with free isocyanide on one end and a thiol protected with a bulky group on the other, as shown in Figure 3.2 (right), with the goal of exerting molecular rectification behavior. A mixed monolayer system was formed with dodecanethiolate as a matrix and the *I/V* curve of the substrate was studied using STM.[35] The monolayer formation involved anchoring the isocyanide terminus to the gold surface. The *I/V* curve for the molecular film involving isocyano anchored linker showed opposite rectification with a meager rectifying ratio of 1.9 when compared to the rectification ratio of 7.4 documented for the analoguous system featuring the thiolate anchoring group (Figure 3.2, left).[35] The observed reverse rectification was caused by differences in the induced bond dipole at the surface for the otherwise similar molecules. The thiolate anchoring group supported higher rectification while the isocyano anchoring group in their studies had very low rectification.

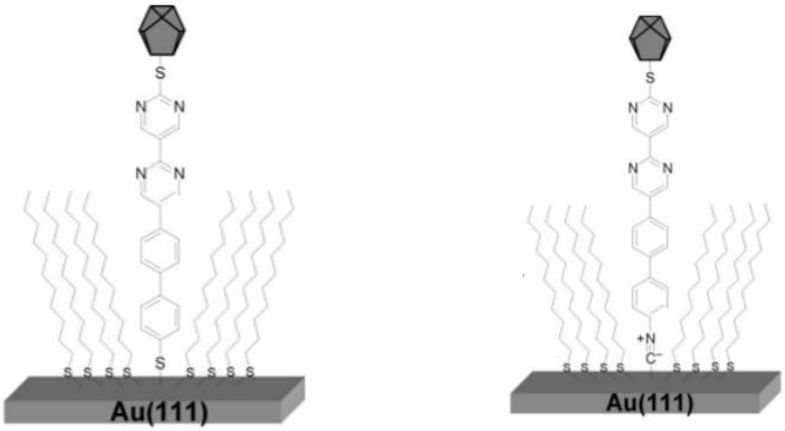

Figure 3.2. Illustration of molecules assembled on Au (111) for exerting molecular diode behavior. Reprinted with permission from Ref. 35. Copyright (2009) American Chemical Society.

More recently, a 2017 publication with our collaborator, Michael Zharnikov, featured azulene terminated with cyano and thiolate groups for potential conductance and maybe rectification purposes.[12] Importantly, only the thiolate group can act as a junction unit in this design due to the fact that the cyano group has a very low affinity for binding to the gold substrate.[37] Their goal for the study was to discern the dynamics of electron transfer along azulenic molecular axis. Figure 3.3 shows the assembled molecule on the gold substrate with cyano group attached as the terminal substituent and thiol as the head group. The SAMs of this system on gold films were analyzed using near-edge X-ray photoelectron spectroscopy (NEXAFS) and high resonant XPS. The SAMs were reported to orient upright with respect to the gold film with tilt and twists to the gold surfaces.[12] The electron dynamics of the framework were studied using Auger electron spectroscopy. From the NEXAFS result, two well-defined resonances were observed.[12] This

observed resonance is due to conjugation of the π* orbitals of the seven membered-ring of azulene and the cyano unit, hence the splitting of the degenerate π(C≡N*) orbital, leading to the two observed resonances at different energies (that is π_1* and π_3*). The π_3*, solely localized in the cyano group, and the π_1*, delocalized across the seven membered ring and the cyano group, were used for studying resonant excitation during the Auger spectroscopy analysis.[12] The strongly conjugated orbital (π_1*) between the cyano and the azulenic framework, showed electron transfer time of *ca.* 22 fs while the localized orbital on the cyano group (π_3*) showed *ca.* 120 fs.[12] Importantly, it was observed that the electron transfer pathway across the azulene backbone to the gold substrate showed that the nitrile groups were electronically perturbed when the azulene molecule was coordinated to the gold substrate. Therefore, both the molecular backbone length and strong conjugations play a vital role in controlling the dynamics of electron transfer.

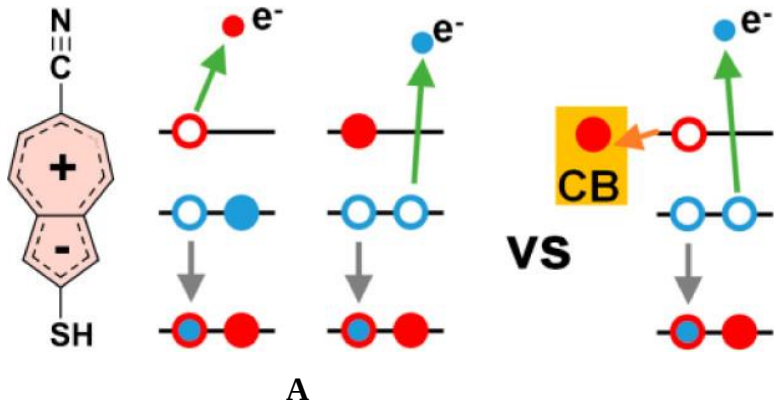

Figure 3.3. Dynamics of electron transfer in 2-mercapto-6-cyanoazulene assembled on Au (111) using Auger electron spectroscopy.[12] An illustration of core de-excitation routes for the nitrile group in NC-AzuS/Au upon the resonant excitation. The red and blue colors represent electron and hole, respectively. The excitation by A) or B) **Vs** CB (conduction band of the substrate) is close and electron transfer may occur. Reprinted with permission from Ref. 12. Copyright (2017) American Chemical Society.

III.3. Molecular orientation, packing, and conductance

Understanding molecular packing, orientation and conductivity of SAM films are essential for their use in electronic applications. Some of the established methods in interpreting SAM packing, orientation, and charge transport properties are ellipsometry, infrared reflection spectra, SERS, XPS, conductive probe atomic force microscopy (AFM), and scanning tunneling microscopy (STM). The head group used as a junction between the conductive substrate and the SAM influences packing, orientation, and charge transport behavior of the SAMs. This section summarizes recent advances primarily focused on thiol and isocyanide head groups used in SAM formation relevant to potential applications in molecular electronics. The molecular conductance, assessed using a variety of techniques involving these head groups, is discussed as well.

Molecular packing and orientation of SAMs have been studied by many researchers mainly focusing on their head groups and influences on the film formation and physicochemical characteristics.[38-39] Although the intermolecular interaction between the molecules influences the packing of the SAMs, the junction group (head group) plays a crucial role in the packing and orientation of the SAMs. Several head groups have been studied in SAMs, but the isocyano and thiolate head groups are the most studied using different techniques.[40-48] Density functional theory (DFT) analyses have been used to describe the packing of some SAMs on gold substrates. The dominant, or most energetically favored, packing geometry of organothiolate SAMs on gold films is characterized by the $(\sqrt{3}$ Å x $\sqrt{3}$ Å) rotated 30 ° from the gold.[10, 39, 48-49] Also, the tail groups are known to influence molecular packing in SAM films. STM studies by Christopher B. Gorman *et al.* focused on SAMs containing tail groups of alkene, cyano, and carboxylic acid- terminated organothiol SAMs.[49] A hexagonal ($\sqrt{3}$ x $\sqrt{3}$)R30 lattice with a spacing of 5 Å and a c(4 x 2)

superlattice was observed for alkene-terminated SAMs.[49] The ($\sqrt{3}$ x $\sqrt{3}$)R30 has been reported in alkanethiol by many researchers.[10, 39, 48-49] The carboxylic acid-terminated and cyano-terminated SAMs were indistinguishable and formed complicated zigzag head-to-tail geometries that lay flat, and do not form well-packed monolayers. This was due to strong dipole-dipole repulsion in the tail groups. In aromatic ring SAMs on gold, the π-π interaction may influence molecular packing in SAMS. Diisocyanoarene assembled on gold film reported in a 2008 article had ($2\sqrt{3}$ Å x $\sqrt{3}$ Å) herringbone pattern and densely packed SAMs were observed due to intermolecular attraction.[50] In an attempt to probe the charge transport of the diisocyanoarene assembled on gold film, theoretical calculations on spatial distribution of induced charge density was done. Their observations showed that the induced charge density decays from the molecule-surface interface in an oscillating mode.[50]

Conduction mechanisms and charge transports in SAMs have been investigated by many researchers for straight alkyl chains and in conjugated systems. Tunneling and hopping are the two mechanisms that have been considered. While non-resonant tunneling occurs in monolayers containing alkyl chains, resonant tunneling has been seen to happen in conjugated systems due to relatively small HOMO-LUMO gaps.[51] The STM measurements reported by Mallick Govind *et al.* showed that the tunneling currents in conjugated molecules were approximately three orders of magnitude higher than those in straight alkyl chains of hexadecanethiol and octadecanethiols.[51] This implies that the nature of molecular backbone affects electron transport. Some researchers have reported that the length of the molecular backbone affects the conductivity of the SAMs.[3, 51-53] Another vital property for high conductivity is the alignment of the Fermi level of the gold electrodes with the frontier molecular orbitals of the linker. Studies by many researchers indicate that the nature of anchoring groups may induce dipole at the interface and internal polarization

within the molecule that is essential in the alignment of the Fermi energy level of the gold electrode with the orbitals of the linker.[35, 54] The measured I/V curve by Yu *et al*. showed that the Fermi level of the gold electrode increased or decreased when an anchoring group formed a covalent bond with the gold substrate and that this alignment made electron tunneling through the LUMO or HOMO feasible.[35] Different anchoring groups, which include thiolates, isocyanides, nitriles, carboxylates, amines, pyridines, and phosphoric acids have been reported. Thiols and isocyanides are the most studied of these anchoring groups.

Kubiak *et al.* investigated four families of conjugated molecules with isocyano and thiol junction groups on a gold substrate using RAIR, STM, SERS, optical ellipsometry, and contact angle measurements.[48] They compared the Fermi energy level to the HOMO energies of the corresponding SAMs made on the gold substrates. They discovered that SAMs made using isocyanide junction groups have larger conductance gap than the analogous SAMs with the thiolate end groups.[48] In the thiolate and dithiolate systems, the Fermi energy level was closer to the HOMO energy level. As the number of phenyl rings increased, the Fermi-HOMO energy difference lessened. In contrast, the opposite trend was observed in the isocyanide and diisocyanide systems.[48] Therefore, careful interpretation of data is important, and the results may differ depending on the terminal groups present in the SAMs.[48] The isocyanide showed an opposing trend due to the electronic property of the isocyanide junction group. The increased π-conjugation between the isocyanide and phenyl rings affected the conductivity of the SAMs. Therefore, increasing the number of the phenyl rings resulted in increased π-conjugation resulting in increased Fermi-HOMO energy. This is consistent with the bathochromic shifts of the stretching frequency of isocyanide from the solution IR to the RAIR after SAM formation.[48]

In work done by Kiguchi *et al.*, conductive properties of single molecule bridges of phenyldithiol, phenyldicyanides, and phenyldiisocyanides were compared with a focus on the effect of the anchoring groups on electron transport.[55] Electrical conductance of these molecules was determined using STM in the study of the tunneling in these films. The conductance was measured by applying a bias between the tip and the substrates. The authors' investigation showed that the dicyano SAMs had little or no conductance which may be attributed to the junction group forming unstable SAMs.[55] No conductance for the dicyano was reported in the article. On the other hand, the dithiolate and diisocyano junction groups gave comparable conductance range based on experimental and theoretical calculations. They concluded that bond strengths played a crucial role in conductivity. The thiolate formed a strong Au-S bond with the gold substrate leading to stable interactions of the metal and molecular orbitals that is essential for high conductance. Though their calculations demonstrated that the Au-CN bond has similar energy difference between the Fermi level and conductance orbitals to that of the Au-S, the bond strengths are significantly different with Au-S being stronger by almost a factor of two .[55] Even though they claimed that the Au-Au bond strength is higher than the Au-NC, but lower than the Au-CN and Au-S bonds, no measured conductance was reported for the monolayer formed from the dicyano analogue.

Head groups, like thiolate and isocyanide, will be useful in designing SAMs with the purpose of molecular conductance in organo-electronics. Moreover, electron donating and withdrawing anchoring groups have been reported to have ability in exerting molecular rectification.[36] The design and investigation of a diode-like molecule, azulene, featuring a thiol and an isocyano anchoring groups is discussed herein. Perhaps, the symmetric analogue of this system, with diisocyano anchoring groups, reported in Barybin *et al.* 2006 Langmuir paper will be a suitable candidate for comparison to this new 2-isocyano-6-azulenylthiolate platform self

assembled on Au (111). Reported in this chapter is SAM formation of the non-alternant fully aromatic scaffold of azulene substituted at the 2,6- positions with isocyanide and thiol groups, respectively. The design presents the first example, to the best of the author's knowledge, of a π-linker equipped with uncomplexed mercapto *and* complexed isocyano anchoring groups.[13] The SAM described herein may be useful in designing and constructing molecular-scale equivalents of solid-state conductors.

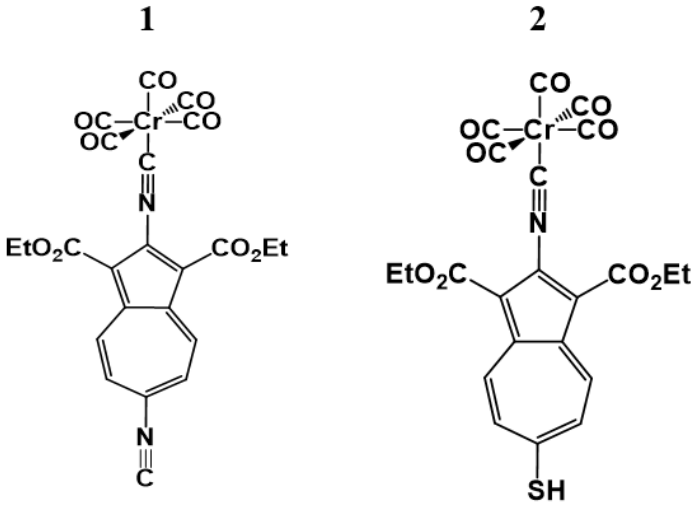

Figure 3.4. Azulene molecules **1** and **2** used in SAM formation.

III.4. Experimental section

III.4.1. General procedures and starting materials

The complexed azulene derivatives in Figure 3.4 used in this study were synthesized by varous Barybin researchers. The synthesis of **1** may be found in Dubose, D. L.; Robinson, R. E.; Holovics, T. C.; Moody, D. R.; Weintrob, E. C.; Berrie, C. L.; Barybin, M. V., Interaction of Mono- and Diisocyanoazulenes with Gold Surfaces: First Examples of Self-assembled Monolayer

Films Involving Azulenic Scaffolds. *Langmuir* **2006**, *22*, 4599-4606. The synthesis of **2** may be found in Applegate, J. C.; Okeowo, M. K.; Erickson, N. R.; Neal, B. M.; Berrie, C. L.; Gerasimchuk, N. N.; Barybin, M. V., First π-Linker Featuring Mercapto and Isocyano Anchoring Groups within the same Molecule: Synthesis, Heterobimetallic Complexation and Self-assembly on Au (111). *Chemical Science* **2016**, *7*, 1422-1429.

Throughout this experiment, commercially available gold-coated silicon substrates, purchased from Platypus Technologies, featuring grains with Au (111) terraces made via deposition, were employed. The silicon wafers used had been first coated with 5 nm Titanium adhesion layer before *ca.* 1000 Å of gold was deposited on the substrates.

Unless specified otherwise, all substrates were soaked in chloroform ($CHCl_3$), acetone, and 200-proof ethanol for two hours in each solvent for cleaning purposes. All solvents were purchased from commercial sources and used as received unless further solvent distillation was performed. Chloroform was distilled over P_2O_5. Dichloromethane was distilled over CaH_2. Following the purification, the distilled solvents were stored under argon. The substrates were thoroughly rinsed again with 200-proof ethanol to remove any physisorbed materials left after the cleaning the substrates and blow-dried with N_2 gas. The ellipsometric physical constants of the cleaned substrates were measured before immersing substrates in solutions of the azulenic compounds to make the SAM-coated substrates.

The ellipsometric physical constants *n and k* values for each sample of the gold substrates were measured at a minimum of five different spots using Rudolph research/Auto EL III fixed wavelength ellipsometer. A cleaned bare silicon wafer was used to calibrate the ellipsometer before collecting the *n and k* values. The bare silicon wafer was cleaned as described in chapter II with 50:50 ethyl ether and methanol followed by drying with a nitrogen stream.[56] The ellipsometer

employed a HeNe laser with a fixed wavelength of 632.8 nm and an incident angle of 70 ° to the surface normal was used for all the measurements. The physical constant, incident angle, and refractive index aided in determining the experimental thicknesses of the SAM-coated substrates. The refractive index of 1.45 was assumed[57-59] for all organic thin films described herein. For each film, the thickness value, including the corresponding standard deviation, was reported. The reported value constitutes an average measurement derived from a minimum of five different spots on the SAMs-coated substrates.

The grazing incidence Reflection Absorption Infra-Red (RAIR) spectra for the SAM-coated substrates were collected with a Thermo Nicolet Nexus 670 FTIR spectrophotometer that has a VeeMax grazing angle accessory set at 70°. The FTIR spectrophotometer is attached to a Kaeser air purifying system to continuously dry the air and reduce CO_2 and H_2O in the background spectrum. The detector employed in the FTIR spectrophotometer is an MCT detector, continuously cooled with liquid nitrogen. Background spectra were collected using a freshly cleaned bare gold substrate before acquisition of any spectra for each sample. Ten thousand scans from 600 cm^{-1} to 4000 cm^{-1} at a resolution of 4 cm^{-1} were employed for each background/sample combination. Automated background subtraction from the spectrum was done for all the samples.

III.4.1.1. SAM formation of a 2,6-diisocyano azulene capped with a $Cr(CO)_5$ complex unit at the 2-isocyano terminal (1) on a gold film

SAM films of **1** were prepared following a procedure similar to that previously described by Barybin, M. V. *et al.*[10] Before use, approximately 1 × 1 cm^2 gold substrates were cleaned with hot Piranha solution (**Warning**: extreme care should be used when handling Piranha solution due to violent reaction of the oxidant with organic substances). The substrates were rinsed with large volumes of Millipore water and dried with nitrogen gas. Further cleaning was done by

sequential soaking of substrates in chloroform, acetone, and 200- proof ethanol for two hours in each solvent. The substrates were rinsed with ethanol and dried with nitrogen gas before the ellipsometric physical constants, *n and k*, were measured. The films were then immersed in a 2 mM solution of **1** in distilled $CHCl_3$ for *ca.* 24 hours. SAM-coated substrates were thoroughly rinsed with distilled chloroform to remove unbound physisorbed molecules and blow-dried in a flow of N_2 gas before carrying out any analysis. No precaution to exclude air or ambient laboratory lighting was exercised in the SAM experiments.

Surface IR (RAIR) and ellipsometry analyses were measured on SAM-coated film of **1**. The RAIR spectra were collected as described in the general procedures and starting materials section, 10 000 scans were collected for three SAM-coated films at 4 cm^{-1} resolution. The ellipsometric thicknesses of the SAM-coated films of **1** were obtained at five different spots using the average optical constants *n = 0.143 (0.001) and k = 3.465 (0.004)* while assuming a refractive index of 1.45 for the organic thin films.

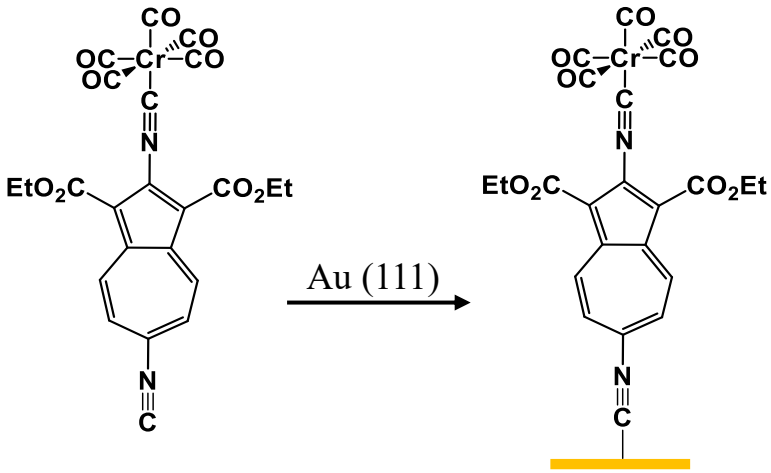

Figure 3.5. Illustration showing how molecules of **1** are self-assembled on the gold substrate via anchoring through the isocyanide junction in an upright orientation.

III.4.1.2. SAM formation of 2-isocyano-6-mercaptoazulene capped with a $Cr(CO)_5$ complex unit at the 2-isocyano terminal (2) on gold film

SAM films of **2** were prepared on the Au (111) surface using commercial gold-coated silicon substrates. The bare gold substrates were cleaned, as described in the general procedures and starting material section, using distilled chloroform, acetone, and 200- proof ethanol for two hours in each solvent before SAM films were made. The bare gold substrates were thoroughly dried under a stream of N_2 gas and their ellipsometric physical constants (*n and k*) values were measured at five different spots. SAM films of the compound were formed by placing the freshly cleaned gold substrate into a 2 mM solution of **2** in $CHCl_3$ for *ca.* 24 hrs. Prior to their analysis, the SAM-coated substrates were rinsed thoroughly with $CHCl_3$ and dried in a flow of N_2 gas. No precautions to exclude air or ambient laboratory lighting were exercised during these SAM experiments.

Surface IR (RAIR) and ellipsometry for the SAM-coated films of **2** were measured. The RAIR analyses were done following the general procedures and starting materials section. A background spectrum was collected using a freshly cleaned bare gold substrate before acquiring the spectrum of each sample. One thousand scans from 600 to 4000 cm^{-1} for three samples at a resolution of 4 cm^{-1} were obtained for each background/sample combination. The ellipsometric thicknesses were measured at five different spots using the average optical constants *n = 0.146 (0.001) and k = 3.532 (0.002)* while assuming a refractive index of 1.45 for the organic thin films.

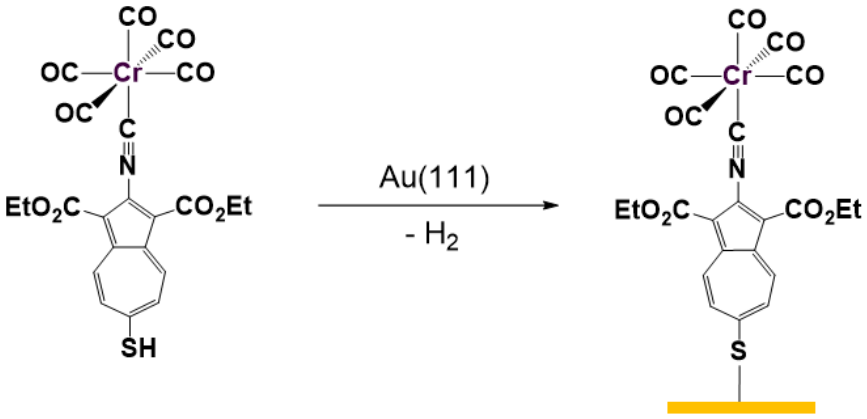

Figure 3.6. Illustration showing how molecules of **2** are self-assembled on the gold substrate via anchoring through the thiolate junction in an upright orientation.

III.4.1.3. Experimental procedures pertinent to SAM displacement investigations

Adsorption competition studies were conducted to compare the relative affinities of **1** and **2** to Au (111) substrates. The SAMs of **1** on Au (111) was formed as described earlier in this chapter and characterized using both ellipsometry and RAIR spectroscopy to affirm the monolayer formation. The preform SAM-coated substrates of **1** were immersed in a 2 mM $CHCl_3$ solution of **2** for *ca.* 24 hours. The resulting films were thoroughly rinsed using $CHCl_3$ and blow-dried in a flow of N_2 before being subjected to ellipsometric and RAIR spectroscopic analyses.

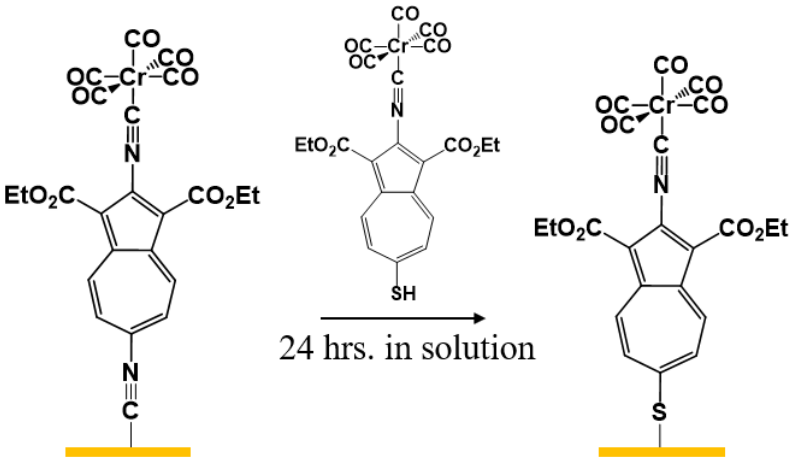

Figure 3.7. An illustration of the competitive SAM displacement experiment.

III.5. Results and Discussion

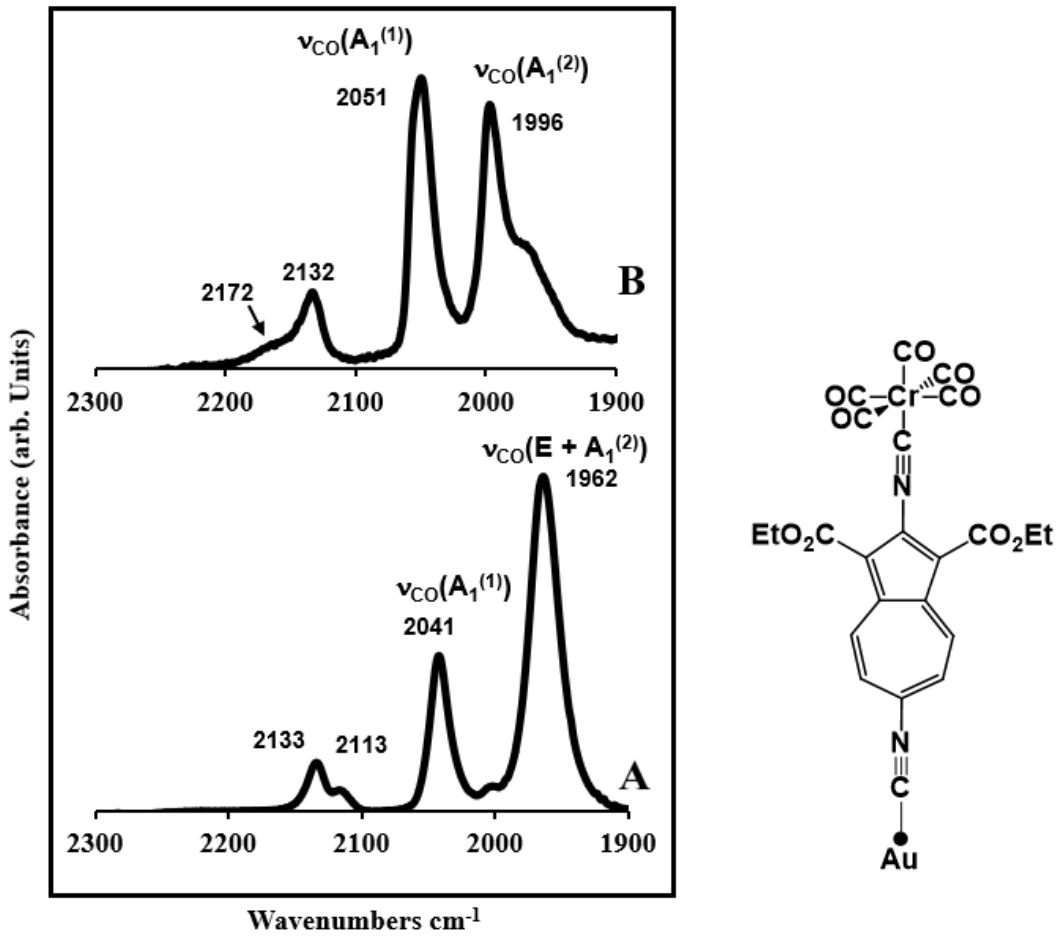

Figure 3.8. (A) FTIR spectrum of a solution of **1** in distilled $CHCl_3$. (B) RAIR spectrum of **1** adsorbed on Au (111) film. (C) Illustration of the upright coordination mode of **1** adsorbed on Au (111) via the isocyanide junction group.

The solution FTIR spectrum before SAM formation and the Reflection-Absorption Infra-Red (RAIR) spectrum after the monolayer formation for (**1**) are presented in Figure 3.8. In the solution IR spectrum of **1** (Figure 3.8a), there should be five IR-active bands in the ν(CO) and ν(CN) stretching regions although only four distinct bands are observed in the spectrum. The two

bands occuring at 2113 cm^{-1} and 2133 cm^{-1} in the spectrum are indicative of the uncomplexed isocyanide group and the Cr-bound isocyanide group, respectively. There should be three bands arising from the vibrations of the carbonyl ligands attached to the Cr^0 center: two symmetric vibrations of A_1 symmetry and a degenerate vibration of E symmetry. Note that only two IR peaks corresponding to these expected three ν(CO) vibrational modes are seen in the spectrum because the E band overlaps with one of the A_1 bands. Based on the literature precedent[60] and the DFT calculations done in our group by Nate Erickson, the C_{4v}-symmetry of the complex $[Cr(CO)_5CNR]$ should give rise to four ν(CO) stretching modes: two of A_1 symmetry, as well as B_1, and E bands as illustrated in Figure 3.9. The B_1 ν(CO) vibration is IR-forbidden while the A and E ν(CO) modes are IR-active. Therefore, the first and second A_1 bands labeled as $A_1^{(1)}$ and $A_1^{(2)}$ in the solution IR spectrum of **1** shown in Figure 3.8 occur at 2041 cm^{-1} and 1962 cm^{-1}, respectively.

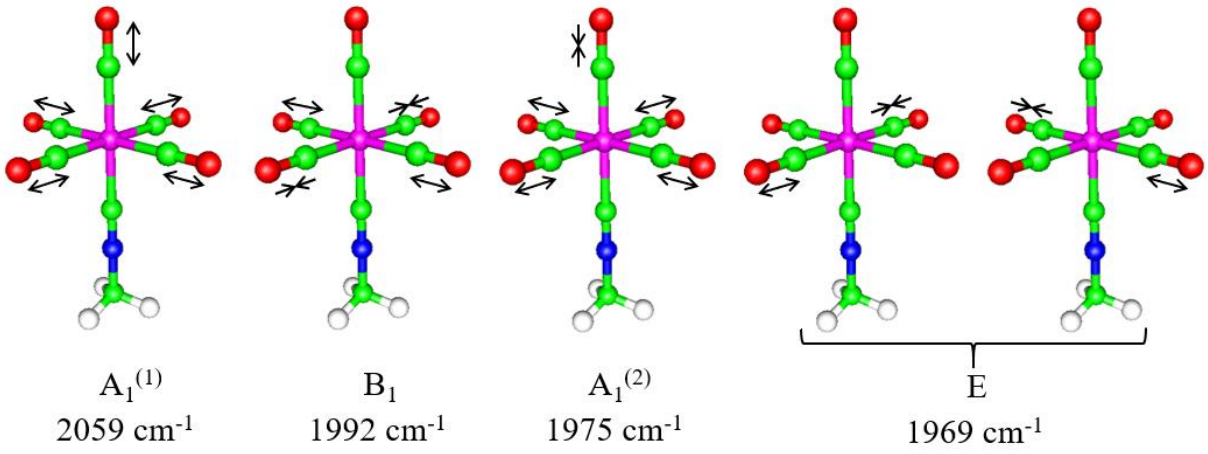

Figure 3.9. DFT-calculated ν(CO) vibrational profile for $(MeNC)Cr(CO)_5$ in the gas phase. [13, 60]

Upon preparation of the SAM of **1**, its RAIR spectrum was recorded. The RAIR spectrum of **1** adsorbed on Au(111) features four IR bands. Based on the selection rules of the RAIR spectroscopy, only vibrations that have a non-zero component perpendicular to the surface would be IR-active, whereas oscillators vibrating parallel to the surface would have IR-forbidden vibrational signatures. Consequently, the E band overlapping with the $A_1^{(2)}$ band in the solution IR spectrum loses its intensity upon adsorption of the molecule on the Au(111) surface. The peak at 1996 cm^{-1} in the RAIR spectrum shown in Figure 3.8b corresponds to the $A_1^{(2)}$ stretching mode of the $[Cr(CO)_5]$ unit, whereas the small shoulder at the lower energy is attributed to the E band not disappearing completely due to the *cis*-CO ligands not being strictly parallel to the metal surface (i.e., not a perfectly upright orientation of **1** with respect to the Au(111) surface). This is due to the molecular packing within the film that may result in small tilts of the individual molecules within the monolayer. Notably, upon adsorption of **1** on the gold surface, the $A_1^{(2)}$ ν(CO) band moves to a higher energy compared to its position in the solution FTIR spectrum of **1**. Also, the $A_1^{(1)}$ ν(CO) band for the adsorbed **1** gains intensity and undergoes a blue shift (to 2051 cm^{-1}) compared to its characteristics in the corresponding solution FTIR spectrum. The higher energies of the two ν(CO) bands of A_1 symmetry in the RAIR spectrum of the surface-bound **1** compared to the corresponding values documented for the solution FTIR spectrum of **1** suggest reduction in the electron richness of the Cr(0) center upon adsorption of **1** (i.e., lower extent of $Cr(d\pi) \rightarrow p\pi^*(CO)$ back-bonding). This is consistent with the gold surface functioning as an electron withdrawer and the 2,6-diisocyanoazulenic bridge mediating electron polarization from the Cr(0) center to the Au(111) surface. The lone electron pair of the free isocyanide carbon in **1** is donated to the gold atoms upon SAM formation. Such coordination is reflected in the RAIR spectrum of **1** adsorbed on gold. Indeed, the ν(CN) band at 2113 cm^{-1} for the 6-isocyano terminus in the solution IR spectrum of **1**

moved to 2172 cm^{-1} upon adsorption of **1** on the Au surface via the 6-isocyano junction. The ν(CN) value of 2133 cm^{-1} for the Cr-bound isocyanide group in the solution IR spectrum of **1** essentially did not change (2132 cm^{-1}) upon adsorption of **1**. Noticeably, the relative intensities of the ν(CO) bands in the RAIR and solution IR spectra are switched due to depletion of the intensity of the E band as dictated by the surface IR selection rules. The findings discussed above suggest a nearly upright coordination of the molecules of **1** within the self-assembled monolayer on the Au(111) surface. The experimentally determined thickness of the SAM was also consistent with an upright orientation of the molecules bound to the gold surface. The calculated thickness of the SAM, that corresponds to a completely upright orientation of the molecular constituents, was estimated to be *ca.* 17 Å assuming a 2.05 Å distance for the Au–C junction.[6-7, 47, 61] The observed SAM thickness corroborates nicely with the calculated thicknesses, as summarized in Table 3.1.

Exposing *ca.* 1 × 1 cm^2 gold substrates to a 2 mM solution of **2** in $CHCl_3$ without protection from air and ambient lighting reproducibly afforded self-assembled monolayer (SAM) films of **2** on the Au (111) surface. This chemisorption process is presumably accompanied by the formation of the thiolate junction and the release of H_2.[62-64] The solution FTIR and the Reflection-Absorption Infra-Red (RAIR) spectrum of the SAM of **2** on Au(111) are illustrated in Figure 3.10. The solution IR spectrum of **2** shows a weak ν(SH) band at 2583 cm^{-1} which goes away when the monolayer is formed as depicted in the insets in Figure 3.10. In addition to the ν(CN) absorption at 2135 cm^{-1}, the RAIR spectrum of **2** adsorbed on gold features two ν(CO) bands. The ν(CO) region in the RAIR spectrum and solution IR have peak intensities that are switched and the energies experience blue shift. The lowest energy ν(CO) band in the solution IR spectrum of **2**, which is primarily attributed to the ν(CO) mode of E symmetry, practically vanishes upon the SAM formation, while simultaneously uncovering the hidden $A_1^{(2)}$ band of much lower

intensity. This observation implies approximately parallel orientation of the *cis*-CO ligands with respect to the gold surface. Indeed, surface IR selection rules[65-66] dictate that only vibrations contributing to dipole changes perpendicular to the surface are IR-active. Consequently, any vibrations occurring nearly parallel to the surface would have low IR intensity. Given that the C–N–C–Cr unit in **2,** as seen in Figure 3.10(c), is expected to be nearly linear, the appearance of the RAIR spectrum in Figure 3.10(a) suggests upright orientation of the molecules in the SAMs of **2**.

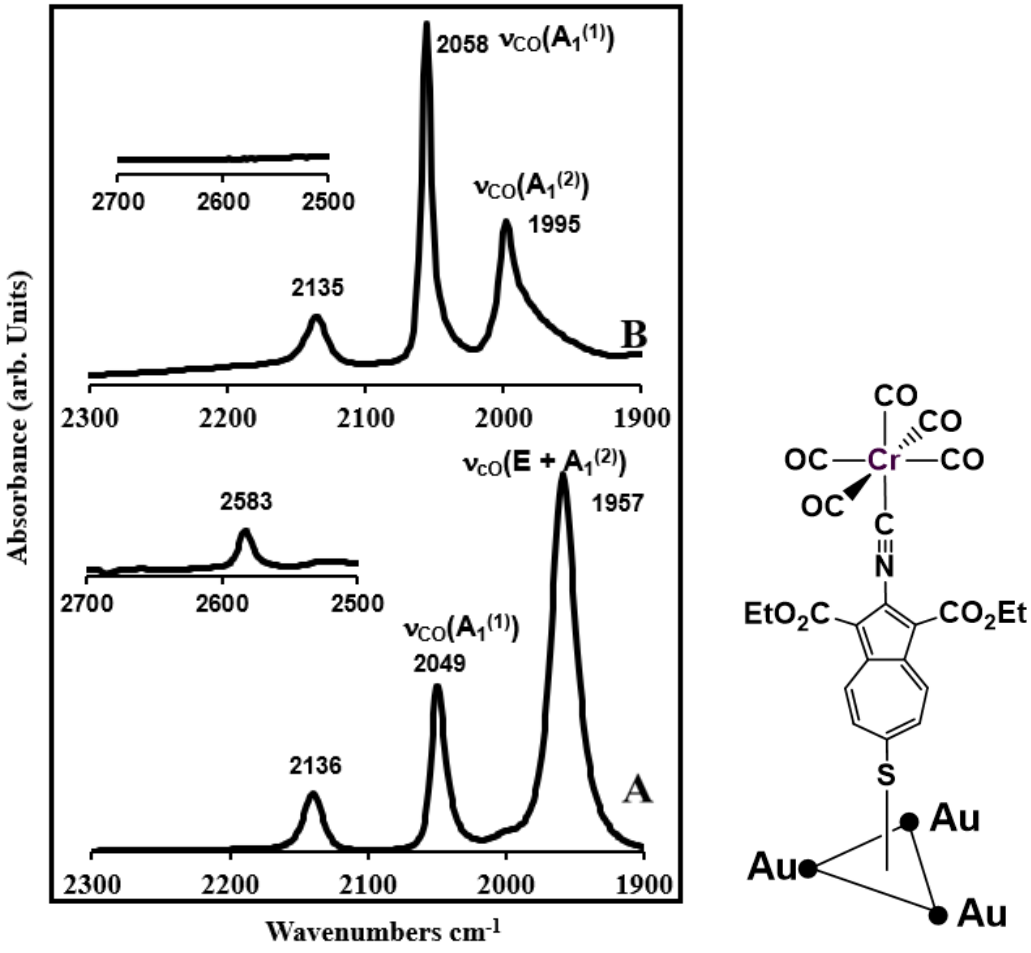

Figure 3.10. (A) FTIR solution spectrum of **2** in $CHCl_3$ (B) RAIR spectrum of **2** on Au (111) film (C) Illustration of the hollow-linear coordination of the SAM on gold film via thiolate junction group.[13]

The "hollow-linear" coordination of organic thiolates in their SAMs on Au(111), akin to that depicted in Figure 3.10(c), has been predicted to accommodate the strongest S–Au interaction and induce S→Au(111) charge transfer *via* S(*3p*)–Au π-bonding.[67-68] In the context of the chemistry presented herein, this demonstrates that the gold surface would effectively function as an electron-withdrawing "substituent," thus, enhancing π-acidity of the 2-isocyanoazulene ligand and, in turn, decreasing electron richness of the [$Cr(CO)_5$] unit. The $A_1^{(1)}$ and $A_1^{(2)}$ ν(CO) bands at 2058 and 1995 cm^{-1} in the RAIR spectrum in Figure 3.10(b) both exhibit significant blue shifts compared to the corresponding ν(CO) bands in the solution FTIR spectrum of the molecule which showed bands at 2049 and 1958 cm^{-1} (Figure 3.10(a)). The magnitudes of these shifts appear to be too high, especially in the case of the $A_1^{(2)}$ mode, to be attributed solely to differences in intermolecular interactions within the SAM *vs.* solution of **2**. The larger change in energy of the ν(CO) $A_1^{(2)}$ mode compared to that of the $A_1^{(1)}$ mode upon chemisorption of **2** stems from the greater contribution of the *trans*-CO stretch to the former.

The tilt angle of the aromatic moiety in SAMs of benzenoid mercaptoarenes on Au(111) can be highly variable.[62] We have recently shown that 2-mercaptoazulene, and several of its derivatives, form monolayer films on Au(111) with the approximately upright assembly of the azulenylthiolate constituents.[11] Our optical ellipsometry measurements on multiple SAM samples of **1** provided consistent SAM thickness values that nicely corroborate the monolayer nature of these films and upright orientation of the molecules on the gold surface (Table 3.1). The calculated thicknesses of SAMs of **2**, derived from the crystallographic measurements documented for **2**,[13] are comparable to the measured thicknesses. In terms of their composition, the SAMs of **1** and **2** on Au (111) differ only in the surface anchoring group (thiolate *vs.* isocyanide) and appear to exhibit

essentially identical thicknesses.[8] Notably, neither RAIR spectroscopic nor ellipsometric data collected for the SAMs of **2** on Au(111) would be consistent with the "on-top-bent" [66] or any other adsorption models of **2** invoking a bent C–S–$Au_{surface}$ geometry. The ellipsometric measurements on SAM films formed from our recently reported[69] 6-mercapto-1,3-diethoxycarbonyl-azulene and 6-mercapto-2-chloro-1,3-diethoxycarbonylazulene also corroborate that these 6-mercaptoazulenes self-assemble on Au(111) surfaces in the upright fashion (Table 3.1).

Table 3.1. Observed ellipsometric ($\boldsymbol{D}_{obs}$) and calculated ($\boldsymbol{D}_{calc}$) film thicknesses (in Å) of the SAMs of 1,3-diethoxycarbonyl-2-isocyanochromiumpentacarbonyl-6-isocyanoazulene**,** 1,3-diethoxycarbonyl-2-isocyanochromiumpentacarbonyl-6-mercaptoazulene**,** 6-mercapto-1,3-diethoxycarbonylazulene, and 6-mercapto-2-chloro-1,3-diethoxycarbonylazulene

Compounds	$\mathbf{D}_{obs.}$	$\mathbf{D}_{calc.}$
1. 1,3-diethoxycarbonyl-2-isocyanochromiumpntacarbonyl-6-isocyanoazulene	18 ± 3	17.1
2. 1,3-diethoxycarbonyl-2-isocyanochromiumpntacarbonyl-6-mercaptoazulene	18 ± 2	17
3. 6-mercapto-1,3-diethoxycarbonyl-azulene	13 ± 2	13.3
4. 6-mercapto-2-chloro-1,3-diethoxycarbonylazulene	15 ± 2	13.3

III.5.1. Results and discussion on SAM displacement studies involving 1 and 2 adsorbed on Au(111) either via isocyano and mercapto junction groups

The ellipsometric and RAIR measurements on SAM-coated Au (111) films containing chemisorbed **1** were repeatedly taken to validate the quality of the films before their use in the SAM displacement studies. As described earlier, four IR bands in the ν(CN) and ν(CO) region were observed in the RAIR spectrum of **1** adsorbed on Au(111) as reproduced in Figure 3.11(a). Two of the peaks were attributed to the symmetric ν(CO) vibrational modes, labeled as $A_1^{(1)}$ and $A_1^{(2)}$, while the other two peaks are due to the ν(CN) vibrations of the Cr-bound and Au-bound junctions on the films. Upon immersion of the SAM of **1** on the Au(111) substrate into a solution of **2** in $CHCl_3$, the SAM of **1** was completely stripped from the metal surface and a new SAM formed, as indicated by ellipsometric and RAIR spectroscopic measurements. The new SAM differs from the original SAM only in the junction group: instead of the gold-isocyanide bonding it involves the gold-thiolate anchoring. The RAIR spectrum of the resulting new film featuring **2** adsorbed on Au(111) exhibits only three IR bands in the ν(CN)/ν(CO) region, two of which correspond to the ν(CO) vibrations of the $[Cr(CO)_5]$ unit labeled as $A_1^{(1)}$ and $A_1^{(2)}$ and the third being the ν(CN) band corresponding to the Cr-bound isocyanide group (Figure 3.11(b)). The broader ν(CO) band of $A_1^{(2)}$ symmetry in Figure 3.11 (B) may also include contribution from the ν(CO) vibration of E symmetry due to a slight tilt in the molecular packing within the film. The disappearance of the peak at 2170 cm^{-1} indicates desorption of **1** from the gold surface upon immersing its SAM on Au(111) into the solution of **2**. This implies that the thiolate-bound monolayers exibit a stronger gold-junction bonding than the isocyano-anchored monolayers. Aside from the fact that the Au-S bond is approximately 20 kcal/mol stronger than the Au–CN bond [11, 70-71], researchers have speculated that thiolate anchoring groups are suitable junction groups for molecular conductance.

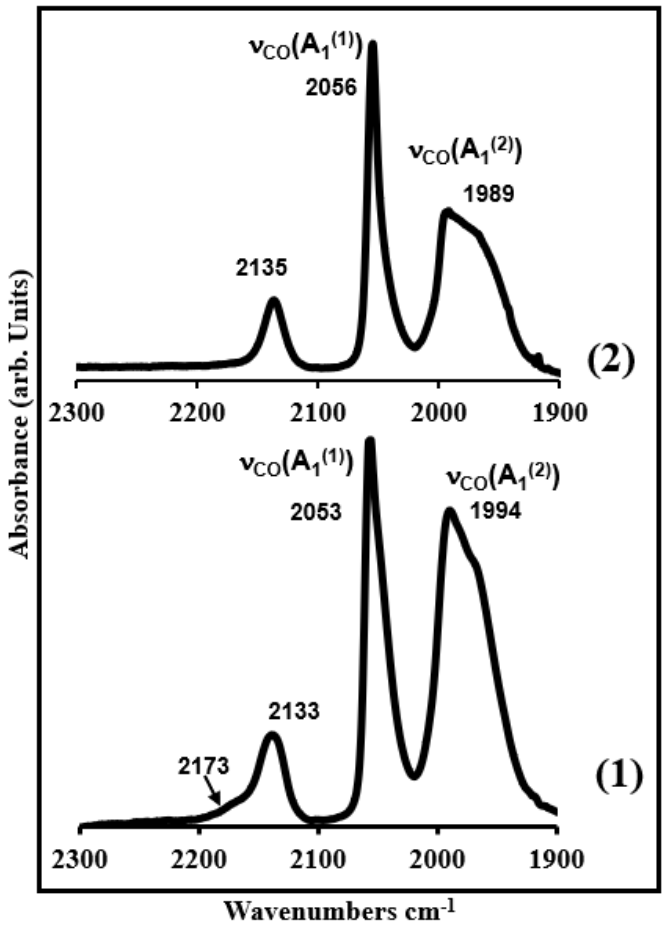

Figure 3.11. RAIR spectra from the displacement studies of the SAM of **1** before (**A**) and after (**B**) its immersion into a solution of **2** in $CHCl_3$.

III.6. Conclusions and outlook

In this chapter, the formation and characterization of the first self-assembled monolayer films involving isocyanoazulenylthiolate derivative SAMs have been presented. This asymmetric non-benzenoid aromatic framework of azulene proved to be a convenient platform for accessing the π-linker terminated with both thiol and isocyano junction moieties. The IR and ellipsometric analyses suggest that the monolayer was adsorbed onto the gold surface and the monolayer was

oriented in an upright fashion with respect to the gold film. In **2**, the thiol group were converted into thiolate junctions upon adsorption of the molecule to the gold surface. The C_{4v}-symmetric [$Cr(CO)_5CN$-] moiety served as a distinctly informative infrared reporter, supporting an upright orientation of the monolayers, for probing self-assembly of the 6-thiolateazulenic motif on the Au(111) surface. The study of the competitive adsorption, between **1** and **2,** emphasizes the stronger binding affinity of the thiolate junction group in **1** to gold than in **2**.

The monoazulenic system described in this chapter can be extended to biazulenic, terazulenic, or possibly, polyazulenic derivatives with isocyano and thiolate junction groups self-assembly. These extended systems may provide opportunities to designing potential molecular wires. A biazulene linker, featuring both -N≡C and -SH termini within the same molecule, adsorbed on Au (111), utilizing the bi-6,6′-azulenic core, for the purpose of electron transport from one electrode to the other will be discussed in chapter IV. Atomic Force Microscope (AFM) techniques may provide further information on the packing geometry, molecular packing, and periodicity of the azulenic SAMs relative to the gold film will be discussed in detail in a later chapter.

III.7. References

1. Aviram, A.; Ratner, M. A., Molecular Rectifiers. *Chemical Physics Letters* **1974**, *29*, 277-283.
2. Krzeminski, C.; Delerue, C.; Allan, G.; Vuillaume, D.; Metzger, R. M., Theory of Electrical Rectification in a Molecular Monolayer. *Physical Review B* **2001**, *64*, 085405-085406.
3. Querebillo, C. J.; Terfort, A.; Allara, D. L.; Zharnikov, M., Static Conductance of Nitrile-Substituted Oligophenylene and Oligo(phenylene ethynylene) Self-Assembled Monolayers Studied by the Mercury-Drop Method. *The Journal of Physical Chemistry C* **2013**, *117*, 25556-25561.
4. Kao, P.; Neppl, S.; Feulner, P.; Allara, D. L.; Zharnikov, M., Charge Transfer Time in Alkanethiolate Self-Assembled Mono layers via Resonant Auger Electron Spectroscopy. *The Journal of Physical Chemistry C* **2010**, *114*, 13766-13773.
5. Zhou, K.-g.; Zhang, Y.-h.; Wang, L.-j.; Xie, K.-f.; Xiong, Y.-q.; Zhang, H.-l.; Wang, C.-w., Can Azulene-Like Molecules Function as Substitution-Free Molecular Rectifiers? *Physical Chemistry Chemical Physics* **2011**, *13*, 15882-15890.
6. Barybin, M.; Chisholm, M.; Dalal, N.; Holovics, T.; Patmore, N.; Robinson, R.; Zipse, D., Long-range Electronic Coupling of MM Quadruple Bonds (M = Mo or W) via a 2,6-Azulenedicarboxylate Bridge. *Journal of the American Chemical Society* **2005**, *127*, 15182-15190.
7. Robinson, R.; Holovics, T. C.; Deplazes, S.; Powell, D.; Lushington, G.; Thompson, W.; Barybin, M., Five Possible Isocyanoazulenes and Electron- Rich Complexes Thereof: A Quantitative Organometallic Approach for Probing Electronic Inhomogeneity of the Azulenic Framework. *Organometallics* **2005**, *24*, 2386-2397.
8. Dubose, D. L.; Robinson, R. E.; Holovics, T. C.; Moody, D. R.; Weintrob, E. C.; Berrie, C. L.; Barybin, M. V., Interaction of Mono- and Diisocyanoazulenes with Gold Surfaces: First Examples of Self-assembled Monolayer Films Involving Azulenic Scaffolds. *Langmuir : The ACS Journal of Surfaces and Colloids* **2006**, *22*, 4599-4606.
9. Holovics, T. C.; Robinson, R. E.; Weintrob, E. C.; Toriyama, M.; Lushington, G. H.; Barybin, M. V., The 2,6- Diisocyanoazulene Motif: Synthesis and Efficient Mono- and Heterobimetallic Complexation with Controlled Orientation of the Azulenic Dipole. *Journal of the American Chemical Society* **2006**, *128*, 2300-2309.
10. Barybin, M. V., Nonbenzenoid Aromatic Isocyanides: New Coordination Building Blocks for Organometallic and Surface Chemistry. *Coordination Chemistry Reviews* **2010**, *254*, 1240-1252.
11. Neal, B. M.; Vorushilov, A.; Delarosa, A.; Robinson, R.; Berrie, C.; Barybin, M., Ancillary nitrile substituents as convenient IR spectroscopic reporters for self- assembly of mercapto- and isocyanoazulenes on Au(111). *Chemical Communications* **2011**, *47*, 10803-10805.
12. Wächter, T.; Scheetz, K. J.; Spaeth, A. D.; Barybin, M. V.; Zharnikov, M., Dynamics of Electron Transfer in Azulene- Based Self-Assembled Monolayers. *The Journal of Physical Chemistry C* **2017**, *121*, 13777-13785.
13. Applegate, J. C.; Okeowo, M. K.; Erickson, N. R.; Neal, B. M.; Berrie, C. L.; Gerasimchuk, N. N.; Barybin, M. V., First π-Linker Featuring Mercapto and Isocyano Anchoring Groups within the same Molecule: Synthesis, Heterobimetallic Complexation and Self-assembly on Au(111). *Chemical Science* **2016**, *7*, 1422-1429.
14. Schwarz, F., Charge Transport and Conductance Switching of Redox-Active Azulene Derivatives. *Angewandte Chemie International Edition* **2016**, *55*, 11781-11786.

15. Schwarz, F.; Koch, M.; Kastlunger, G.; Berke, H.; Stadler, R.; Venkatesan, K.; Loertscher, E., Charge Transport and Conductance Switching of Redox- active Azulene Derivatives. *Angewandte Chemie International Edition* **2016**, *55*, 11781-11786.
16. Barybin, M. V., Book Review of Functional Supramolecular Architectures: For Organic Electronics and Nanotechnology, Vols. 1– 2. . *Journal of the American Chemical Society* **2011**, *133*, 8774-8774.
17. M., L.; J., A. R., Modern Surface Organometallic Chemistry. *Wiley-VCH* **2009**, *Weinheim*, 513-556.
18. Buerkle, M.; Viljas, J. K.; Vonlanthen, D.; Mishchenko, A.; Schoen, G.; Mayor, M.; Wandlowski, T.; Pauly, F., Conduction mechanisms in biphenyl dithiol single-molecule junctions. *Physical Reviews B: Condensed Matter Material Physics* **2012**, *85*, 075417/075411-075417/075412.
19. Haekkinen, H., The gold-sulfur interface at the nanoscale. *Nat Chem* **2012**, *4*, 443-455.
20. Morari, C.; Rignanese, G. M.; Melinte, S., Electronic properties of 1-4, dicyanobenzene and 1-4, phenylene diisocyanide molecules contacted between Pt and Pd electrodes: First-principles study. *Physical Reviews B: Condensed Matter Material Physics* **2007**, *76*, 115428/115421-115428/115426.
21. Li, Y.; Lu, D.; Swanson, S. A.; Scott, J. C.; Galli, G., Microscopic Characterization of the Interface between Aromatic Isocyanides and Au(111): A First-Principles Investigation. *The Journal of Physical Chemistry C* **2008**, *112*, 6413-6421.
22. Chu, C.; Ayres, J. A.; Stefanescu, D. M.; Walker, B. R.; Gorman, C. B.; Parsons, G. N., Enhanced Conduction through Isocyanide Terminal Groups in Alkane and Biphenylene Molecules Measured in Molecule/Nanoparticle/Molecule Junctions. *The Journal of Physical Chemistry C* **2007**, *111*, 8080-8085.
23. Pontes, R. B.; Rocha, A. R.; Sanvito, S.; Fazzio, A.; Roque da Silva, A. J., Ab Initio Calculations of Structural Evolution and Conductance of Benzene-1,4-dithiol on Gold Leads. *ACS Nano* **2011**, *5*, 795-804.
24. Samori, P.; Cacialli, F.; Editors, *Functional Supramolecular Architectures for Organic Electronics and Nanotechnology, Volume 2*. Wiley-VCH Verlag GmbH & Co. KGaA, **2011**.
25. Samori, P.; Cacialli, F.; Editors, *Functional Supramolecular Architectures: For Organic Electronics And Nanotechnology, Volume 1*. Wiley-VCH Verlag GmbH & Co. KGaA, **2011**.
26. Barybin, M. V.; Jr., J. J. M.; Neal, B. M., Isocyanide Chemistry - Applications in Synthesis and Material Science. In *Isocyanide Chemistry - Applications in Synthesis and Material Science*, Nenajdenko, V., Ed. Wiley-VCH: Weinheim, **2012**, 493-529.
27. Lasar, M.; Angelici, R. J., Modern Surace Organometallic Chemistry. In *Modern Surace Organometallic Chemistry*, Basset, J.-M.; Psaro, R.; Roberto, D.; Ugo, R., Eds. Wiley-VCH: Weinheim, **2009**, 493-529.
28. Xiang, D.; Wang, X.; Jia, C.; Lee, T.; Guo, X., Molecular-Scale Electronics: From Concept to Function. *Chemical Reviews* **2016**, *116*, 4318-4440.
29. Kestell, J.; Abuflaha, R.; Garvey, M.; Tysoe, W. T., Self-Assembled Oligomeric Structures from 1,4-Benzenedithiol on Au(111) and the Formation of Conductive Linkers between Gold Nanoparticles. *The Journal of Physical Chemistry C* **2015**, *119*, 23042-23051.
30. Bruot, C.; Hihath, J.; Tao, N., Mechanically controlled molecular orbital alignment in single molecule junctions. *Nature Nanotechnology* **2012**, *7*, 35-40.
31. Kim, Y.-S.; Pietsch, T.; Erbe, A.; Belzig, W.; Scheer, E., Benzenedithiol: A broad-range single-channel molecular conductor. *Nano Letters* **2011**, *11*, 3734-3738.

32. Kim, B.; Choi, S. H.; Zhu, X. Y.; Frisbie, C. D., Molecular Tunnel Junctions Based on π-Conjugated Oligoacene Thiols and Dithiols between Ag, Au, and Pt Contacts: Effect of Surface Linking Group and Metal Work Function. *Journal of the American Chemical Society* **2011**, *133*, 19864-19877.
33. Murphy, K. L.; Tysoe, W. T.; Bennett, D. W., A Comparative Investigation of Aryl Isocyanides Chemisorbed to Palladium and Gold: An ATR-IR Spectroscopic Study. *Langmuir* **2004**, *20*, 1732-1738.
34. Kim; Beebe, J. M.; Jun, Y.; Zhu, X. Y.; Frisbie, C. D., Correlation between HOMO Alignment and Contact Resistance in Molecular Junctions: Aromatic Thiols versus Aromatic Isocyanides. *Journal of the American Chemical Society* **2006**, *128*, 4970-4971.
35. Lee, Y.; Carsten, B.; Yu, L., Understanding the Anchoring Group Effect of Molecular Diodes on Rectification. *Langmuir* **2009**, *25*, 1495-1499.
36. Van Dyck, C.; Ratner, M. A., Molecular Rectifiers: A New Design Based on Asymmetric Anchoring Moieties. *Nano Letters* **2015**, *15*, 1577-1584.
37. Rodríguez-Bolívar, S.; Gómez-Campos, F. M.; Álvarez de Cienfuegos, L.; Fuentes, N.; Cárdenas, D. J.; Buñuel, E.; Carceller, J. E.; Parra, A.; Cuerva, J. M., Conductance and Application of Organic Molecule Pairs as Nanofuses. *Physical Review B* **2011**, *83*, 125424-125411.
38. Porter, M. D.; Bright, T. B.; Allara, D. L.; Chidsey, C. E. D., Spontaneously Organized Molecular Assemblies. 4. Structural Characterization of N-Alkyl Thiol Monolayers on Gold by Optical Ellipsometry, Infrared Spectroscopy, and Electrochemistry. *Journal of the American Chemical Society* **1987**, *109*, 3559-3568.
39. Ulman, A., Formation and Structure of Self-Assembled Monolayers. *Chemical Reviews* **1996**, *96*, 1533-1554.
40. Stapleton, J. J.; Daniel, T. A.; Uppili, S.; Cabarcos, O. M.; Naciri, J.; Shashidhar, R.; Allara, D. L., Self-assembly, Characterization, and Chemical Stability of Isocyanide- Bound Molecular Wire Monolayers on Gold and Palladium Surfaces. *Langmuir : The ACS Journal of Surfaces and Colloids* **2005**, *21*, 11061-11070.
41. Swanson, S. A.; McClain, R.; Lovejoy, K. S.; Alamdari, N. B.; Hamilton, J. S.; Scott, J. C., Self-Assembled Diisocyanide Monolayer Films on Gold and Palladium. *Langmuir : The ACS Journal of Surfaces and Colloids* **2005**, *21*, 5034-5039.
42. Sohn, Y.; White, J., Solely Sigma-atop Site Bonding of Phenyl Isocyanide on Au(111)? Comparison with on Cu(111). *The Journal of Physical Chemistry C* **2008**, *112*, 5006-5013.
43. Boscoboinik, J.; Calaza, F. C.; Habeeb, Z.; Bennett, D.; Stacchiola, D.; Purino, M.; Tysoe, W., One- dimensional supramolecular surface structures: 1,4- diisocyanobenzene on Au(111) surfaces. *Physical Chemistry Chemical Physics* **2010**, *12*.
44. Boscoboinik, J.; Kestell, J.; Garvey, M.; Weinert, M.; Tysoe, W., Creation of Low-Coordination Gold Sites on Au(111) Surface by 1,4-phenylene Diisocyanide Adsorption. *Topics in Catalysis* **2011**, *54*, 20-25.
45. Noh, J.; Ito, E.; Hara, M., Self- assembled monolayers of benzenethiol and benzenemethanethiol on Au(1 1 1): Influence of an alkyl spacer on the structure and thermal desorption behavior. *Journal of Colloid and Interface Science* **2010**, *342*, 513-517.
46. Kang, H.; Park, T.; Choi, I.; Lee, Y.; Ito, E.; Hara, M.; Noh, J., Formation of Large Ordered Domains in Benzenethiol Self-assembled Monolayers on Au(111) Observed by Scanning Tunneling Microscopy. *Ultramicroscopy* **2009**, *109*, 1011-1014.

47. Kang, J.; Ulman, A.; Liao, S.; Jordan, R.; Yang, G.; Liu, G., Self-Assembled Rigid Monolayers of 4 '- Substituted- 4- Mercaptobiphenyls on Gold and Silver Surfaces. *Langmuir* **2001**, *17*, 95-106.
48. Hong, S.; Reifenberger, R.; Tian, W.; Datta, S.; Henderson, J. I.; Kubiak, C. P., Molecular Conductance Spectroscopy of Conjugated, Phenyl- Based Molecules on Au(111): The Effect of End Groups on Molecular Conduction. *Superlattices and Microstructures* **2000**, *28*, 289-303.
49. Gorman, C.; He, Y.; Carroll, R., The Influence of Headgroup on the Structure of Self-Assembled Monolayers as Viewed by Scanning Tunneling Microscopy. *Langmuir* **2001**, *17*, 5324-5328.
50. Li, Y.; Lu, D.; Swanson, S. A.; Scott, J.; Galli, G., Microscopic characterization of the interface between aromatic isocyanides and Au(111): A first-principles investigation. *The Journal of Physical Chemistry C* **2008**, *112*, 6413-6421.
51. Mallick, G., *Scanning Tunneling Microscopic Characterization of an Engineered Organic Molecule*. Aberdeen Proving Ground, MD : Army Research Laboratory, Aberdeen Proving Ground, MD, **2011**.
52. Kim, B. S.; Choi, S. H.; Zhu, X.-Y.; Frisbie, C. D., Molecular Tunnel Junctions Based on π-Conjugated Oligoacene Thiols and Dithiols between Ag, Au, and Pt Contacts: Effect of Surface Linking Group and Metal Work Function. *Journal of the American Chemical Society* **2011**, *133*, 19864-19877.
53. Nijhuis, C. A., Charge Transport and Rectification in Arrays of SAM-Based Tunneling Junctions. *Nano Letters* **2010**, *10*, 3611-3619.
54. Heimel, G.; Romaner, L.; Zojer, E.; Bredas, J. L., Toward Control of the Metal-Organic Interfacial Electronic Structure in Molecular Electronics: A First-Principles Study on Self-Assembled Monolayers of Pi-Conjugated Molecules on Noble Metals. *Nano Letters* **2007**, *7*, 932-940.
55. Kiguchi, M.; Miura, S.; Hara, K.; Sawamura, M.; Murakoshi, K., Conductance of a Single Molecule Anchored by an Isocyanide Substituent to Gold Electrodes. *Applied Physics Letters* **2006**, *89*, 213104-213103.
56. Automatic Refractometer: Rudolph Research Analytical. *Laboratory Equipment* **2003**, *39*, 87.
57. Wasserman, S. R.; Whitesides, G. M.; Tidswell, I. M.; Ocko, B. M.; Pershan, P. S.; Axe, J. D., The Structure of Self-Assembled Monolayers of Alkylsiloxanes on Silicon: A Comparison of Results from Ellipsometry and Low-Angle X-Ray Reflectivity. *Journal of the American Chemical Society* **1989**, *111*, 5852-5861.
58. Le Grange, J. D.; Markham, J. L.; Kurkjian, C. R., Effects of Surface Hydration on the Deposition of Silane Monolayers on Silica. *Langmuir* **1993**, *9*, 1749-1753.
59. Clear, S. C.; Nealey, P. F., Lateral Force Microscopy Study of the Frictional Behavior of Self-Assembled Monolayers of Octadecyltrichlorosilane on Silicon/Silicon Dioxide Immersed in n-Alcohols. *Langmuir* **2001**, *17*, 720-732.
60. Wang, J.; Li, G.; Li, Q.-S.; Xie, Y.; King, R. B., Isocyanide Versus Nitrile Ligands and Methyl Versus Trifluoromethyl Substituents in Metal Carbonyl Chemistry. *Polyhedron* **2012**, *47*, 165-172.
61. Gottschalck, J.; Hammer, B., A Density Functional Theory Study of the Adsorption of Sulfur, Mercapto, And Methylthiolate on Au(111). *The Journal of chemical physics* **2002**, *116*, 784-790.

62. Love, J.; Estroff, L.; Kriebel, J.; Nuzzo, R. G.; Whitesides, G., Self-Assembled Monolayers of Thiolates on Metals as a Form of Nanotechnology. *Chemical Reviews* **2005**, *105*, 1103-1169.
63. Chu, C.; Ayres, J. A.; Stefanescu, D. M.; Walker, B. R.; Gorman, C. B.; Parsons, G. N., Enhanced Conduction through Isocyanide Terminal Groups in Alkane and Biphenylene Molecules Measured in Molecule/Nanoparticle/Molecule Junctions. *The Journal of Physical Chemistry C* **2007**, *111*, 8080-8085.
64. Cossaro, A.; Mazzarello, R.; Rousseau, R.; Casalis, L.; Verdini, A.; Kohlmeyer, A.; Floreano, L.; Scandolo, S.; Morgante, A.; Klein, M. L.; Scoles, G., X-ray Diffraction and Computation Yield the Structure of Alkanethiols on Gold(111). *Science* **2008**, *321*, 943-946.
65. Harris, D. C.; Bertolucci, M. D., Symmetry and Spectroscopy : An Introduction to Vibrational and Electronic Spectroscopy. Bertolucci, M. D., Ed. New York : Dover Publications: New York, **1989**, 151-159.
66. Pearce, H. A.; Sheppard, N., Possible Importance of a "Metal-Surface Selection Rule" in the Interpretation of the Infrared Spectra of Molecules Adsorbed on Particulate Metals; Infrared Spectra from Ethylene Chemisorbed on Silica-Supported Metal Catalysts. *Surface Science* **1976**, *59*, 205-217.
67. Tachiban, M.; Yoshizawa, K.; Ogawa, A.; Fujimoto, H.; Hoffman, R., Sulfur- Gold Orbital Interactions, which Determine the Structure of Alkanethiolate/ Au (111) Self- Assembled Monolayer Systems. *Journal of Physical Chemistry B* **2002**, *106*, 12727-12736.
68. Sellers H., U. A.; Shnidman Y.; E., E. J., Modeling Chemisorption Processes with Metal Cluster Systems: III. Model Thio-Alkyls on Gold Surfaces. *NATO ASI Series (Series B: Physics)* **1992**, *283*, 441-452.
69. Scheetz, K. J.; Spaeth, A. D.; Vorushilov, A. S.; Powell, D. R.; Day, V. W.; Barybin, M. V., The 2,6-dimercaptoazulene Motif: Efficient Synthesis and Completely Regioselective Metallation of its 6-mercapto Terminus. *Chemical Science* **2013**, *4*, 4267-4272.
70. Dubois, L. H.; Nuzzo, R. G., Synthesis, Structure, and Properties of Model Organic Surfaces. *Annual Review of Physical Chemistry* **1992**, *43*, 437-463.
71. Nuzzo, R. G.; Zegarski, B. R.; Dubois, L. H., Fundamental Studies of the Chemisorption of Organosulfur Compounds on Gold(111). Implications for Molecular Self-assembly on Gold Surfaces. *Journal of the American Chemical Society* **1987**, *109*, 733-740.

Chapter IV:

SAMs of biazulenic scaffolds featuring mercapto and isocyano anchoring groups within the same molecule adsorbed on Au (111) substrates

IV.1. Symmetric and asymmetric strategic anchoring of a 6,6'-biazulene scaffold for molecular conductivity and possibly, molecular rectification

The surface chemistry of the SAMs of biazulenic linkers, equipped with asymmetric anchoring, involving isocyanide and thiolate junction groups within the same molecule is described herein. This chapter, featuring a biazulenic system, is an extension of the monoazulenic systems, asymmetrically anchored to a gold substrate, described in chapter III. Here, two molecules with 6,6'-biazulenic motifs have either thiolate or isocyanide junction group connected to the Au (111) surface (see figure 4.1). Similar to the linear azulenic linker presented in chapter III, both molecules described in this work have an isocyanide terminus connected to the zero-valent chromium center of the $Cr(CO)_5$ motif. The frequencies and intensities of the IR bands corresponding to the CO stretching vibrations of the chromium pentacarbonyl remote infrared reporters provide indirect information about orientation of the adsorbed molecules with respect to the gold surface. Both molecules, seen in Figure 4.1, chemisorbed to the gold substrate result in perpendicular orientation to the surface. Though the influence of the junction groups, on SAM formation, differs and may result in different conductance behavior, the junction groups aid the upright orientation observed. The junction groups, either an isocyanide or a thiolate, form an isocyano-gold or a thiolate-gold junction upon self-assembly of the organochromium biazulene scaffolds on the gold substrate. While the isocyanide-anchored SAMs feature linear Au-C≡NR coordination, the thiolate-anchored SAMs involve a “hollow-linear’ Au-S-R coordination at the gold-SAM interface. A competitive adsorption study was performed, in order to assess the relative binding affinities, for the molecules with two different junction groups to the surface. Ellipsometric and RAIR spectroscopic studies were conducted to elucidate the molecular packing, including orientation within the SAMs.

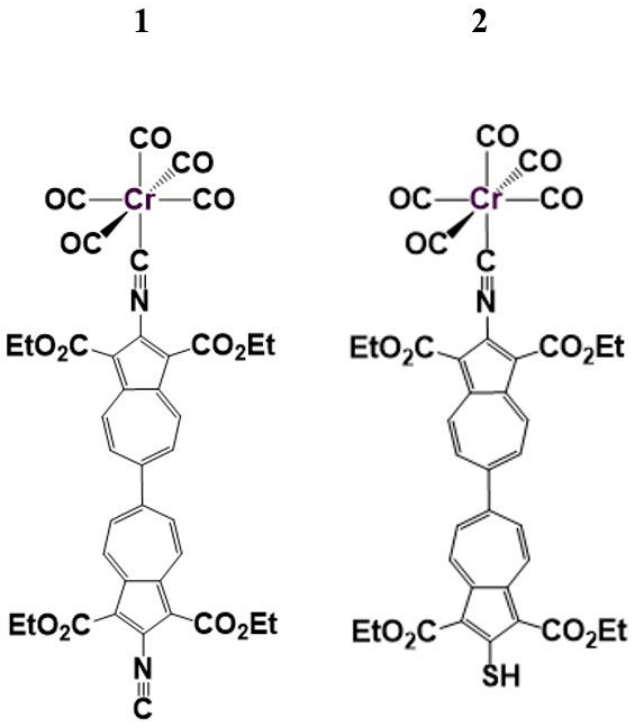

Figure 4.1. Biazulenic molecules used in SAM formation.

Azulene and its derivatives are attractive building blocks in the design of electronic materials, particularly, because of the charge separation between the two rings.[1-5] The intramolecular charge transfer from the 7-membered ring to the 5-membered ring of the azulenic scaffold leads to Huckel aromaticity within both rings. The zwitter-ionic resonance structure, depicted in Figure 4.2, exerts a ground state dipole moment of about one Debye. In addition to this characteristic, azulene has frontier (HOMO and LUMO) orbital density distributions with complementary features where the HOMO density is primarily centered on the odd-numbered carbon atoms of the scaffold and the LUMO density is on the even-numbered carbon atoms.[6] Independent tuning of the energies of the frontier orbitals is achievable via substitution at the

azulenic core. Substitution at the odd- and even-numbered positions changes the energy of either HOMO or LUMO, but not both, because of the complementary nature of the orbital density within these molecular orbitals.[2, 7] The Barybin and Berrie research groups explore functionalization of the azulenic scaffold, along the molecular axis, in order to take advantage of azulene's dipole moment in molecular charge delocalization and transport settings. This is accomplished by installing substituents at the 2 or/and 6 position(s) of the azulenic scaffold, such as isocyanide, thiolate, cyanide or/and carboxylate, that can serve as junctions between the azulenic moiety and metal atoms, ions, or surfaces. The coordination and surface chemistry of azulene-based organometallics has been studied for more than a decade in the Barybin and Berrie labs due to their tremendous potential applications in nanotechnology.[2-4, 7-11]

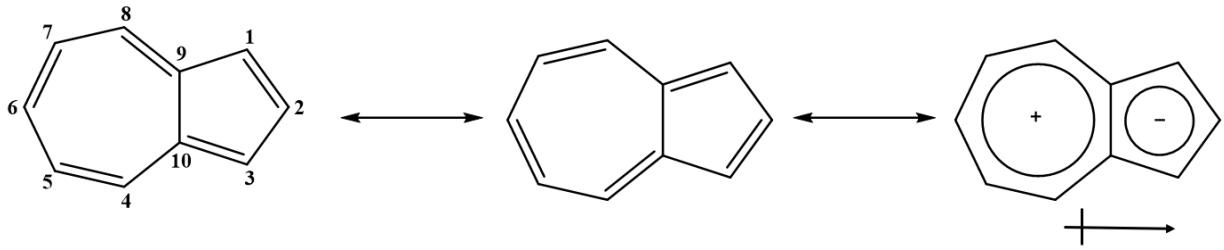

Figure 4.2. The atom numbering scheme for azulene, its resonance structures, and the direction of its molecular dipole.

Azulene has been considered useful in designing of organoelectronic materials due to its electronic asymmetry.[1, 5, 12] Also, azulene derivatives are versatile building blocks for designing functional materials and molecular wires.[8, 13-14] The connection of properly functionalized azulene derivatives to a conductive substrate for developing advanced materials has been studied. The junction group used in connecting the azulenic framework to a metal substrate like gold plays a crucial role in conductance properties of the SAM films.[13, 15-17] The theoretical study by Ratner *et al.* predicted that a molecular rectifier should be comprised of donor and acceptor subunits and

should include a π-decoupling unit which enhances the rectification by separating the spatially independent Fermi-level pinned HOMO and LUMO orbitals.[15] Also, the use of conjugated molecules employed for designing the molecular rectifier should have two lateral fragments connected, but no π-coupling of the fragments is advised.[15]

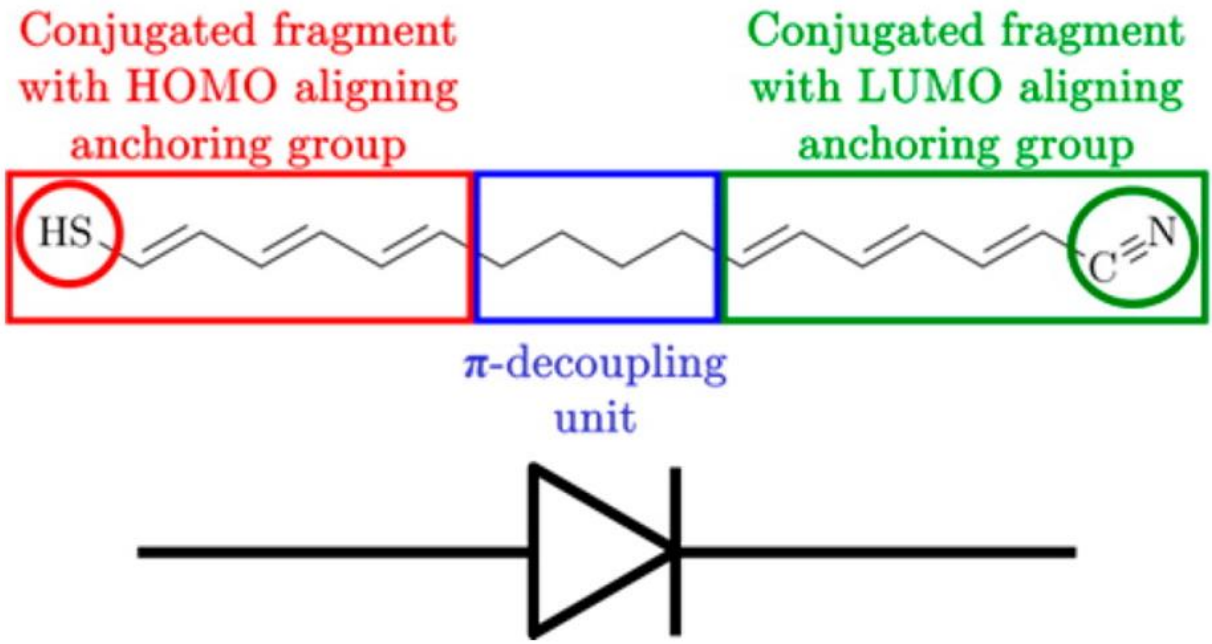

Figure 4.3. An illustration of the proposed design for molecular rectification. At each end is a donating (mercapto) and accepting (cyano) anchoring groups, the mercaptan promotes alignment of the HOMO while cyano supports alignment of LUMO. Presence of two decoupled lateral conjugated fragments complete the model for rectification. Reprinted with permission from Ref. 15. Copyright (2015) American Chemical Society.

The theoretical study by Ratner *et al.* in 2015 showed that importantly, the complete model for rectification requires at least three components, illustrated in Figure 4.3.[15] The researchers used cyano and mercapto termini as the electron donating and withdrawing groups, respectively,

to connect the molecule of interest to a gold surface. The proposed molecule was a combination of two hexatrienyls fragments separated by a saturated tetramethylene bridge.[15] Ratner and coworkers suggested that the rectification behavior is due to the opposition between resonant and non-resonant tunneling, hence the use of a saturated bridge. The anchoring groups should be able to aid alignment of either the HOMO or the LUMO to the Fermi level of the gold, as shown in Figure 4.4., with the purpose of separating the spatially independent fermi-level pinned HOMO and LUMO orbitals.[15] The presence of appropriate frontier orbital energy levels in the transmission region (dashed lines) lead to the significant resonant tunneling, in the negative bias region (Figure 4.4b), but in the positive bias (Figure 4.4a), transitions from the less efficient non-resonant tunneling were observed. This difference in the tunneling by both positive and negative bias lead to significant rectification.[15] Ratner's findings based on DFT calculations suggested an increase in performance of rectification by two orders of magnitude. The calculations done on the model showed that the rectifying ratio increased with increased bias, with a maximum of 150 as the rectifying ratio at 1.2 V, surpassing existing literature values.[15] Ratner's theoretical study poses significant drawback due to the lack of molecular rigidity, which would complicate experimental probing. Moreover, the π-decoupling unit, tetramethylene, would significantly reduce the extent of conductivity. The asymmetric anchoring, however, of the conjugated π-systems with electron donating and withdrawing junctions at opposite ends, for the purpose of Fermi level pinning, as previously mentioned, is important. The influence of electron donating and withdrawing junction groups pose a substantial effect on rectification. A 2011 theoretical work by Wang *et al.* proposed that azulenic or biazulenic linker anchored via suitable electron withdrawing and donating groups to a conductive substrate may exert significant rectification ratio.[1] They suggested that linking one or two azulenic units used as an electronic bridge may influence positively rectification.[1]

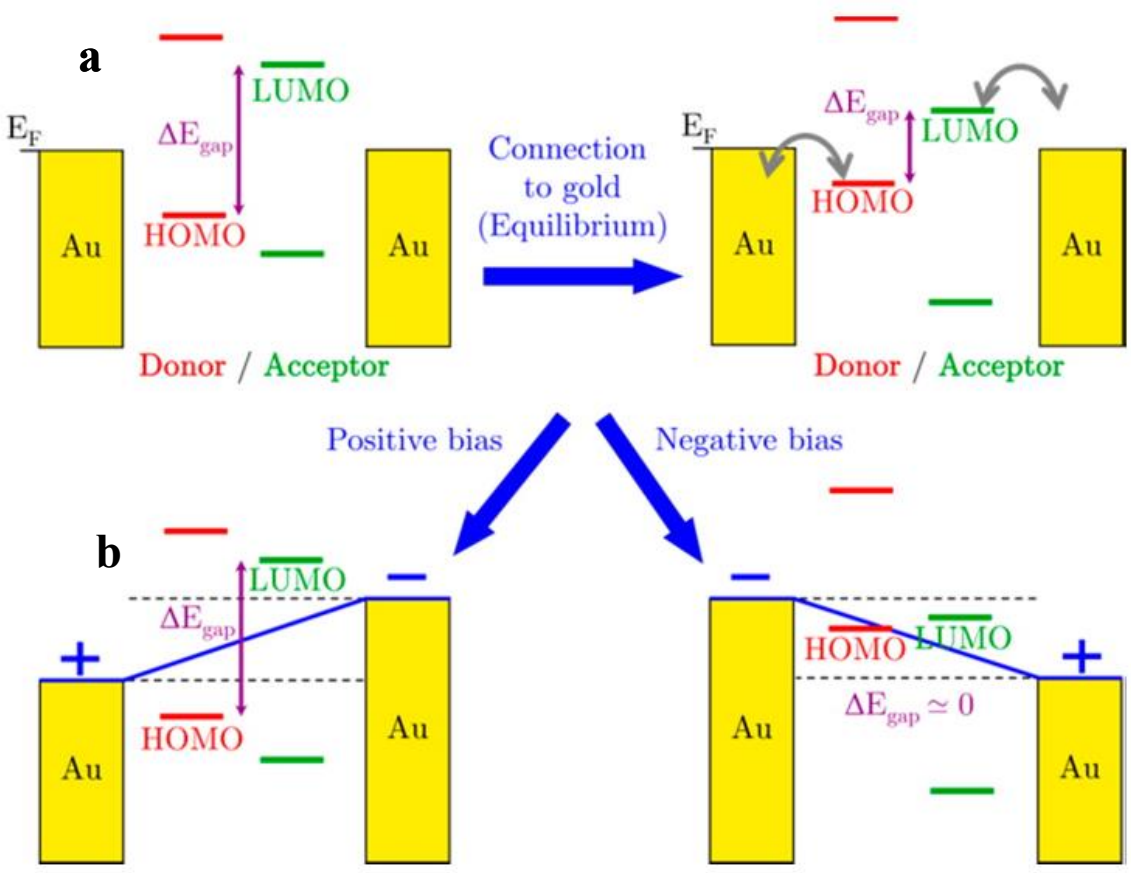

Figure 4.4. Schematic representation of the Ratner's proposed rectification mechanism showing (a) the connection of the gold electrodes to the molecule, (b) mechanism for positive bias and negative bias. The blue lines in the positive and negative bias show the electrostatic potentials. Reprinted with permission from Ref. 15. Copyright (2009) American Chemical Society.

Increasing the number of azulene motifs, connected in a 2,2'-, 2,6-, and a 6,6'-moieties along the molecular axis to make biazulenes, terazulenes, or polyazulenes can be useful tool for molecular wires. The Barybin group has carried out extensive breakthrough investigations, as the first research group, on the biazulenes derivatives via synthetic, computational, and surface chemistry studies. The π-conjugation and frontier molecular orbital overlap between the azulenic units decrease in the order 2,2'-, 2,6-, and a 6,6'-biazulenes, allowing for less π-electron

delocalization respectively with the 6,6'-biazulene as the least coupled. The torsional angles of rotation are governed by steric interactions of the hydrogen atoms closest to the point at which the azulenic units connect.[18] The torsional angles, based on DFT studies with our collaborator Thompson *et al.*, for the 2,2'-, 2,6-, and 6,6'-diisocyanobiazulenes are 5°, 28°, and 50°, respectively.[18] This torsional angle magnitude, between the azulenic units, is inversely related to the π-conjugation and orbital overlap between the azulenic units. Therefore, the biazulenic derivatives, specifically 6,6'-biazulenes, might be capable of separating the donor and acceptor units of a molecular linker in the design without compromising the conductance pathway. [19-20]

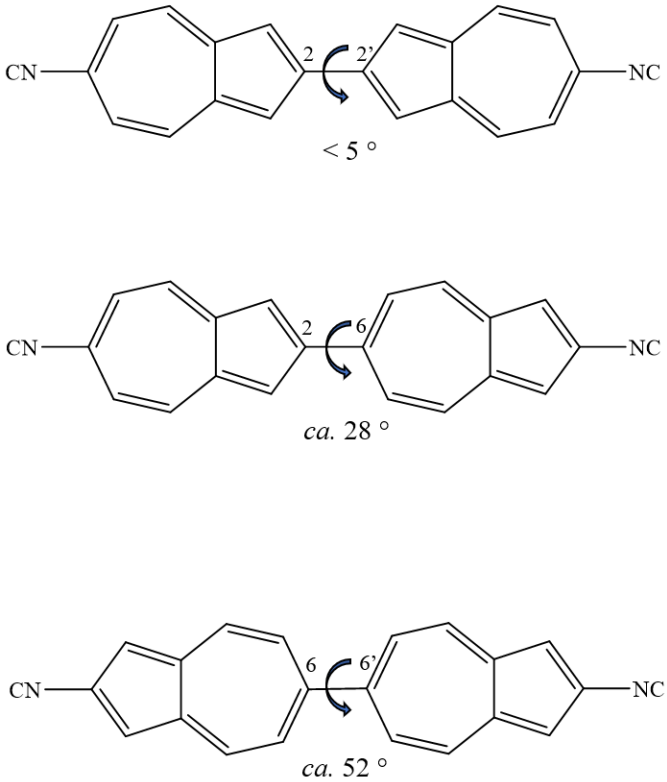

Figure 4.5. Structural drawings of three linearly functionalized diisocyanobiazulenes and the corresponding DFT-calculated interplanar torsional angles.[18]

The coupling within any of the biazulenic units shown above, especially the 2,6- unit, makes them good potential candidates for conductance which may be useful in designing molecular wires. In 2010, a diisocyanobiazulene with connectivity at the 6,6'- was synthesized in the Barybin Lab. The crystal structure of the molecule showed a torsional angle of 66.9°, DFT calculations show that the 6,6'- connectivity are electronically coupled.[18] In 2017, Chen *et al.* described the function of our 2,2'-diisocyano-6,6'-biazulene in Figure 4.5 as a molecular rectifier.[21] Their conductive AFM analysis supported the potential use of this biazulene unit in rectification based on a rectifying ratio of 6.5 as highest at 0.31V for the studied biazulene film. [21]

The work described herein features SAMs of 6,6'- biazulene molecule with asymmetric anchoring using isocyano and thiol groups **2** and are compared to the symmetric diisocyano anchoring analogue **1** (see Figure 4.1). The molecules were synthesized in the Barybin lab by Jason Applegate.[22] The ethoxycarbonyl substituents at the 1-, 1'-, 3-, and 3'- positions of the biazulenic scaffold are necessary for synthetic purposes and ensuring good solubility of the compound in organic solvents. The molecules have complexed zero-valent chromium center of the $Cr(CO)_5$ motif bound to the isocyanide and either a free mercapto or isocyano termini. The SAM formation, molecular packing, the influence of junction groups, and stability characteristics are discussed. Importantly, it is expected that **1** and **2** coordinates through the unbound junction groups to the gold surface and that the molecules will approximately orient vertically on the substrates. Also, competition studies on the isocyano and thiolate junction groups carried out provide information on packing and stability of the films. Overall, the garnered information from this study present an opportunity to experimentally probe the conductive behavior of the films relevant to organic electronics.

IV.2. Experimental section

IV.2.1. General procedures and starting materials

The syntheses of the biazulenes used in these studies were developed and performed by Jason Applegate of the Barybin group and will be reported in Applegate, J. C.; Okeowo, M. K.; Erickson, N. R.; Neal, B. M.; Berrie, C. L.; Gerasimchuk, N. N.; Barybin, M. V., Biazulenic π-linker featuring isocyano and mercapto anchoring termini in the same molecule: Synthesis, self-assembly on gold film, redox behavior, and heterobimetallic complexation, Manuscript in preparation.[22]

Commercially available gold-coated silicon substrates featuring grains with Au (111) terraces made via deposition were employed throughout this experiment. The gold substrates were purchased from Platypus Technologies. The silicon wafers had been coated with 5 nm titanium adhesion layer before *ca.* 100 nm of gold was deposited on the substrates.

Unless specified otherwise, all substrates were cleaned by soaking sequentially in chloroform, acetone, and 200-proof ethanol for two hours in each solvent. All solvents were obtained from commercial sources and used as received or distilled before use. Chloroform was distilled over P_2O_5. Dichloromethane was distilled over CaH_2. Following the purification, the distilled solvents were stored under argon. After being soaked, the substrates were rinsed with 200-proof ethanol and then dried with a stream of nitrogen gas. The optical constants for bare gold substrates were measured before immersing the substrates into *ca.* 2 mM solutions of the biazulenic compounds to make the SAM-coated substrates. The values of the optical constants, *n and k,* for each sample of the gold substrates were obtained at a minimum of five different spots using Rudolph research/Auto EL III fixed wavelength ellipsometer. A standard calibration of the ellipsometer was done with a silicon wafer control sample before collecting the *n and k* values. All

measurements were conducted using a HeNe laser with a wavelength of 632.8 nm and an incident angle of 70° to the surface normal. The optical constants, incident angle, and a refractive index were used to determine the experimental thicknesses of the adsorbed SAMs. The refractive index of 1.45 was assumed[23-25] for all organic thin films described herein. The average thickness values and the corresponding standard deviations given in parentheses were determined from ellipsometric measurements at a minimum of five separate spots on the SAM substrate.

The grazing incidence Reflection Absorption Infra-Red (RAIR) spectra for the SAM-coated substrates were recorded using a Thermo Nicolet Nexus 670 FTIR spectrophotometer with a VeeMax grazing angle accessory set at an angle of 70 ° and an MCT detector. The detector of the FTIR spectrophotometer was cooled continuously with liquid nitrogen, and the spectrophotometer was connected to Kaeser air purifying system to dry the air and reduce background spectrum interference from CO_2 and H_2O. Background spectra were collected using a freshly cleaned bare gold substrate before acquiring any spectra for each sample. Ten thousand scans from 600 to 4000 cm^{-1} at 4 cm^{-1} resolution were obtained for each background/sample combination.

IV.2.1.1. SAM formation of 2,2'-diisocyano-1,1',3,3'-tetraethoxycarbonyl-6,6'-biazulene capped with a $Cr(CO)_5$ moiety at the 2-isocyano terminus (1) on Au (111) film

Freshly cut 1 x 1 cm^2 gold-coated silicon substrates were cleaned with hot Piranha solution, flushed with large volumes of Milli-Q water, and dried in a stream of N_2 gas (**Warning:** extreme care must be used when handling Piranha solution. The solution reacts violently with organic substances and poses an explosion danger). The dried substrates were cleaned by soaking sequentially in chloroform, acetone, and 200-proof ethanol for 2 hours each. The cleaned

substrates were thoroughly dried in a stream of nitrogen gas before the optical characteristics (*n and k*) of the film were measured.

Monolayer assembly of **1** was done by placing a freshly cleaned gold substrate into a 3 mM solution of **1** in distilled dichloromethane for *ca.* 24 hours. SAM-coated substrates were thoroughly rinsed with distilled dichloromethane to remove any physisorbed molecules and dried with N_2 gas before further analyses. Surface RAIR spectra of and ellipsometric measurements on the resulting were then obtained. No precaution to exclude air or ambient laboratory lighting was exercised during these SAM experiments.

The solution infrared spectrum of **1** used in SAM formation was recorded on a PerkinElmer Spectrum 100 FTIR spectrometer with samples sealed into a 0.1 mm gas tight NaCl cell. A background spectrum was first collected for the dichloromethane solvent before the sample measurement. The surface IR (RAIR) spectra were obtained by collecting a background spectrum followed by that of the sample film as described in the general procedure and starting materials section. One thousand scans were collected for three SAM-coated films at a resolution of 2 cm^{-1} while the instrument was cooled continuously with liquid nitrogen. After each sample exchange, the water and CO peaks were monitored as they decreased while the system was purged with dry air to reduce these peaks as much as possible. Analyses to determine the ellipsometric thickness of **1** were done as described in the general procedures and starting materials section. The average of optical properties of the bare gold substrate used to determine the thickness of **1** were *n = 0.141 (0.003) and k = 3.435 (0.024).*

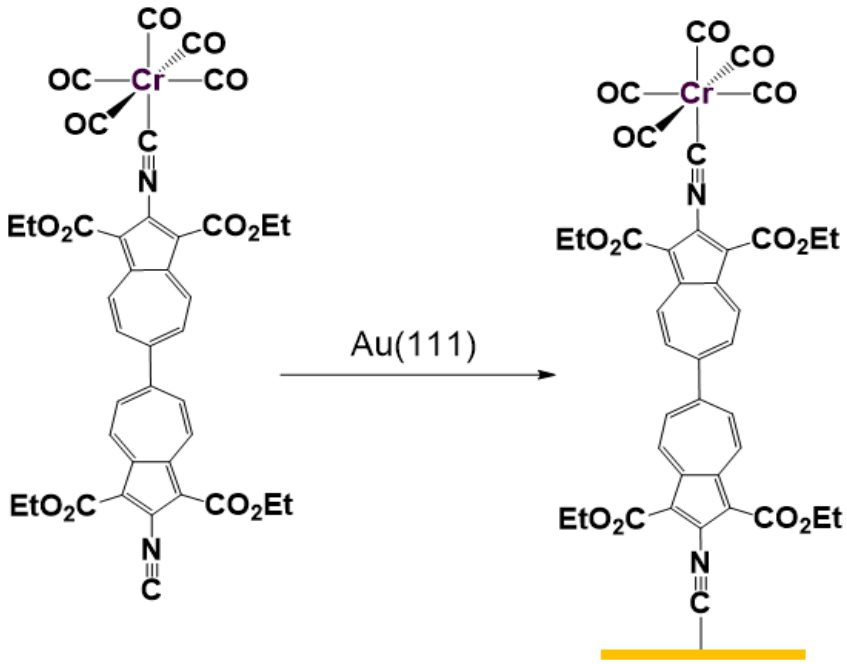

Figure 4.7. Illustration showing how the molecules of **1** bind to the gold substrates via anchoring through the isocyanide junction group in an upright orientation.

IV.2.1.2. SAM formation of 2-isocyano-2'-mercapto-1,1',3,3'-tetraethoxycarbonyl-6,6'-biazulene capped with a $Cr(CO)_5$ moiety at the 2-isocyano terminus (2) on Au (111) film

The gold-coated silicon substrates were cleaned and SAMs of **2** were formed following the protocol described in the general procedures and starting materials section. The SAM-coated substrates were rinsed with chloroform to remove any physisorbed molecules on the films, dried with a stream of nitrogen gas and stored in a clean vial for analyses. No precaution to exclude air or ambient laboratory lighting was exercised during these SAM experiments.

Surface IR (RAIR) and ellipsometry analyses were performed on the SAMs of **2**. The surface IR measurements were conducted as described in the general procedures and starting materials section' 10,000 scans of the spectrum were collected at a resolution of 2 cm^{-1}. The ellipsometric thickness of the SAM was obtained at five different spots using average optical

constants *n = 0.151 (0.007) and k = 3.420 (0.006)* for **2** while assuming a refractive index of 1.45 for the organic thin film.

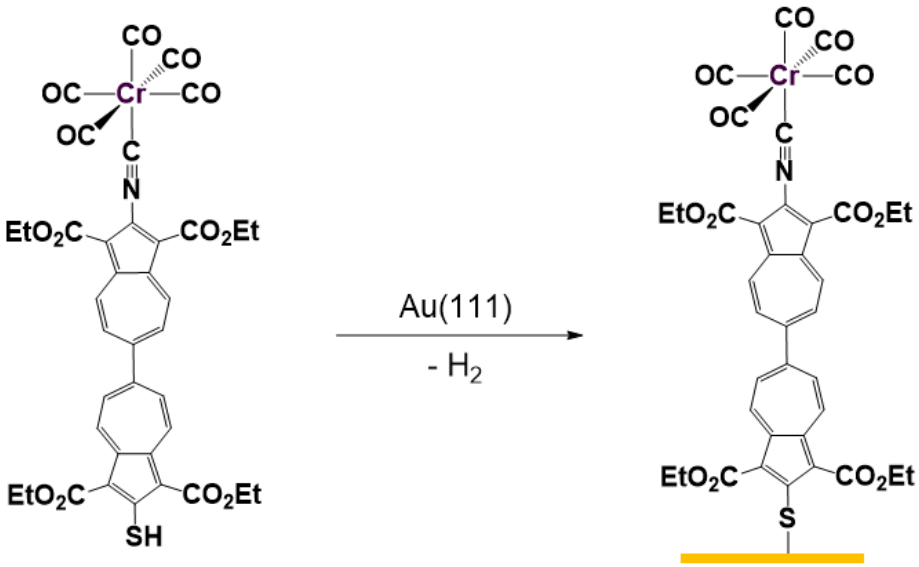

Figure 4.8. Illustration showing how molecules of **2** bind to the gold substrates via anchoring through the thiolate junction in an upright orientation.

IV.2.1.3. Experimental procedures for SAM Displacement

An adsorption competition study aimed to analyze the relative stability and binding affinity of **1** vs. **2** on gold substrates was carried out. The SAMs of **1** were formed by immersing gold substrates into a 2 mM solution of **1** in chloroform. After the SAMs of **1** were made, the films were thoroughly rinsed with chloroform to remove any physisorbed molecules, dried with a stream of nitrogen gas, and characterized by both optical ellipsometry and RAIR spectroscopy to affirm the monolayer formation. After these analyses, the SAMs of **1** on gold were placed in a 2 mM solution of **2** in chloroform for *ca.* 24 hours to determine if the SAM of **1** would undergo displacement with the molecules of **2**. The resulting films were thoroughly rinsed with chloroform, blow-dried with

a stream of nitrogen gas, and characterized using ellipsometry and RAIR. A trial to reverse the new monolayer of **2** on the substrate back to that of **1** was performed to check if the displacement of the molecules on the film were reversible. A SAM film of compound **2** on Au (111) was immersed back into *ca.* 2 mM solution of **1** in chloroform for 48 hours followed by the RAIR spectroscopic analysis.

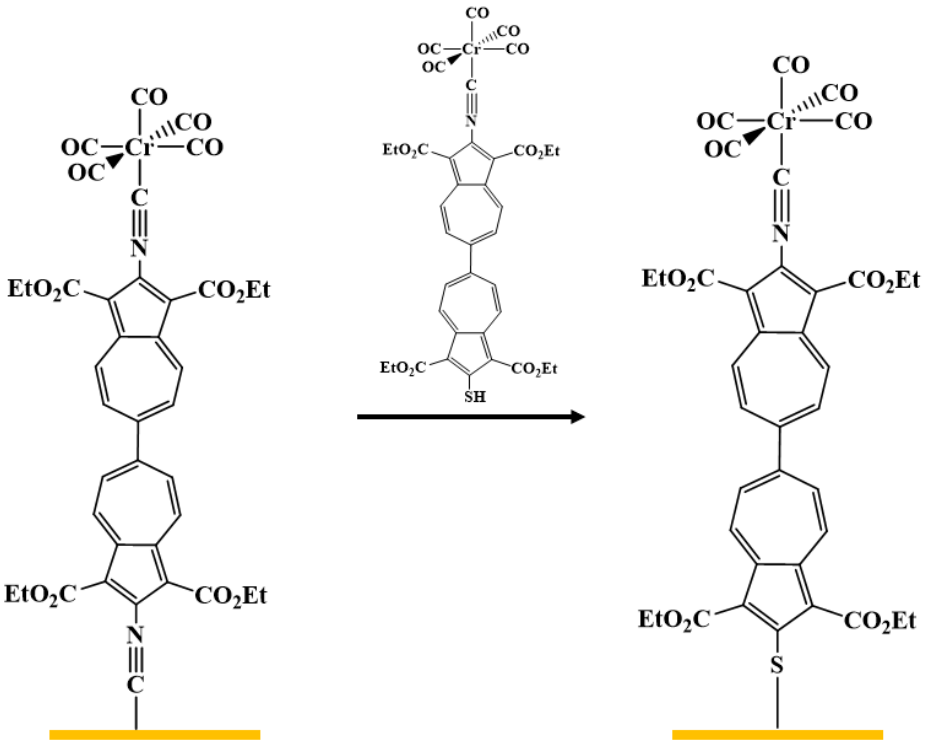

Figure 4.9. An illustration of the competitive displacement experiment.

IV.3. Results and Discussion

SAMs, made using a 3 mM solution of **1** in distilled dichloromethane and a 2 mM solution of **2** in chloroform without protection from air, were observed to have average thicknesses of 23.8*(2.5)* Å and 20.12*(3.7)* Å, respectively. The calculated SAM thicknesses for **1** and **2** binding in the upright orientation, are 23.7 Å and 23.3 Å; well within the error of the experimental results. The theoretical thicknesses were calculated based on X-ray crystallographic measurements. For the calculations, 2.45 Å was added to the computed thickness to account for an Au–S bond length while for the Au–C bond length, 2 Å is included to account for the Au-C bond. The calculation supports that the film is a single layer thick on the surface indicating no formation of multilayers. But assessing binding, packing, and orientation of our molecules on the substrate through ellipsometric thickness alone is impossible. The use of infrared spectroscopy provides further information on the molecular binding, packing, and orientation of the molecule on the gold substrate. IR provides information about the binding groups used to make junctions at the surface and about the orientation of the molecules on the substrate.

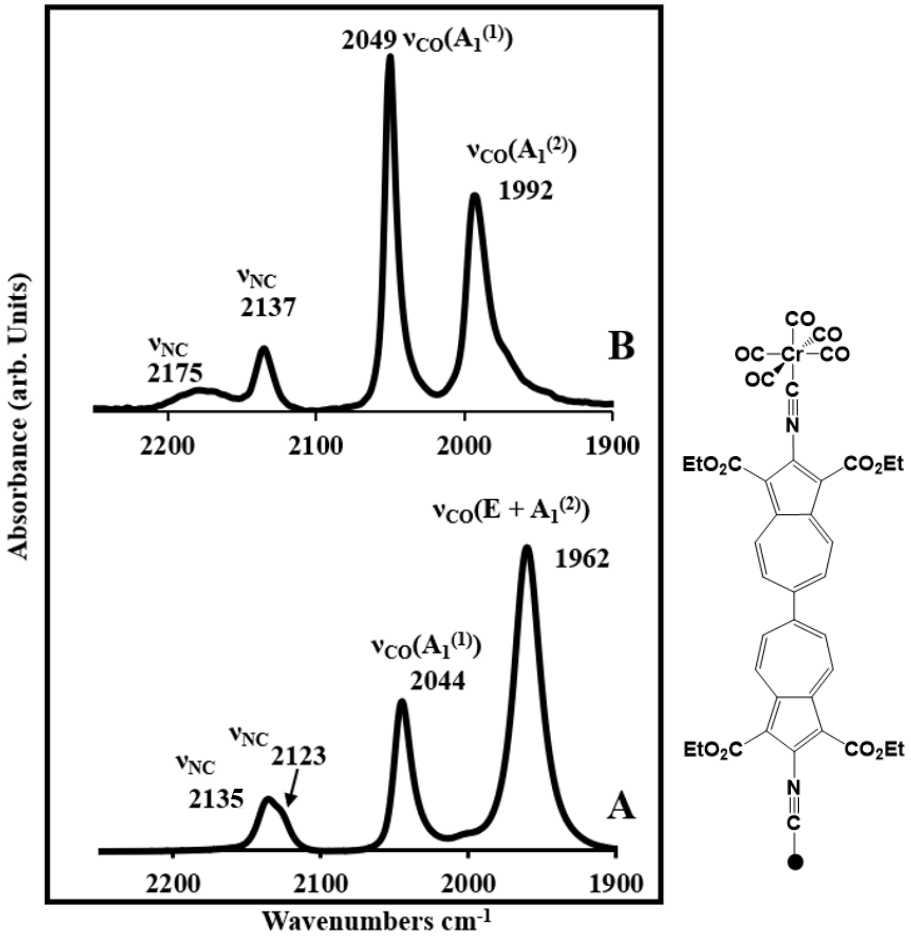

Figure 4.10. (A) FTIR spectrum of **1** in dichloromethane solution; (B) RAIR spectrum of **1** adsorbed on Au (111) film. (C) Illustration of the upright coordination of **1** adsorbed on the gold substrate via the isocyanide junction group.

The solution IR spectrum of **1** and the RAIR spectrum of **1** adsorbed on Au(111) film are shown in Figure 4.10 and illustrate the vibrational signatures of **1** before and after SAM formation. These IR spectra focus on the ν(CN) and ν(CO) vibrational regions and appear quite different from each other because of the fundamental differences in the bulk versus surface. Similar to the observed RAIR of **1** in chapter 3, there should be five IR-active stretching vibrations for **1** in the ν(CO) and ν(CN) IR regions, but the peaks are not resolved due to broad overlapping band, hence four bands are seen. Two of the bands correspond to the ν(CN) stretching vibrations of the

uncomplexed isocyanide group and the Cr-bound isocyanide group. Whereas the Cr-bound isocyanide stretching frequency does not change much upon adsorption of **1,** the ν(CN) value for the uncomplexed isocyanide shifts dramatically upon the SAM formation on Au(111). Indeed, in the solution-phase FTIR spectrum, the Cr-bound isocyanide stretching frequency is 2135 cm^{-1} while the uncomplexed isocyanide group's ν(CN) is at 2123 cm^{-1} (see Figure 4.10). Upon adsorption of **1** on the gold surface, the ν(CN) band for the Cr-bound isocyanide group is at 2137 cm^{-1} and the ν(CN) band for the gold-bound 2-isocyano terminus undergoes a blue shift to 2175 cm^{-1} indicating chemisorption of **1** on the gold substrate. The free isocyanide's carbon lone pair is donated to the gold upon SAM formation, thereby strengthening the junction's C≡N bond. If the molecules of **1** are oriented upright within the SAM on gold, the four *cis*-CO ligands of the $[Cr(CO)_5]$ moiety would be positioned approximately parallel to the Au surface and, therefore, the ν(CO) vibration of E symmetry would be forbidden according to the surface IR selection rules. As a result, only two ν(CO) vibrations of the $[Cr(CO)_5]$ unit, both of A_1 symmetry, would be surface IR allowed. The E ν(CO) band at 1962 cm^{-1} overlapping with the $A_1^{(2)}$ ν(CO) band in the solution IR spectrum of **1** loses its intensity upon the SAM formation of **1**, which uncovers the significantly blue-shifted $A_1^{(2)}$ ν(CO) band. The other symmetric ν(CO) vibration, $A_1^{(1)}$, that corresponds to the band at 2044 cm^{-1} in the solution IR spectrum of **1**, also undergoes a blue shift and gains intensity with respect to other ν(CN)/ν(CO) bands upon adsorption of **1** on the gold surface. This indicates reduction in the $d\pi(Cr) \rightarrow p\pi^*(CO)$ backbonding and suggests the electron-withdrawing effect of the gold surface that is communicated through the 6,6′-biazulenic linker. Therefore, the $[Cr(CO)_5CNR]$ fragment is sensitive to electronic perturbation induced by the adsorption of the isocyano anchoring group of **1** to the gold surface. The RAIR spectroscopic and ellipsometric data

discussed above suggest an upright orientation of the molecules of **1** upon their adsorption to the Au(111) surface via the isocyanide anchoring groups.

The FTIR spectrum of **2** in solution features four distinct bands in the ν(CN)/ν(CO)/ν(SH) regions as shown in Figure 4.11a. The IR band at 2587 cm^{-1} in the solution FTIR spectrum of **2** corresponds to the stretching vibration of the thiol group (see inset in Figure 4.11a), whereas the band at 2137 cm^{-1} reflects the ν(CN) vibration of the Cr-bound isocyano group. The group theoretical analysis predicts three ν(CO) bands for the C_{4v}-symmetric [$Cr(CO)_5$] unit if no overap occurs: two symmetric vibrations of A_1 symmetry and a degenerate ν(CO) vibration of E symmetry. Similar to the case of compound **1**, one of the ν(CO) bands of A_1 symmetry ($A_1^{(2)}$) overlaps with the intense E-band in the solution FTIR spectrum of **2**. These overlapping $A_1^{(2)}$ and E ν(CO) bands for **2** occur at 1960 cm^{-1} while the remaining $A_1^{(2)}$ ν(CO) peak is at 2046 cm^{-1}. Figure 4.11b illustrates the RAIR spectrum of **2** adsorbed on Au(111). This RAIR spectrum shows no ν(SH) band since the chemisorption of **2** involves formation of the thiolate junction and, presumably, release of H_2. [27-29] As in the case of **1** adsorbed on Au(111), the gold surface in the SAM of **2** on Au(111) exerts an electron-withdrawing effect, thereby increasing the π-acidity of the 2-isocyanoazulene junction at the opposite end of the biazulenic linker. This decreases the electron richness of the chromium(0) center, which is manifested via blue shifts of both ν(CO) bands of A_1 symmetry upon formation of the thiolate-anchored SAM. The SAM formation involves a hollow-linear coordination of the thiolate junctions to the gold surface, inducing an S→Au(111) charge transfer *via* S(*3p*)–Au(*π*) bonding.[30-31] Only one ν(CN) band is observed in both the solution IR and the RAIR at *ca.* 2138 cm^{-1} implying that there is no change in ν(CN) upon chemisorption. The ν(Au–S) vibration expected at *ca.* 400 cm^{-1} would be impossible to document using the FTIR spectrometer's frequency window (600 cm^{-1} – 4000 cm^{-1}) employed in this study.

The chromium pentacarbonyl moiety, however, is an excellent infrared reporter, and the observed ν(CO) bands clearly indicate an approximately upright orientation of the molecules of **2** (minus H•) on the gold film. In the RAIR spectrum shown in Figure 4.11b, the two ν(CO) bands are labeled as $A_1^{(1)}$ and $A_1^{(2)}$ and occur at 2052 cm^{-1} and 1986 cm^{-1}, respectively. The ν(CO) vibration of E symmetry would be IR-forbidden in the RAIR spectrum of **2** on Au(111) if the cis-CO ligands are positioned strictly parallel to the gold surface. The weak shoulder at the lower energy side of the ν(CO) $A_1^{(2)}$ band likely to corresponds to the ν(CO) vibration of E symmetry. This E ν(CO) band would not vanish completely upon chemisorption of **2** if the molecules within the SAM are even slightly tilted with respect to the gold surface. Another key observation is the blue shifts in energy for the $A_1^{(1)}$ and $A_1^{(2)}$ ν(CO) bands upon going from the solution IR spectrum of **2** to the corresponding RAIR spectrum. The larger shift the $A_1^{(2)}$ ν(CO) band compared to the $A_1^{(1)}$ ν(CO) band is due to greater contribution of the *trans*-CO stretch to the former.[8,35] Both the RAIR spectroscopic and ellipsometric data support the conclusion that **2** adsorbs on the Au(111) surface via anchoring of the thiolate junction and the molecules within the resulting SAM are oriented nearly perpendicular to the gold surface.

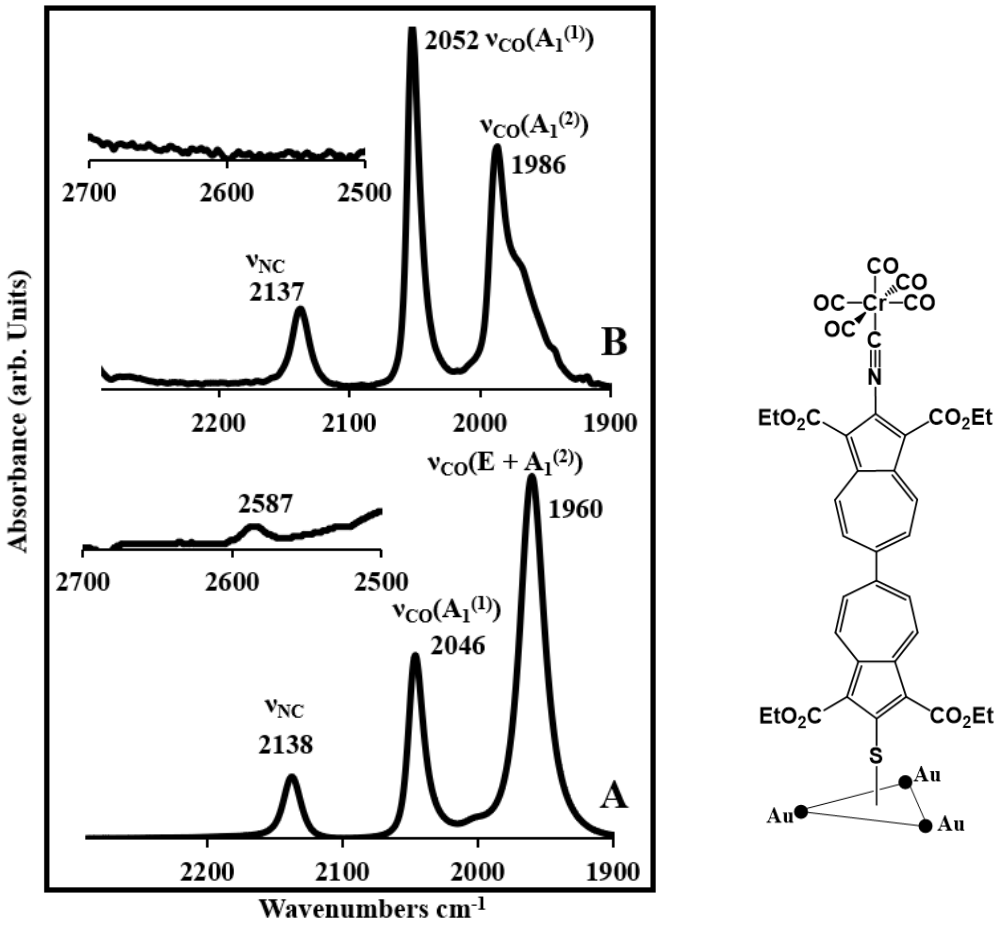

Figure 4.11. (A) FTIR spectrum of **2** in CH_2Cl_2 solution. (B) RAIR spectrum of **2** adsorbed on Au (111) film. (C) Illustration of the hollow-linear coordination of SAM of **2** adsorbed on the gold substrate via the thiolate junction.

Analyses of SAM of **1** were done to verify the quality of the film before using the film for the displacement competition. Ellipsometry and RAIR analysis showed that the molecules on the film were a layer thick and are coordinated vertically on the gold substrates. The four IR bands in the RAIR spectrum depicted in Figure 4.12a indicate ν(CN) stretching frequencies for the Cr-bound isocyanide group and the Au-coordinated isocyanide group at 2137 cm^{-1} and 2175 cm^{-1} respectively, and two symmetric ν(CO) stretching frequencies for $A_1^{(1)}$ and $A_1^{(2)}$ at 2049 cm^{-1} and

1992 cm^{-1} respectively. Note that the peak at 2175 cm^{-1} represents the formation of ν(C≡N) bond when the isocyanide coordinate to the gold substrate. The SAM displacement analyses done suggested that SAM of **1** was entirely displaced by **2,** forming a layer thick SAM of **2** on the gold film. The ellipsometry and the RAIR were used to analyze the new film. The disappearance of the peak at 2175 cm^{-1} is indicative that no ν(C≡N) bond is present in the film. The RAIR results of the new film (Figure 4.12b) reveal only three IR-active bands in the ν(CN)/ν(CO) region, corresponding to the vibrations from the Cr-bound isocyanide group and the [$Cr(CO)_5$] fragment. Hence, a Au–S bond must have been formed during the displacement of **1** by **2** on the gold film. The observed results imply that desorption of isocyano-bound monolayers and formation of thiolate-bound monolayers occurred upon immersing the SAM of **1** in 2. When the SAM of **2** was immersed back into a solution of **1**, no spectroscopic evidence of **1** displacing **2** was observed even after 48 h. The Au–S bond energy is about 20 kcal/mol stronger than the Au–C bond[32-34] which corroborates the above findings. The RAIR spectrum shows almost no shoulder peaks at the lower energy side of the ν(CO) band of $A_1^{(2)}$ symmetry as compared to Figure 4.11b. When the SAM films of **1** were immersed in the solution of **2,** the molecules in the solution vertically attach themselves to the gold film, displacing **1** and better ordered monolayer (see Figure 4.11b) is observed for the newly formed SAMs resulting in better molecular packing of the film.

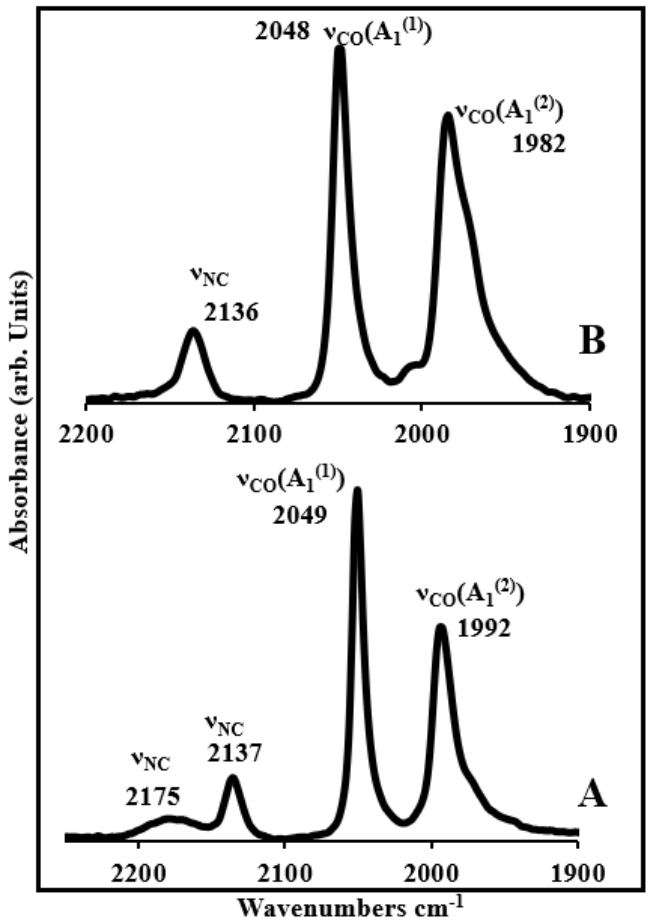

Figure 4.12. RAIR spectrum from the displacement studies of the SAM of **1** (A) before immersion and (B) after immersion into a solution of **2** in chloroform.

IV.4. Conclusions and outlook

In this chapter, the molecular packing, orientation, thickness, the influence of junction groups on SAM formation, and stability using SAM displacement analysis were studied. The first SAMs involving biazulenic scaffolds, with asymmetric anchoring on gold film, using isocyano and thiolate junction groups have been presented. The infrared results suggested that either coordination via the isocyano or thiolate junction group would result in upright orientation of the adsorbed molecules on the gold surface. Moreover, the C_{4v}-symmetric $[Cr(CO)_5CN-]$ moiety

served as a remote informative infrared reporter supporting the upright orientation of the monolayers. The ellipsometric thicknesses corroborate with the conclusions, that the molecules are uprightly oriented, derived from infrared spectroscopy. Both junction groups employed in this work form stable SAM films although the displacement competition supports that thiolate-anchored monolayers show stronger gold-junction bonding/interaction than the isocyano-anchored monolayers. The findings in this work show that SAM displacement route will influence the molecular packing. Carrying out imaging studies using microscopy techniques, AFM, to investigate the molecular packing of SAM films made via SAM displacement method may help probe the topography images in AFM analysis. Athough the ethoxycarbonyl substituents present in **1** and **2** may be undesirable due to steric hindrances exerted in the vicinity of the junction groups which may affect the molecular packing of the films made, the measured ellipsometric thickness and RAIR spectroscopic data showed any influence of the substituents on the SAM film does not affect the binding of the molecule to the gold. Perhaps it will be interesting to qualitatively analyze the packing density of the SAM films.

The well-defined molecular films described in this work may open opportunity to experimentally probe the conductive behavior of an asymmetrically anchored biazulenyl framework for molecular electronics. Hence, the use of STM to study charge transport may be considered since topography and conductivity can be simultaneously addressed during an experiment.

IV.5. References

1. Zhou, K.-g.; Zhang, Y.-h.; Wang, L.-j.; Xie, K.-f.; Xiong, Y.-q.; Zhang, H.-l.; Wang, C.-w., Can Azulene-Like Molecules Function as Substitution-Free Molecular Rectifiers? *Physical Chemistry Chemical Physics* **2011**, *13*, 15882-15890.
2. Barybin, M. V., Nonbenzenoid Aromatic Isocyanides: New Coordination Building Blocks for Organometallic and Surface Chemistry. *Coordination Chemistry Reviews* **2010**, *254*, 1240-1252.
3. Robinson, R.; Holovics, T. C.; Deplazes, S.; Powell, D.; Lushington, G.; Thompson, W.; Barybin, M., Five Possible Isocyanoazulenes and Electron- Rich Complexes Thereof: A Quantitative Organometallic Approach for Probing Electronic Inhomogeneity of the Azulenic Framework. *Organometallics* **2005**, *24*, 2386-2397.
4. Barybin, M.; Chisholm, M.; Dalal, N.; Holovics, T.; Patmore, N.; Robinson, R.; Zipse, D., Long-range Electronic Coupling of MM Quadruple Bonds (M = Mo or W) via a 2,6-Azulenedicarboxylate Bridge. *Journal of the American Chemical Society* **2005**, *127*, 15182-15190.
5. Treboux, G.; Lapstun, P.; Silverbrook, K., Asymmetric I / V Characteristics in Nonalternant Carbon Networks. *The Journal of Physical Chemistry B* **1998**, *102*, 8978-8980.
6. Shevyakov, S. V.; Li, H.; Muthyala, R.; Asato, A. E.; Croney, J. C.; Jameson, D. M.; Liu, R. S. H., Orbital Control of the Color and Excited State Properties of Formylated and Fluorinated Derivatives of Azulene. *The Journal of Physical Chemistry A* **2003**, *107*, 3295-3299.
7. Holovics, T. C.; Robinson, R. E.; Weintrob, E. C.; Toriyama, M.; Lushington, G. H.; Barybin, M. V., The 2,6- Diisocyanoazulene Motif: Synthesis and Efficient Mono- and Heterobimetallic Complexation with Controlled Orientation of the Azulenic Dipole. *Journal of the American Chemical Society* **2006**, *128*, 2300-2309.
8. Applegate, J. C.; Okeowo, M. K.; Erickson, N. R.; Neal, B. M.; Berrie, C. L.; Gerasimchuk, N. N.; Barybin, M. V., First π-Linker Featuring Mercapto and Isocyano Anchoring Groups within the same Molecule: Synthesis, Heterobimetallic Complexation and Self-assembly on Au(111). *Chemical Science* **2016**, *7*, 1422-1429.
9. Maher, T. R.; Meyers, J. J.; Spaeth, A. D.; Lemley, K. R.; Barybin, M. V., Diisocyanoarene- linked Pentacarbonylvanadate(I) ions as Building Blocks in a Supramolecular Charge-transfer Framework Assembled through Noncovalent and Contact Ion Interactions. *Dalton Transactions* **2012**, *41*, 7845-7848.
10. Neal, B. M.; Vorushilov, A.; Delarosa, A.; Robinson, R.; Berrie, C.; Barybin, M., Ancillary Nitrile Substituents as Convenient IR Spectroscopic Reporters for Self-assembly of Mercapto- and Isocyanoazulenes on Au(111). *Chemical Communications* **2011**, *47*, 10803-10805.
11. Maher, T.; Spaeth, A. D.; Neal, B. M.; Berrie, C.; Thompson, W.; Day, V.; Barybin, M., Linear 6,6 '- Biazulenyl Framework Featuring Isocyanide Termini: Synthesis, Structure, Redox Behavior, Complexation, and Self- Assembly on Au(111). *Journal of the American Chemical Society* **2010**, *132*, 15924-15926.
12. Dutta, S.; Lakshmi, S.; Pati, S., Comparative Study of Electron Conduction in Azulene and Naphthalene. *Bulletin of Materials Science* **2008**, *31*, 353-358.
13. Wächter, T.; Scheetz, K. J.; Spaeth, A. D.; Barybin, M. V.; Zharnikov, M., Dynamics of Electron Transfer in Azulene- Based Self-Assembled Monolayers. *The Journal of Physical Chemistry C* **2017**, *121*, 13777-13785.

14. Schwarz, F., Charge Transport and Conductance Switching of Redox-Active Azulene Derivatives. *Angewandte Chemie International Edition* **2016**, *55*, 11781-11786.
15. Van Dyck, C.; Ratner, M. A., Molecular Rectifiers: A New Design Based on Asymmetric Anchoring Moieties. *Nano Letters* **2015**, *15*, 1577-1584.
16. Lee, Y.; Carsten, B.; Yu, L., Understanding the Anchoring Group Effect of Molecular Diodes on Rectification. *Langmuir* **2009**, *25*, 1495-1499.
17. Mallick, G., *Scanning Tunneling Microscopic Characterization of an Engineered Organic Molecule*. Aberdeen Proving Ground, MD : Army Research Laboratory: Aberdeen Proving Ground, MD, **2011**.
18. Maher, T. R.; Spaeth, A. D.; Neal, B. M.; Berrie, C. L.; Thompson, W. H.; Day, V. W.; Barybin, M. V., Linear 6,6′-Biazulenyl Framework Featuring Isocyanide Termini: Synthesis, Structure, Redox Behavior, Complexation, and Self-Assembly on Au(111). *Journal of the American Chemical Society* **2010**, *132*, 15924-15926.
19. Van Dyck, C.; Ratner, M. A., Molecular Rectifiers: A New Design Based on Asymmetric Anchoring Moieties. *Nano Letters* **2015**, *15*, 1577-1584.
20. Su, W.-X.; Zuo, X.; Xie, Z.; Zhang, G.-P.; Wang, C.-K., Obvious modulation of rectifying performance by conjugation breaking of the bridging fragment in donor-bridge-acceptor molecular diodes. *RSC Advances* **2017**, *7*, 14200-14205.
21. Sun, S.; Zhuang, X.; Wang, L.; Zhang, B.; Ding, J.; Zhang, F.; Chen, Y., Azulene-bridged Coordinated Framework Based Quasi-molecular Rectifier. *Journal of Materials Chemistry C* **2017**, *5*, 2223-2229.
22. Applegate, J. C.; Okeowo, M. K.; Erickson, N. R.; Berrie, C.; Gerasimchuk, N. N.; Barybin, M. V., ., Biazulenic π-linker featuring isocyano and mercapto anchoring termini in the same molecule: Synthesis, self-assembly on gold film, redox behavior, and heterobimetallic complexation. *Manuscript In Preparation*.
23. Wasserman, S. R.; Whitesides, G. M.; Tidswell, I. M.; Ocko, B. M.; Pershan, P. S.; Axe, J. D., The Structure of Self-Assembled Monolayers of Alkylsiloxanes on Silicon: A Comparison of Results from Ellipsometry and Low-Angle X-Ray Reflectivity. *Journal of the American Chemical Society* **1989**, *111*, 5852-5861.
24. Le Grange, J. D.; Markham, J. L.; Kurkjian, C. R., Effects of Surface Hydration on the Deposition of Silane Monolayers on Silica. *Langmuir* **1993**, *9*, 1749-1753.
25. Clear, S. C.; Nealey, P. F., Lateral Force Microscopy Study of the Frictional Behavior of Self-Assembled Monolayers of Octadecyltrichlorosilane on Silicon/Silicon Dioxide Immersed in n-Alcohols. *Langmuir* **2001**, *17*, 720-732.
26. Wang, J.; Li, G.; Li, Q.-S.; Xie, Y.; King, R. B., Isocyanide Versus Nitrile Ligands and Methyl Versus Trifluoromethyl Substituents in Metal Carbonyl Chemistry. *Polyhedron* **2012**, *47*, 165-172.
27. Love, J.; Estroff, L.; Kriebel, J.; Nuzzo, R. G.; Whitesides, G., Self-Assembled Monolayers of Thiolates on Metals as a Form of Nanotechnology. *Chemical Reviews* **2005**, *105*, 1103-1169.
28. Chu, C.; Ayres, J. A.; Stefanescu, D. M.; Walker, B. R.; Gorman, C. B.; Parsons, G. N., Enhanced Conduction through Isocyanide Terminal Groups in Alkane and Biphenylene Molecules Measured in Molecule/Nanoparticle/Molecule Junctions. *The Journal of Physical Chemistry C* **2007**, *111*, 8080-8085.
29. Cossaro, A.; Mazzarello, R.; Rousseau, R.; Casalis, L.; Verdini, A.; Kohlmeyer, A.; Floreano, L.; Scandolo, S.; Morgante, A.; Klein, M. L.; Scoles, G., X-ray Diffraction and Computation Yield the Structure of Alkanethiols on Gold(111). *Science* **2008**, *321*, 943-946.

30. Tachiban, M.; Yoshizawa, K.; Ogawa, A.; Fujimoto, H.; Hoffman, R., Sulfur- Gold Orbital Interactions, which Determine the Structure of Alkanethiolate/ Au (111) Self- Assembled Monolayer Systems. *Journal of Physical Chemistry B* **2002**, *106*, 12727-12736.
31. Sellers H., U. A.; Shnidman Y.; E., E. J., Modeling Chemisorption Processes with Metal Cluster Systems: III. Model Thio-Alkyls on Gold Surfaces. *NATO ASI Series (Series B: Physics)* **1992**, *283*, 441-452.
32. Dubois, L. H.; Nuzzo, R. G., Synthesis, Structure, and Properties of Model Organic Surfaces. *Annual Review of Physical Chemistry* **1992**, *43*, 437-463.
33. Nuzzo, R. G.; Zegarski, B. R.; Dubois, L. H., Fundamental Studies of the Chemisorption of Organosulfur Compounds on Gold(111). Implications for Molecular Self-assembly on Gold Surfaces. *Journal of the American Chemical Society* **1987**, *109*, 733-740.
34. Neal, B. M.; Vorushilov, A.; Delarosa, A.; Robinson, R.; Berrie, C. L.; Barybin, M. V., Ancillary nitrile substituents as convenient IR spectroscopic reporters for self- assembly of mercapto- and isocyanoazulenes on Au(111). *Chemical Communications* **2011**, *47*, 10803-10805.

35. Davies, M. S.; Armstrong, R. S.; Aroney, M. J.; Chronika, C., Metal-ligand p bonding in LM(CO)5 Complexes - A Vibrational Spectroscopy Study. *New Series* **1995**, *24*, 233-252.

Chapter V:

Assessment of periodicity and packing of self-assembled monolayer films of isocyano- and mercaptoazulenes adsorbed on Au (111) using atomic force microscopy (AFM)

V.1. Structural arrangement and topography of azulenic self-assembled monolayer films on the Au (111) surface

Isocyano- and mercaptoazulene self-assembled monolayers (SAMs) on metal substrates with potential use in organic electronics were investigated using atomic force microscopy (AFM) techniques. Information on molecular packing, stability, and molecular orientation of azulenic films on gold have been studied using different analytical techniques, such as ellipsometry, RAIR, AES, and XPS, but experimental information on either the topography, packing geometry, or periodicity has been hitherto unavailable. Resolved molecular-scale images of azulenic SAMs from microscopy experiments may facilitate assessment of the packing of the azulenic molecules within the films.

Contact mode AFM measurements in ambient conditions were conducted to investigate the packing of the azulenic molecules relative to the Au(111) lattice of the substrate. Molecular layers formed from molecules with both isocyanide and thiol linkers were investigated to determine the influence of the linker's nature on packing. Ordered arrays of the azulenyl thiolates were obtained using a two-step displacement procedure to improve the ordering of the film and reduce the number of defects. Specifically, the first molecular resolution images of 2-isocyanoazulene and 2-mercaptoazulene adsorbed on the Au (111) using contact mode AFM were obtained with an emphasis placed on the structural arrangement, molecular packing, stability, geometry, and periodicity.

V.2. Introduction to scanning probe microscopy

Scanning probe microscopy (SPM) refers to a range of techniques in which scanning probe tips are used to spatially resolve different materials' properties including topography, conductivity, friction, adhesion, magnetization, etc. [1-5] Atomic force microscopy (AFM) is a type of SPM

technique employed in this study. In AFM, a sharp probe tip is raster scanned across the surface to build a topographic image of the sample with angstrom resolution. Other types of SPM are scanning tunneling microscope STM, conductive AFM, lateral force microscope LFM, force modulation microscopy, magnetic force microscopy MFM, electric force microscopy EFM, and surface potential microscopy, etc.[6] Different surface physical properties can be investigated using a combination of these techniques. Features like the electrostatic potential, surface roughness, nanomechanical properties or molecular geometry may be evaluated depending on the experimental set-up employed. [1-5]

The technique used in an experimental analysis depends on the type of sample surface and the desired information required from the analysis. The most popular methods for analyzing surface roughness and morphology are the STM and AFM. STM and AFM were invented in 1982 (by Binning, Rohrer, Gerber, and Weihel) and 1986 (by Binning, Quate, and Gerber), respectively, at IBM (STM) and Stanford University (AFM). In STM, a conducting or semiconducting sample is required. Tunneling current under an applied bias or tip-sample distance as a function of constant current is measured.[6] AFM is based on the interaction forces between the tip and sample, therefore it does not rely on measuring current.[6] One of the most powerful characteristics of AFM is its flexibility in the types of substrates that can be investigated and the environmental conditions in which it is operated. Also, AFM can be used in both liquid and gas environments. AFM sharp probe tip is made of silicon or silicon nitride on a cantilever. The probe movement reveals surface topography. Figure 5.1 is a diagrammatic representation of an AFM experiment. In general, two main components are involved in AFM: a piezoelectric scanner and AFM detection system.

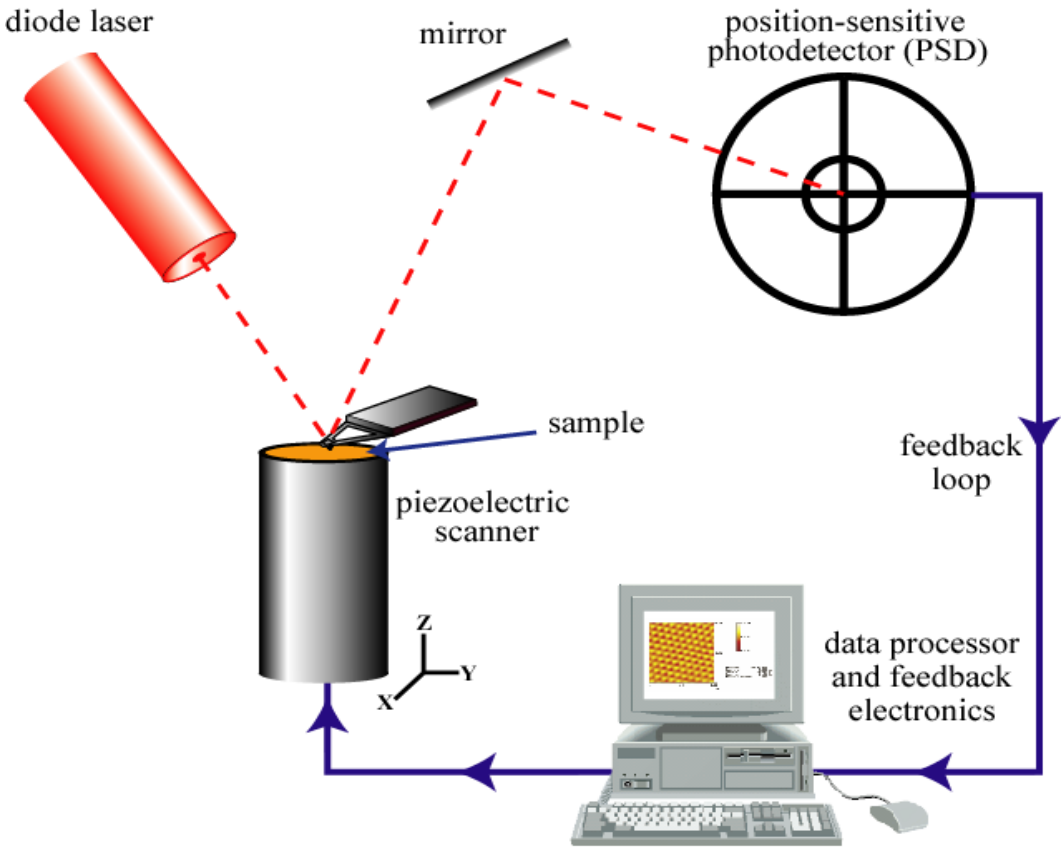

Figure 5.1. Diagrammatic representation of an AFM experiment. (Courtesy of Dr. Jill Headrick).

The general operation of AFM involves monitoring the interaction forces between the tips and sample.[7-8] The sample is placed on a piezoelectric scanner and a voltage is applied to the piezo material.[9] The piezoelectric material can change shape and move in a controlled way due to the application of different voltages. Thus, scanning the applied voltage allows precise angstrom level motion of the sample on the scanner. A setpoint force is chosen, and as the tip scans over the sample, the voltage on the z-piezo is adjusted to move the sample up or down to keep the force constant. Monitoring the z-piezo voltage allows the topography of the surface to be mapped. The laser is focused on the reflective cantilever tip and the movement of the laser. As the sample is scanned across, the response is monitored by a position-sensitive photodetector (PSD).[9] The

signals obtained are then sent to the computer control feedback loop as illustrated in Figure 5.1. The feedback loop keeps the cantilever deflection constant by adjusting the applied voltage to the Z scanner while the cantilever tip is in contact with the substrate. The cantilever tip used in this work is a robust silicon nitride AFM probe. Different cantilever lengths, materials, and shapes allow for varied spring constants and resonant frequencies. The spring constant and resonant frequencies employed during AFM imaging are determined by the kind of surface/sample being imaged.

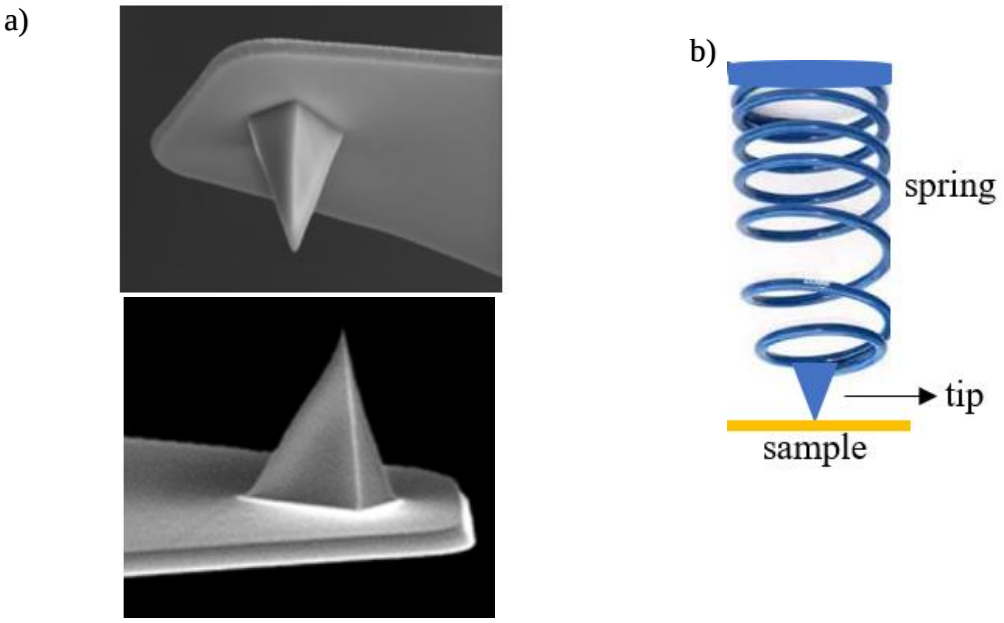

Figure 5.2. a) SEM image of a typical probe tip employed. DNP tip (top) and MSNL tip (bottom).[39] b) Spring depiction of the cantilever.

Figure 5.2 (a) shows a scanning electron microscope image (SEM) of the probe tip used in this work. The MSNL tip is made sharper than the DNP tip. The force exerted between the probe tip and the sample is dependent on the probe-sample distance and the spring constant of a flexible cantilever that supports the probe. The force is governed by Hooke's Law $F = -kx$, *where k*

represents the spring constant (N/m) and x is the cantilever deflection from its rest position. Typical spring constants of the tip used range from 0.01 N/m - 14 N/m. The quality of AFM cantilevers is dependent not only on the spring constant but also the resonant frequency and tip radius of curvature. The resonance frequency at which the tip oscillates usually ranges from 7 kHz - 400 kHz, depending on its stiffness. The tip shape and radius of curvature affect the image resolution. The tip radius usually ranges from 5 nm - 50 nm. The sharper the tip, the better the image resolution.

A force curve is usually employed to set the imaging force in contact mode and measure the surface mechanical properties, like stiffness and tip-surface interaction. The force curve graph shown in Figure 5.3 represents the tip-sample interaction plots, for both approach and retract curves, where the vertical axis is the cantilever deflection while the horizontal axis is the distance of the scanner movement. The force curve reflects tip-sample attractive, repulsive, and adhesive interactions. The tip deflects upward or downward before making contact with the sample whenever the tip experiences long-range attractive or repulsive interactions, as shown in Figure 5.3. As the cantilever tip approaches the surface (A), it may experience enough attractive forces that cause the tip to bend and contact (B) the substrate. Once the tip is in contact (C) with the substrate, the fixed end of the cantilever moves closer to the surface, causing an increase in the cantilever deflection until it is retracted. When the cantilever reaches a maximum predefined force value, the approach curve ends and the retract curve begins. Due to adhesion (D), the cantilever oftentimes remains in contact with the surface beyond the point of jump-to-contact in the attract curve. As the cantilever is withdrawn, the restoring force in the cantilever overcomes the adhesion force between the tip and the sample and the tip pops off the surface and returns to its free deflection position (E), possibly causing the cycle to restart.

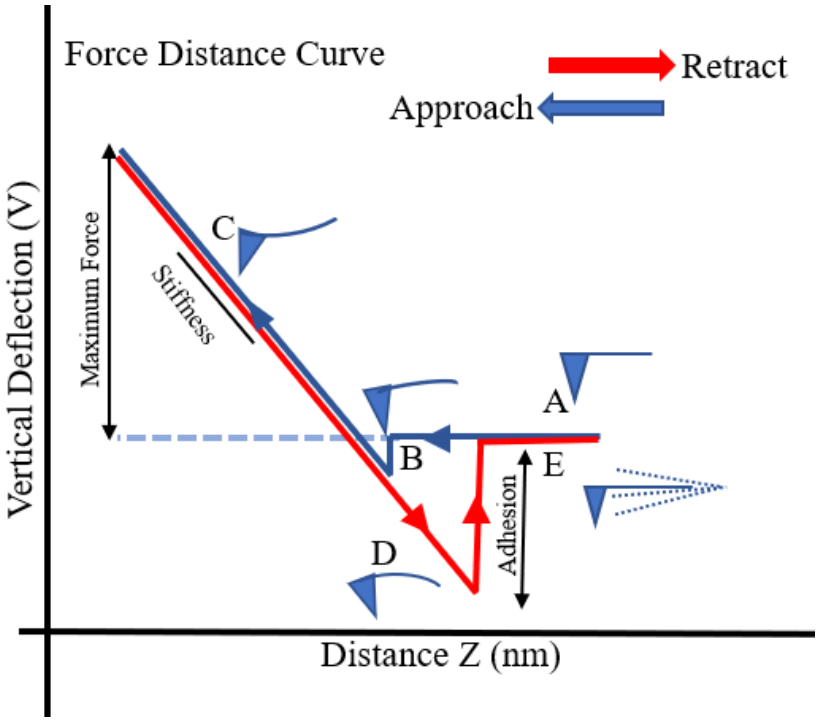

Figure 5.3. Schematic depiction of a Force calibration plot. The horizontal axis, describes Distance Z (nm), is the distance of the scanner movement, and the vertical axis refers to the vertical deflection (V) of the cantilever tip.[10]

The AFM instrument scans in three modes: contact mode, non-contact mode, and tapping mode as illustrated in Figure 5.4.[6, 10] The contact mode AFM operates with the AFM tip in contact with the surface through the adsorbed fluid layer. The contact mode is heavily influenced by adhesion and frictional forces. There are possibilities of distorting the image data or damaging the sample due to the applied force. In the non-contact mode AFM, the tip does not make contact with the sample surface, but rather oscillates above the adsorbed fluid layer on the surface during scanning.[6, 10-11] Low resolution and high resolution topographic images are possible in non-contact mode and the contaminated fluid layer can interfere with the oscillation during scanning.[6, 10-11] The tapping mode AFM operates by the probe tip lightly "tapping" the sample surface during

scanning, contacting the surface according to the changes in amplitude.[6] the tapping mode may prevent the drawbacks associated with both contact and non-contact modes when the cantilever is oscillating with sufficient amplitude.[6] The contact mode AFM is employed throughout this work to scan substrate surfaces with high resolution under ambient conditions

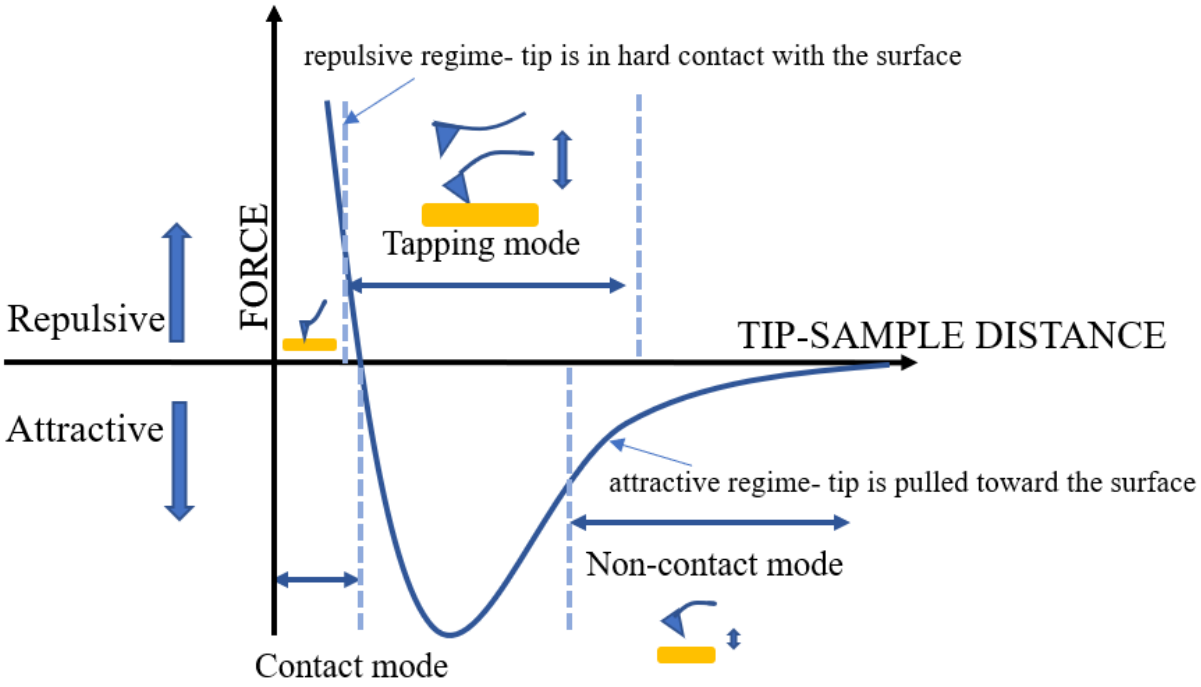

Figure 5.4. Schematic representation of scanning modes in AFM. [6]

The AFM mode employed in this work is the contact mode AFM where the probe tip is in contact with the surface of the sample. The AFM is used to analyze topographic atomic and molecular-scale images of the azulenic SAM films to elucidate the packing, geometry, and periodicity of the azulenic molecules relative to the gold film. The AFM study provides the first molecularly resolved images of SAMs of azulene derivatives which are discussed in detail herein.

V.3. Molecular packing and orientation

Understanding molecular packing, stability, and orientation of SAMs on Au (111) is crucial in organo-electronic designs, reactivity, surface energy, robustness, and many other surface applications. Many analytical methods have been used to monitor the molecular packing, stability, and orientation of SAMs. Some of the analytical methods include FTIR, grazing angled attenuated total reflection IR, mass spectroscopy, X-ray diffraction (XRD), thermal desorption spectroscopy (TDS), AFM, STM, ultraviolet photoelectron spectroscopy (UPS), and X-ray photoelectron spectroscopy (XPS).[12-16] The junction group plays a crucial role in how the molecules are arranged, packed and oriented. Information on the molecular packing influenced by the isocyanide and mercapto junction groups with the gold substrate is essential for designing molecular electronics. Insights on molecular packing and orientation of thiolate- and isocyano-azulene d SAMs on gold substrates have been obtained through studies in our group using both ellipsometry and RAIR spectroscopy. The molecular packing of SAMs on gold substrates is dependent not only on the junction group but also the type of the organic moiety involved in the SAM formation. Figure 5.5 below represents Au (111) (nonpatterned circles) while the positions of the isocyanide and thiolate junction groups are described in patterned circles. The isocyanides are known to form a η^1 linear coordination bond with one gold atom while the thiolate junction coordinates in a hollow fashion with three gold atoms, as depicted in Figure 5.5. The optimum adsorption geometry suggested by the *ab initio* calculations of Ulman *et al.* for CH_3SH adsorbed on Au(111) involves binding of the sulfur atom in triple hollow sites of the Au(111) face.[17] The hexagonal close-packed configuration of gold gives an interatomic gold spacing of *ca* 2.88 Å. The isocyanides and thiolates junctions have wider spacings than the those between gold atoms. The periodic spacing in alkylthiolates SAMs have been measured to have spacings *ca.* 5 Å with a $(\sqrt{3} \times \sqrt{3})R30^{\circ}$ geometry.[17-21] The DFT calculations for the *p*-phenyldiisocyanide (PDI) SAMs on gold adopted a $(2\sqrt{3} \times \sqrt{3})$ ordering.[22]

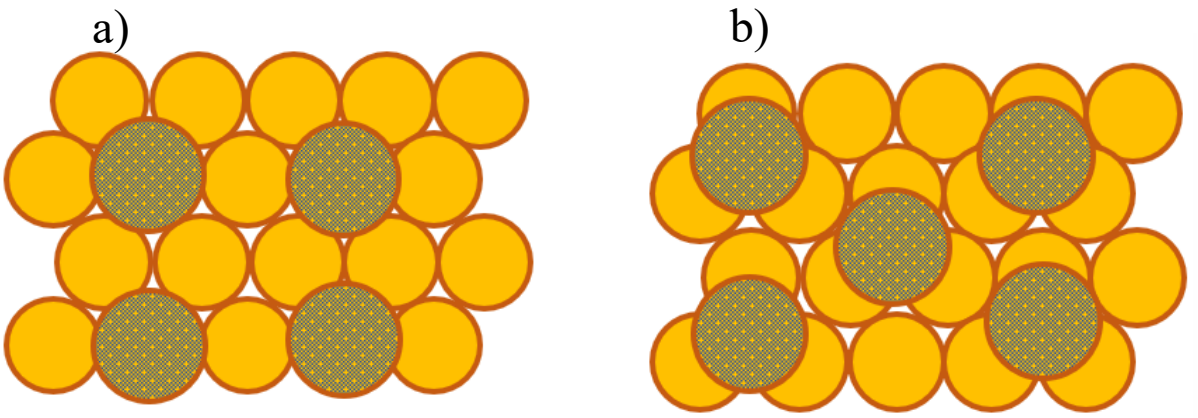

Figure 5.5. Schematic illustration of the structure of SAMs of a) organic isocyanide on gold b) organic thiolate on gold showing molecular packing. The bigger circles represent the isocyano and thiolate groups in a and b, respectively, while the small circles are the Au atoms in the close-packed Au (111) face.

Aside from Au (111), other faces of a golf single crystal have been utilized in SAM formation.[23-25] The investigation of docosylthiol SAMs adsorbed on Au (100), (110), and (111) surfaces by GangYu *et al.* shows that the crystal face of gold substrate influences the structure and packing of SAMs. [25] The study employed low-energy electron diffraction (LEED) technique. The SAMs of docosylthiol adsorbed on Au (111) and (110) showed a commensurate relationship of the thiolate molecule with respect to the surface, while (100) produced incommensurate structures. The sulfur atoms adsorbed on Au (100) showed a (5.97 x 5.97) unit mesh, consistent with the 4-fold symmetry of the underlying gold.[25] This implies that the lattice parameters of the unit cell *a and b* are equal (Figure 5.6). The result was consistent with the c(2 x 2) unit mesh observed for the methyl thiolate SAMs adsorbed on the Au(100) surface. [25] Figure 5.6 illustrates the molecular packing of docosylthiolate film, self-assembled on the Au (100) and Au (110) substrates. The Au (110) surface had a rectangular lattice with a unit mesh of 4.07 x 2.88 Å, while the Au (100) has a square symmetry unit mesh of 2.88 x 2.88 Å, different from the hexagonal Au (111). It was

observed that SAMs made on Au (110) experienced more significant tilt of the molecular constituents as compared to those on Au (111), forming a 4-fold c(2 x 2) arrangement of the sulfur atoms as opposed the 3-fold hollow unit ($\sqrt{3}$ x $\sqrt{3}$)R30° on Au (111).[25] The 4-fold symmetry of the monolayer was due to the missing row in the Au (110) face as shown in Figure 5.6. Therefore, molecular packing is influenced by different junction group-substrate interaction.

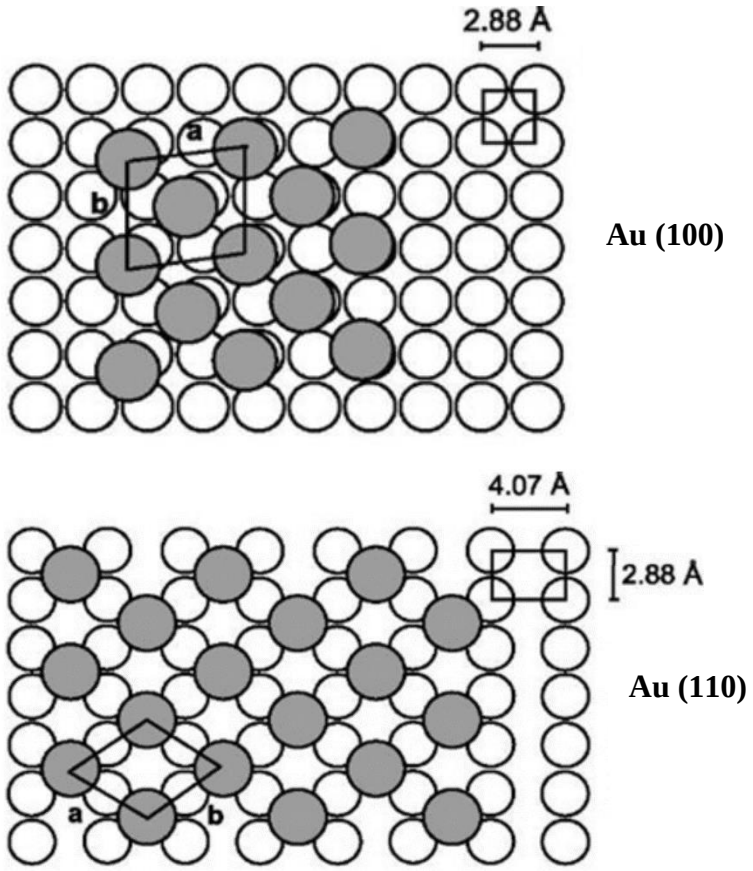

Figure 5.6. Illustration of the structures of SAMs on different gold substrates. Top image: Au (100) showing oblique incommensurate structure with a = b = 5.97 Å and a = 95°. Bottom image: Au (110) sowing commensurate c(2 x 2) unit mesh with a = b=4.99 Å and a = 109.5°. Reprinted with permission from Ref. 25. Copyright (1993) American Chemical Society.

One of the first studies on molecularly resolved images were performed by Gang-yu and coworkers. The long alkanethiol chains adsorbed on Au (111), in ambient conditions, using contact mode AFM were studied. The AFM images were collected using a silicon nitride (Si_3N_4) cantilever tip and a force of 100 nN during the image collection. Gang-yu *et al.* suggested that the alkylthiols adsorbed on Au(111) formed reproducible stable ($\sqrt{3} \times \sqrt{3}$)R30° periodicity with the tilt angle 30° to the surface of the normal.[26] The measured gold hexagonal spacings had an average of *ca.* 0.29 nm.[26] The image of the thiol molecules observed had hexagonal unit spaced by *ca.* 0.5 nm (Figure 5.7) which was consistent with the proposed model from atomic, electron, and X-ray diffraction experiment for thiolate-bound SAMs.[26] The resolved molecular images of the raw data shown in Figure 5.7 were improved using Fourier transformation which filtered out the noise seen in the images. The experiments were conducted at room temperature and atmospheric conditions. Higher resolution images could possibly be obtained at low temperature in vacuum. Experiments at low temperatures, when the molecules are less prone to mobility on the surface, may result in better resolved images. More recent AFM studies have been carried out under ultrahigh vacuum conditions to avoid significant contamination by background gases, to reduce molecule movement during imaging, and to better understand tip-sample interaction. [14, 18, 27-28]

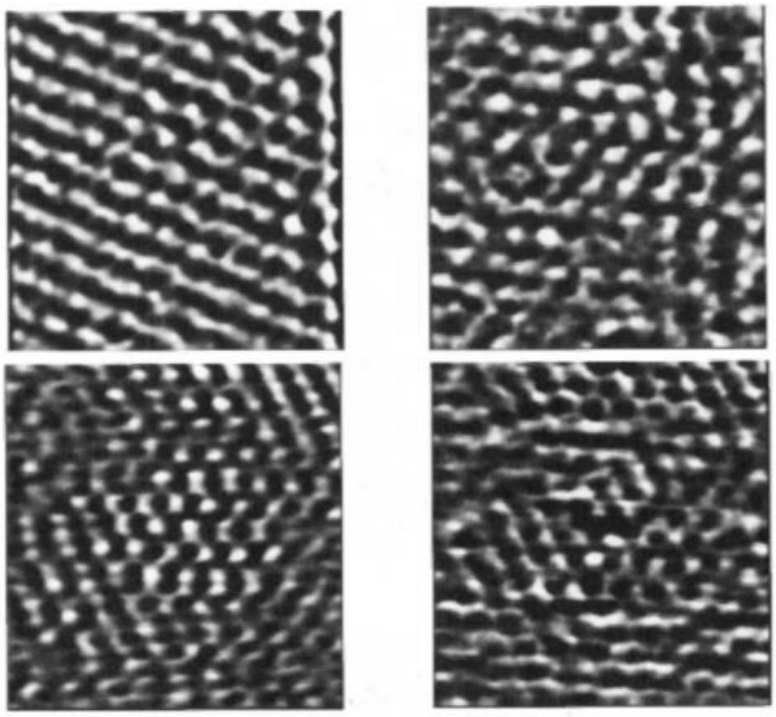

Figure 5.7. AFM images of Left: Topography images of $(CH_2)_9S$ (top image) and $(CH_2)_{17}S$ (bottom image) on Au (111) and Right: corresponding frictional force images collected simultaneously. Reprinted with permission from Ref. 26. Copyright (1994) American Chemical Society.

In more recent studies, different phase structures have been reported suggesting that the observed structures can depend on the type of molecular junction, type of molecular interaction, temperature, substrates, coverage to mention a few.[29-31] G.E Poirier *et al.* showed that the decanethiol could have six distinct phases present which could be (23 x$\sqrt{3}$), (19 x $\sqrt{3}$), ($\sqrt{3}$ x $\sqrt{3}$)R30°, and (3 x 2$\sqrt{3}$) geometries, depending on the coverage.[29-32] These phases were adopted based on either high density or low-density coverage. These decanethiols tend to oxidize on the surface and form decanesulfonates arranged in another phase, (26 x $\sqrt{3}$a) unit cell.[32] In most alkanethiols, it has been seen that the high coverage SAMs may involve a multitude of complex stages like lifting of the (22 x $\sqrt{3}$) Au reconstruction, upright molecular alignment at some specific orientation, and formation of both the most stable ($\sqrt{3}$ x $\sqrt{3}$)R30° and the herringbone patterned

c(4 x 2) superstructures in some other domains as shown in Figure 5.8.[18, 33] Changes in coverage, temperature, or molecular structure can influence the adopted phase observed. The fundamental understanding of how SAMs can have such structural complexity or differences are essential toward the ultimate goals of self-assembly applications in organo electronics.

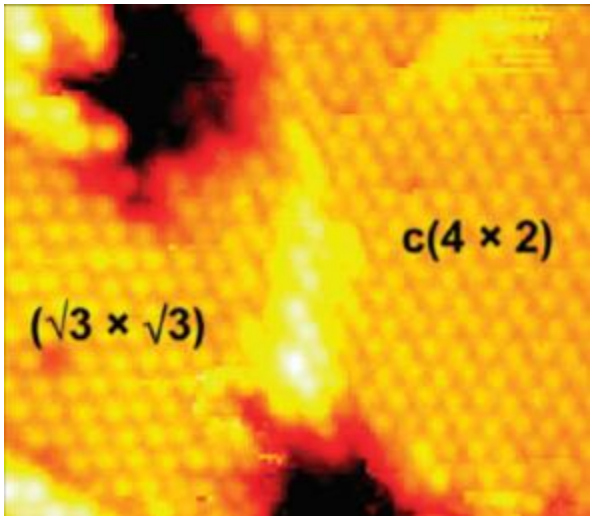

Figure 5.8. Topographic UHV STM image (100 Å x 100 Å, V_s = 1.0 V, I_t = 15 pA) of a C12 SAM. The protruding feature at the center of the image is a domain boundary. Reprinted with permission from Ref. 18. Copyright (2009) American Chemical Society.

Also, conjugated organic rings like benzenethiol SAMs have been studied using AFM/STM measurements. SAMs of 1,4-Benzenedithiol (BDT) adsorbed on Au (111) at 300 K were investigated by W.T. Tysoe *et al.* in a recent 2015 article using an RHK UHV dual AFM/STM. The 1,4-BDT dosed on Au (111) at 300 K and the image acquired at 120 K observed initially showed formation of η^1 gold-sulfur coordination before reassembling of the molecules over time.[27] The reassembling showed both sulfurs bind to the gold substrate with the aryl ring oriented *ca.* parallel to, but substantially above, the gold substrate at room temperature. The STM images showed formation of repeating patterns constrained between the (22 x√3) "herringbone"

reconstructions, hexagonal motifs and chains at low coverage.[27] That is, at high coverage, only one thiolate anchoring group is coordinated to the gold surface, while at low coverage, both thiolate coordinate to the surface, forming chains. Figure 5.9 shows high-resolution UHV STM image of close-packed chains of 1,4-BDT adsorbed on gold at 300 K, with resolvable aryl rings that are hexagonal structures. The measured spacings were approximately 0.65 nm for a parallel aryl rings adsorbed on the gold, with diameters of *ca.* 0.45 nm which are in agreement with literature.[27, 34]

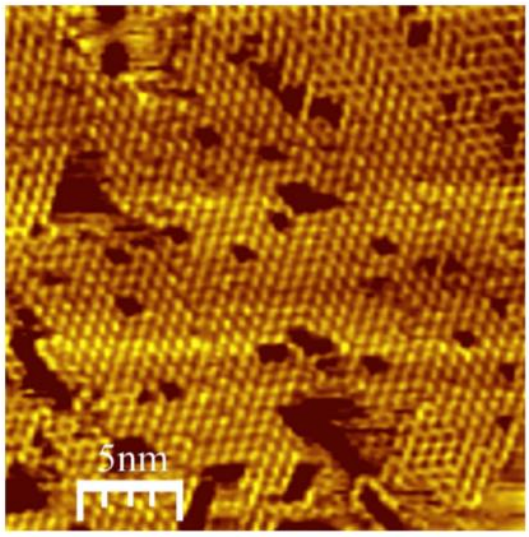

Figure 5.9. STM image of 1,4-DBT adsorbed on gold at 300 K (V_t = 0.25 V_t = 163 pA). Reprinted with permission from Ref. 27. Copyright (2015) American Chemical Society.

AFM/STM images of different SAM films have been investigated in ambient and under ultrahigh vacuum conditions. In ambient conditions, atomically resolved images are harder to collect as compared to imaging under high vacuum due to unavoidable significant gas molecules, liquid layer on the surface, or other adsorbed molecules that interact with the imaging tip and sample surface, this may affect the images collected. Also, most molecules adsorbed on a substrate usually have one anchoring group within the molecule, movement of molecules during imaging in

ambient conditions can affect the topographic images, depending on the strength of interactions in the monolayer and the imaging temperature employed. In 2008, Barybin *et al.* investigated a multipoint anchoring of a metacyclophane to the gold substrate via self-assembly where one isocyanide on each of 4 benzene rings, connected with a short alkyl bridge, all coordinate to the gold as seen in Figure 5.10.[35] This was done to investigate the orientation, binding, stability, and the influence of anchoring via multiple points in a molecule to a gold substrate. The ellipsometric thickness observed for the molecule when all the four isocyanides are bound to the gold was about 5.8 Å which was consistent with calculated thicknesses.[35] Also, the FTIR data showed only one peak, which suggests that all the four isocyanides were bound to the gold substrates and the molecule was oriented in an upright fashion.[35] DFT calculations of the molecule interacting with the gold to estimate the most stable geometry of the molecule on gold was done and it was suggested that the molecule had two lowest possible energy conformations as seen in Figure 5.10 with the intramolecular benzene rings spaced by 0.499 – 0.576 nm.[35] For the first geometry, the interatomic distances between the benzene rings were d_x = 0.499 nm and d_y = *0.499 nm* while the second calculated geometry were d_x = 0.576 nm and d_y = *0.499 nm.* No AFM images were reported. It was suggested that the molecule was very stable due to binding through multiple isocyanides.[35] AFM studies of this molecule adsorbed on gold surface have been obtained recently and are reported herein. Characterization using AFM technique provides further information about the packing and binding of this molecule to the surface.

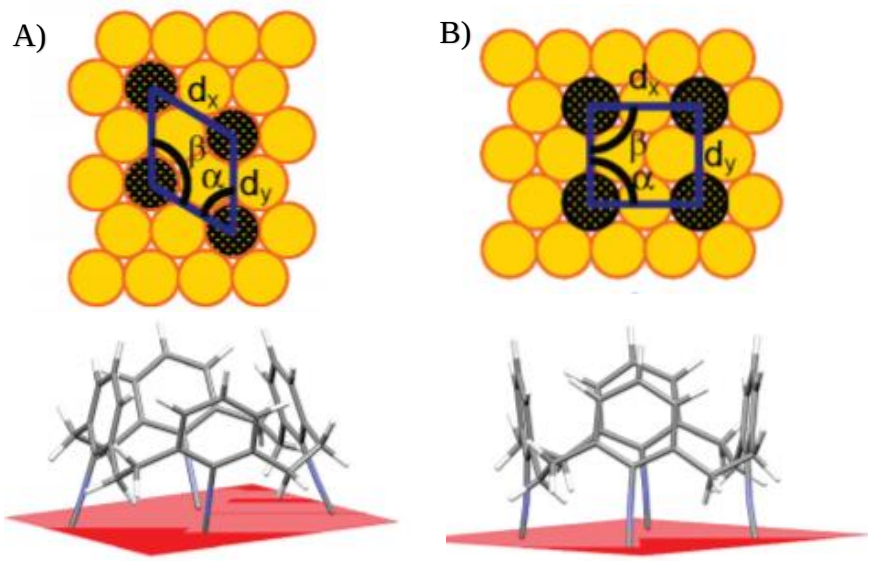

Figure 5.10. A) Top left: Image of the metacyclophane molecule, interatomic distances (d_x = 0.499 nm and d_y = *0.499 nm)*, and the angles (α = 60°and β = *120°*). **B)** Top right: Interatomic distances (d_x = 0.576 nm and d_y = *0.499 nm)* and the angles (α = 90°and β = *90°*) between the gold atoms on the Au(111) surface attributed to Bottom: the lowest energy conformations of the molecule for an upright orientation bound to the Au (111). [35]

Introduced in this work is the AFM characterization of azulenic SAMs with focus on molecular packing, periodicity, and geometry in ambient conditions. Figure 5.11 shows the molecules employed in this work and the materials would likely be used under ambient conditions, so it is important to understand their behavior and packing under ambient conditions. Experiments at low pressure would be more technically challenging and expensive but might provide higher resolution, although under unrealistic conditions. The work described herein features the 2-isocyanoazulene, 2-mercaptoazulene, and a complex metacyclophane. SAM formation and synthesis of the molecules employed have been reported in our previous work. In previous chapters, it was observed that molecular packing and stability can be influenced using SAM displacement experimental route for SAM formation. Hence, investigated in this work is the extent to which this SAM displacement can influence the molecular packing and stability of the azulenic SAMs described.

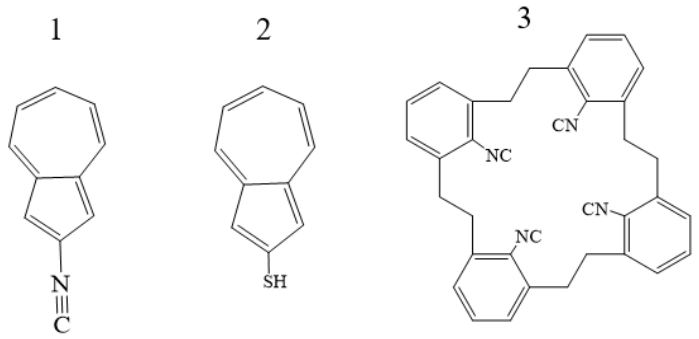

Figure 5.11. 2-isocyanoazulene (**1**), 2-mercaptoazulene (**2**) and 8,16,24,32-tetraisocyano[2.2.2.2]metacyclophane (**3**) adsorbed on gold surfaces for AFM studies.

V.4. Experimental section

V.4.1. General procedures and starting materials

Following the procedures employed in literature, SAMs were made on freshly flame-annealed gold-coated mica, made in the Berrie Lab, without precautions to exclude air or ambient laboratory lighting. In addition, SAMs were made on commercial gold-on-silicon substrates, described in chapter II from Platypus Technologies, for RAIR and ellipsometry analysis of the substrate to confirm the integrity of the SAM formation. Unless stated otherwise, the substrates were cleaned using chloroform ($CHCl_3$), acetone, and 200-proof ethanol for two hours in each solvent for cleaning purposes before SAM formation. All solvents used were purchased from commercial sources and used as received unless solvent distillation was done. Chloroform and dichloromethane were distilled over P_2O_5 and CaH_2 respectively and stored under argon. After cleaning the substrates, ethanol was used to rinse the substrates to remove any physisorbed material on the substrates. The substrates were blow-dried with nitrogen gas before use in SAM formation. The ellipsometric physical constants of the cleaned substrates were measured before immersing substrates in solutions of the azulenic compounds to make the SAM-coated substrates.

Veeco Instruments Multimode AFM Nanoscope® E (Nano E) from Bruker was used for AFM analysis. The calibration of the scanner was done with two different calibration standards, platinum coated calibration grid (PCCG) and highly-ordered pyrolytic graphite (HOPG) substrates, at different scales to ensure that the spacing distances in the sample imaged were accurate. The samples were prepared by attaching the sample to the magnetic sample puck with epoxy (Repro-Rubber, Flexbar Machine Corporation) before transferring to Nano E AFM for imaging analyses. The epoxy glue helps to strongly hold down the sample to the puck in order to avoid any sample movement that may develop during atomic/molecular imaging. The images of both the monolayer and the gold beneath the monolayer were collected, at low and high forces respectively, by applying setpoint voltage on the cantilever tip while the images were collected at 5 nm scan size. The AFM, in contact mode, was used in this study. The instrument was placed on a customized heavy tripod stand, isolating the AFM, inside an acoustically insulated shield to reduce potential acoustic and vibrational noise from the environmental surroundings during the data collection. The probe tip used, except stated otherwise, was a silicon nitride tip on a nitride cantilever purchased from Bruker (Si_3N_4-tip). The tip labeled C, out of four V-shaped cantilevers, with spring constant 0.24 N/m and the resonant frequency of 40 - 75 kHz was used for resolved atomic- and molecular-scaled images. The tip radius of curvature was about 10 - 40 nm, based on manufacturers specifications. The scan size was slowly reduced from 1 μm to 5 nm. The mapped images shown throughout this work, for the atomically or molecularly resolved images, were at 5 nm x 5 nm scan size and at z scale range of 0.5 nm - 1 nm. The AFM parameters; scan rate, scan height, scan size, z-limit, integral gain, proportional gain, and set point were altered accordingly during the image collection to optimize the imaging parameters and image quality for all the

recorded scanned images. Cross section analyses were done for the images to measure the periodic spacings seen on the images.

This work is the first report of molecularly resolved images of azulene derivatives SAM. The imaging parameters, probe tip, and the quality of the monolayer substrate all influence the image quality. Hence, atomically flat gold-coated mica substrates are essential for SAM formation to achieve SAMs with fewer defects and a high packing density on the atomically smooth substrates. Also, not all probe tips can result in atomic and molecular resolution images. Only extremely sharp probes give atomic resolutions. HOPG samples were first imaged at 5 nm scan sizes, due to its flat highly ordered structures, to test the tip quality necessary for image quality, and reproducibility of results.

V.4.1.1. Molecular resolution images of SAMs involving 2-isocyanoazulene (1) on Au (111) surface

*SAMs formation of **1** on gold substrates:*

Flamed-annealed in-house gold-on-mica substrates made in the Berrie Lab were cleaned thoroughly as described in general procedures and starting materials section. The gold substrates were dried in a stream of nitrogen gas before immersing completely in a 2 mM distilled dichloromethane solution of **1** for approximately 24 hrs., to afford a complete monolayer formation. The films were removed, rinsed with distilled dichloromethane to remove physisorbed molecules, dried under a stream of nitrogen gas, and stored in a clean dry vial for AFM analysis.

*Topographic image of SAM-coated films of **1** using contact mode AFM:*

Atomic and molecular resolution images of the gold and monolayers were collected respectively, using contact mode AFM. The SAM-coated substrates were carefully glued on the

sample puck and placed on the AFM as described in general procedures and starting materials. A silicon nitride Si_3N_4 tip was mechanically brought in-contact to the surface of the sample and the images were collected while the AFM parameters were tweaked till atomically resolved images were seen. A setpoint voltage was applied to the cantilever tip, which controls the applied force. The force applied due to the setpoint voltage differs from tip to tip. The images were collected at low forces and high forces. Figure 5.12 is a graphic illustration of how the forces exerted by setpoint voltages can influence the position of the tip. A high applied setpoint voltage may move the molecules away, while the underlying gold surface is imaged. When the setpoint applied is high enough, the molecules are swept from under the tip, allowing the gold surface image to be collected, and the molecules diffuse back once the tip is moved or force is reduced. The monolayer image was collected at low force. The collected images are found in Figure 5.14 in the discussion section.

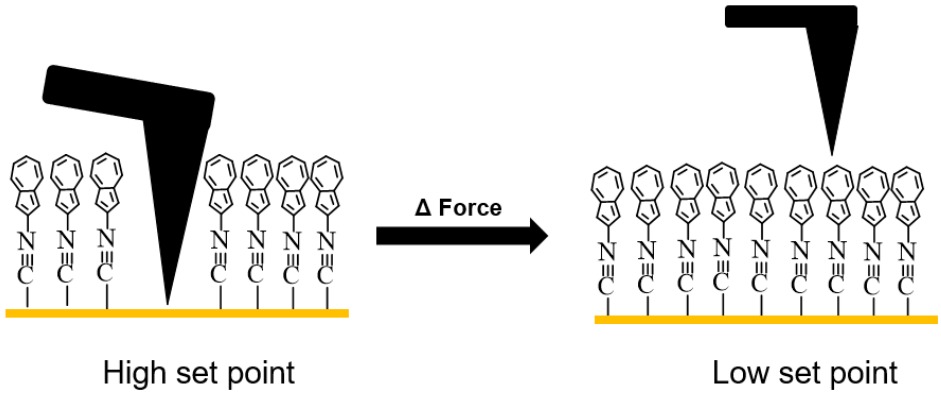

Figure 5.12. A graphic illustration of how AFM probe tip interacts with the surface at high and low force (set point) for imaging the gold substrate and molecular layer of **1** on the gold film respectively.

V.4.1.2. Molecular resolution of SAMs involving 2-mercaptoazulene (2) on Au (111) surface

*SAMs formation of **2** on gold substrates using the displacement method:*

For improvement of the packing and stability of SAM-coated films of **2**, the films were made using the displacement method to prepare the SAMs. SAM-coated films of **1** were first made as described in section 1.2.1 and analyzed using RAIR to verify the expected results. After the analysis verification of SAM-coated films of **1**, the preformed SAM-coated films were immersed in a 2 mM solution of **2** in distilled dichloromethane for *ca.* 24 hrs. Prior to any analysis, the new SAM-coated substrates were rinsed thoroughly with distilled dichloromethane to remove any physisorbed unbound molecules and dried in a flow of N_2 gas.

*Topographic image of SAM-coated films of **2** using contact mode AFM:*

The SAM-coated substrates of **2** were carefully glued on a sample puck using epoxy and contact mode AFM analysis were done as described in the general procedures and starting materials. Tip C on a silicon nitride tip was used brought down in-contact to the surface of the film and images were collected by adjusting all the AFM parameters listed in the general procedure and materials until the atomically resolved images were observed. The collected images are found in Figure 5.15 in the discussion section.

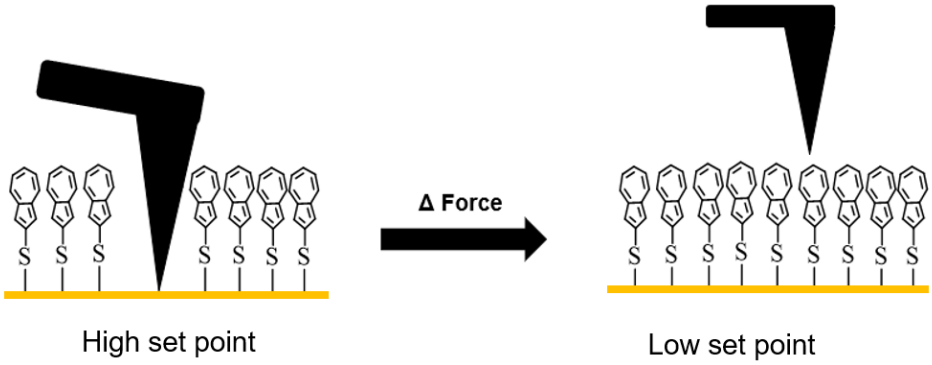

Figure 5.13. Illustration of how AFM probe tip interacts with the surface at high and low force (set point) for imaging the atomic layer and molecular layer of **2** adsorbed the gold film respectively.

V.4.1.3. Molecular resolution of SAMs involving 8,16,24,32-tetraisocyano[2.2.2.2] metacyclo- phane (3) on Au (111) surface

*SAMs formation of **3** on gold substrates:*

Flamed-annealed, freshly made in-house gold-on-mica substrates were cleaned as described in general procedures and starting materials section. SAM-coated films of **3** were made by placing the freshly cleaned gold substrates in a 2 mM solution of **3** in distilled dichloromethane (DCM) for *ca.* 24 hrs. Prior to any analysis, the SAM-coated substrates were rinsed thoroughly with distilled DCM to remove any physisorbed unbound molecules followed by drying under a flow of N_2 gas.

*Topographic image of SAM-coated films of **3** using contact mode AFM:*

A similar imaging method was employed for SAM-coated films of **3**. The film was securely glued on a sample puck using epoxy and transferred onto the AFM in the acoustic shield. Tip C on the cantilever was brought in contact with the surface and images were collected while

optimizing the AFM parameters to give atomically resolved images. (See Figure 5.17 for collected images.)

V.5. Result and Discussion

RAIR spectroscopy and ellipsometry thickness measurements of **1** was done as described in previous chapters. The average thickness of **1** and standard deviation, in parenthesis, at five different spots was 9.5 *(0.2)* Å, and the *ν*(CN) band for the bound 2-isocyanoazulene film was 2176 cm^{-1}. The RAIR and thickness of the SAM results were consistent with previously observed, suggesting upright orientation of the SAM.

AFM images of SAM-coated film of **1** are shown in Figure 5.14. The gold film and the monolayer were sequentially imaged to compare the packing geometries and spacings of the gold to the monolayer. Figure 5.12 represents how the imaging is carried out at high and low forces. The monolayers were temporarily moved away by applying high force on the tip, to image the gold atoms underneath. Since the imaging was done in atmospheric conditions, the molecules that were moved away by the probe tip diffuses back and coordinate with the gold substrates when low forces were applied. At low forces, the molecules were imaged. This is consistent with observations from Gang-yu *et al.*, that when enough force or load is applied to the tip, the molecules move away and diffuse back at a lower load.[26] The hexagonal pattern observed here when the setpoint voltage was 0.3393 V remain constant till the notable change in the pattern at a lower setpoint of 0.1831 V were observed (see Figure 5.14). The force applied was increased and reduced to see the gold and molecules respectively at least three times.

The repeating distances measured at high and low forces were determined through analysis of cross-sectional profiles of the images, by measuring at least 10 different spots. At high force,

the averaged repeating distance and standard deviation in parenthesis for Au-Au separation was 0.31*(0.01)* nm, corresponding to hexagonal geometry of gold spacings from literature. [17-21] At low force, the averaged repeating distances was 0.52*(0.026)* nm. The geometry for the molecular layer is closely related to the ($\sqrt{3}$ x $\sqrt{3}$)R30° seen in the alkylthiol gold films, but the resolution of the image is not great. This may be due to the packing density of the film or imaging conditions. The tilts and twists in the monolayer may provide information on the packing density of the film. Figure 5.15 defines the twist (α) and the tilt (θ) of the monolayer with respect to the gold.

The tilt θ in SAMs adsorbed on gold has been estimated between 25-30°.[36] Gang-yu *et. al.* employed the atomically resolved images and the Fourier transformed analysis to observe the rotation of the unit cell of the molecule (30°) with respect to the unit cell of the underlying gold. The repeated monolayer patterns described here, in the molecularly resolved image in Figure 5.14, are somewhat rotated by 30°. The tilt of the molecule was estimated using ellipsometry thickness. Note that the recorded thickness is an averaged measurement over an area of the substrate. The observed thickness depends on the density packing of the film, which can be lower or higher than the calculated thickness, therefore, the tilt reported is an estimate. In Figure 5.15, the observed thickness is assumed *x* and calculated thickness is *z.* Assuming the calculated thickness of a molecule is tilted which is less than the observed thickness (D_{obs} = 9.5 Å and $D_{calc.}$ = 10.2 Å), then an estimate of the angle at which the molecule is tilted away from the gold surface is given by the equation in Figure 5.15. (The $D_{calc.}$ represents calculated thickness from chapter I and D_{obs} represents observed thickness for SAMs). Note that the assumption is for a completely flat gold surface with no defects. The estimated average tilt angle for 2-isocyanoazulene SAM film was 22 °. The tilt angle normally quoted for alkylthiols on gold is 27 °, and they are quite densely packed.

[36] The tilt in **1** might lead to low coverage. A well-ordered structure of the SAMs at low coverage may be difficult to observe on the AFM.

The image obtained is dependent on the quality of the tip and the sample. The packing of the sample can influence the molecularly resolved images. The image in Figure 5.14b might suggest that the packing is not particularly well-ordered. It could also be that the thermal motion of the molecules makes it difficult to observe. SAM preparation using experimental displacement route are known to provide better molecular packing and stability of SAMs which improves the quality of the film.[37-38] As shown in earlier chapters, mercapto-bound SAMs completely displace isocyanide-bound SAMs on gold substrates. Therefore, this displacement method was employed to make SAM-coated films of **2** for better quality images as shown in Figure 5.15.

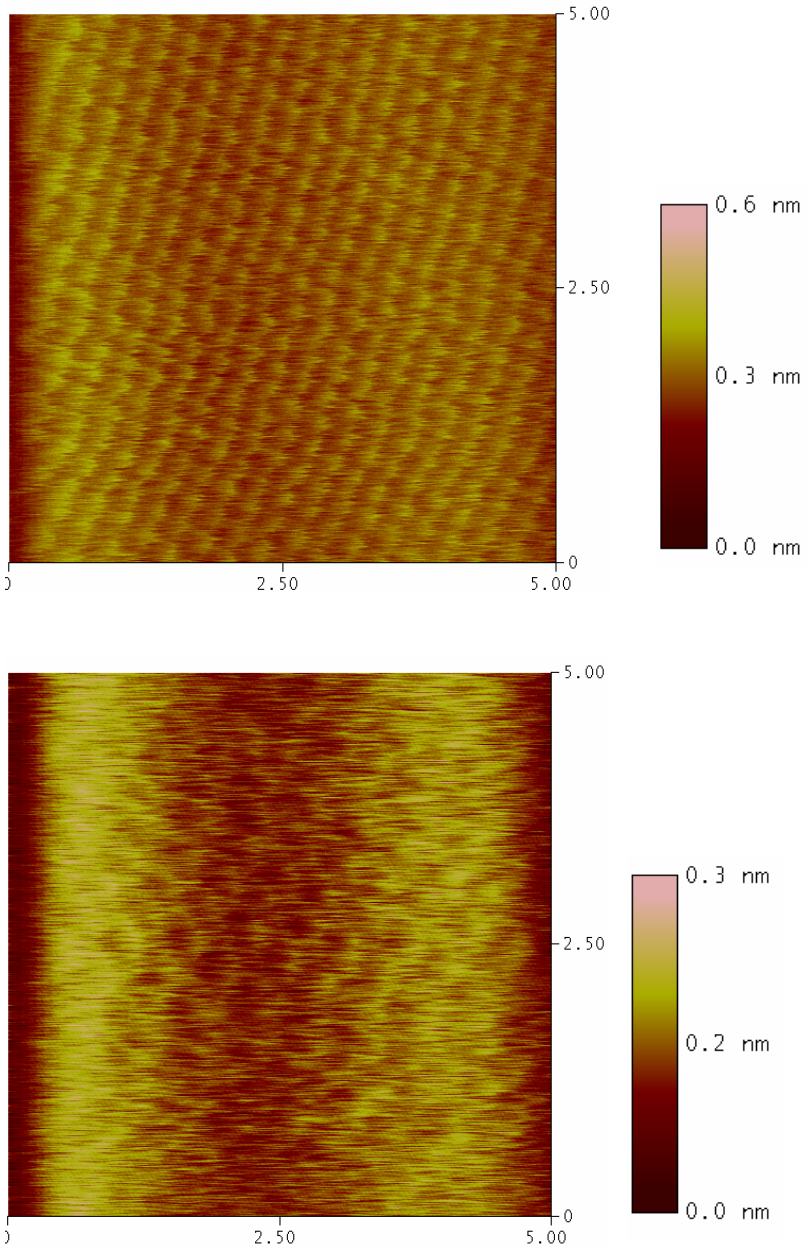

Figure 5.14. AFM unfiltered image of SAM-coated film of **1** a) 5 nm x 5 nm with set point ***0.3393 V***, z scale range 0.6 nm, and atomic spacing ***0.313 (0.007) nm*** b) 5 nm x 5 nm with set point ***0.1831 V***, z scale range 0.3 nm, and molecular spacing ***0.524 (0.026) nm***.

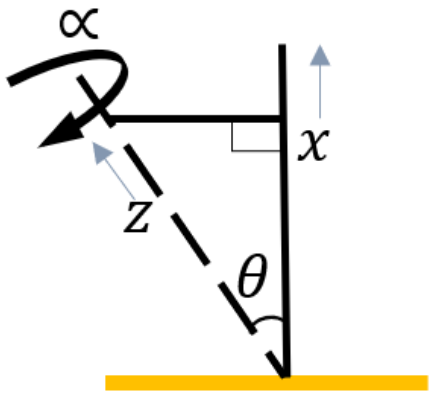

$$\theta^{o} = \cos^{-1}\left(\frac{x}{z}\right)$$

Figure 5.15. Illustration of tilt and twist in SAMs. Assuming *z* represents the molecule on the gold surface, the tilt angle (θ) is defined with respect to the surface normal direction *x*. The twist angle (α) describes the rotation of the molecule plane relative to the plane of the surface normal and the tilted molecule.

The averaged observed thickness D_{obs} and the standard deviation in parenthesis from ellipsometry was 10.9 *(0.1)* Å, similar to the calculated thickness D_{calc}. of 10.4 Å. The observed thickness and the calculated thickness are the same, consistent with the molecules standing upright and densely packed. Note that the tilt angle in **1** is not exact because it is an average value of the film for an assumed atomically flat gold substrate used in monolayer formation. The tilt θ in **2** was not calculated since the observed thickness was higher, unlike in **1**, suggesting possibly higher packing density in **2**. While this is an estimate, it is consistent with the fact that the observed image of **2** are clearer (perhaps more well-packed) than those of **1.** The resolved image in Figure 5.16b is better than Figure 5.14b, indicative of the difference in molecular packing. This may be due to the method of SAM preparation. SAM-coated films of **2** made via displacement methods with better molecular packing were imaged in the air and atmospheric conditions as seen in Figure 5.16. The gold periodicity observed at higher force had the expected Au-Au spacing *ca.* 0.3 nm. The hexagonal pattern was seen at an applied force of 1.350 V and remain unchanged till applied force

was reduced to 0.742 V. At a lower force, the spacing increased, and the molecules were seen at a spacing of 0.53 *(0.049)* nm, measured over at least ten spots. The image 5.16b showed that there is an asymmetric repeating pattern all over the surface. The thiols spaced by 0.53 *(0.049)* nm in one direction, and the other direction by 0.32 *(0.017)* nm. At least a minimum of 10 different spots of the spacings were measured using cross-section analysis on the software. The image in Figure 5.16b is consistent with the molecules being arranged in a face-to-face interaction and tilted in one direction. The yellow and dark features in the images indicate the peak and valleys in the images respectively.

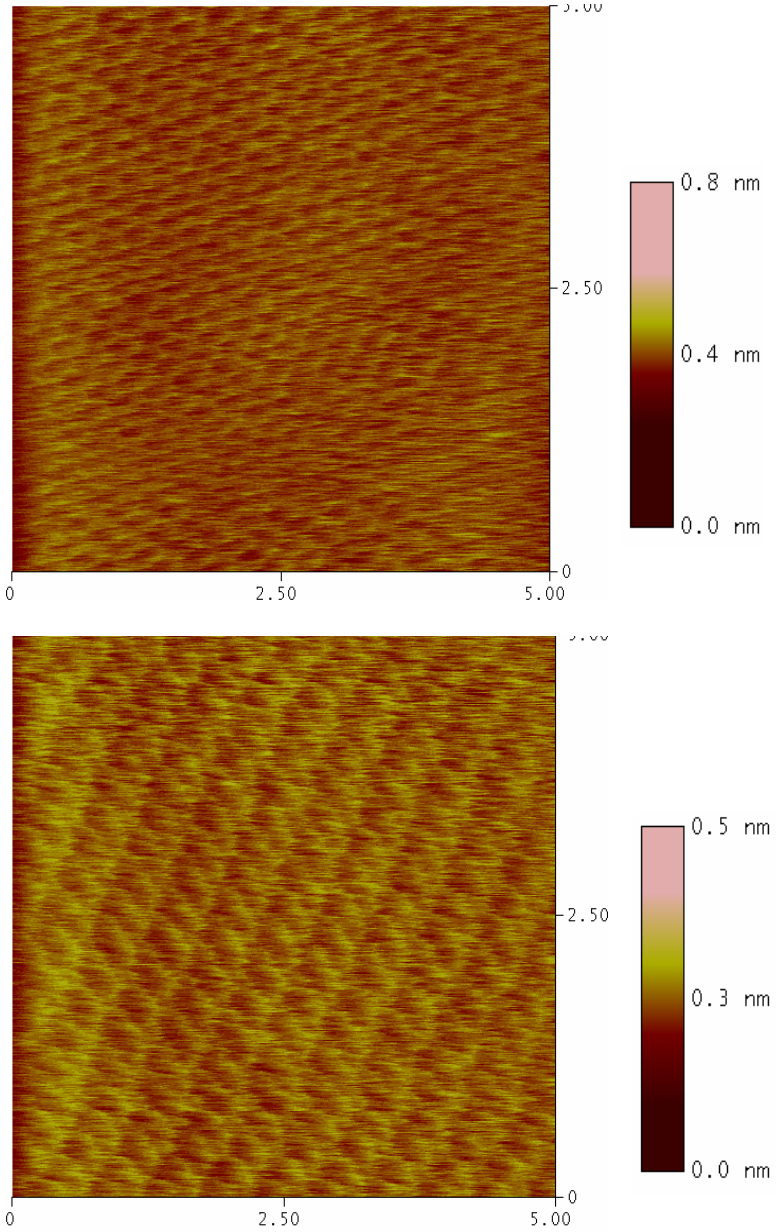

Figure 5.16. AFM unfiltered image of SAM-coated film of **2** made via displacement method a) 5 nm x 5 nm with set point ***1.350 V***, z scale range 0.8 nm, and atomic spacing ***0.332 (0.017) nm*** b) 5 nm x 5 nm with set point ***0.742 V***, z scale range 0.5 nm, and molecular spacing ***0.526 (0.049) nm***.

Comparing the images in Figure 5.16b to 5.14b, the packing of the molecules is different, which may be due to the difference in binding of the junction groups. As discussed in chapter III and IV, the thiolates bind in a three-fold hollow linear fashion to the gold film while a linear gold-

to-isocyanide binding is observed for the isocyanides. This supports the AFM images that show different rectangular unit cell in **2,** not observed in **1**.

The thiolate-bound SAMs on gold substrates were made via displacement experimental procedures in which the thiolate-bound azulene SAMs completely displaced the isocyanides. The packing was enhanced in thiolate-bound SAMs on gold substrate. Perhaps increasing the number of binding junctions, for each molecule, to the gold substrates will aid stronger binding and may result in better molecular packing, and better-resolved images in AFM. Increasing the number of isocyanides bound to the gold substrates will improve the stability of the molecules on the substrates and less movement of the molecules during AFM collection may be observed. Currently, the synthetic work of this type of azulene derivative molecule is in progress.

V.5.1. Discussion on molecular resolution of (3) on Au (111) surface

Contact mode AFM images of SAM-coated films of **3** were collected using an MSNL-tip, labeled D with a spring constant 0.03 N/m, the resonant frequency of 10-20 kHz and tip radius of 2-12 nm. This tip is presumably sharper than the DNP-S tip previously used in the atomic resolution. The images were collected in atmospheric conditions and high applied force yielded images seen in Figure 5.17a representing the Au-Au periodicity. When the high force was applied, the metacyclophane molecules were moved out of the way, and the Au image was collected. The Au-Au spacing measured at ten different spots was consistent with literature values. When the applied force was lowered, the molecules diffused back in and coordinated with the gold substrates to give the images in Figure 5.17b. The measured distances at ten different spots were averaged to *ca.* 0.45*(0.01)* nm. This spacing observed was slightly shorter than the DFT calculated spacings for the interatomic distances of d_x or d_y represented in Figure 5.10 which may be due to the packing of the molecule. The image in Figure 5.17b and the observed spacings are likely due to the packing

of the individual benzene rings in the structure. The packing in this film is quite repeatable and consistent. Also, if the benzene spacing were observed as the picture depicts, the ethyl linkage between each benzene molecule is not visible in the images. High resolution STM images collected under reduced pressure may help in interpreting the images further. The RAIR collected (appendix 4) showed that all the isocyanide in each molecule bind to the gold surface but the ellipsometry thickness measurement for the film was quite short. The thickness for the film images was 3.5 *(0.4)* Å, which is smaller than reported value (5.6 Å).[35] The ellipsometry thickness may suggest low coverage but the image in Figure 5.17b suggest otherwise. This could be that the imaged area on the film had high coverage. The resolution is probably due to the presence of four isocyano anchoring substituent in each molecule. Fourier transformed analysis of the atomic and molecularly resolved images clearly showed that the gold and the molecular images observed are different. While the gold showed a hexagonal pattern and the spacing is consistent with the other images and literature, the molecular layer showed hexagonal arrangements with spacings that are somewhat shorter than expected. The images collected for **3** were made without any SAM displacement. The AFM images shows that the stability of the film is quite high due to multiple anchoring units present in each molecule as compared to the azulenic SAMs in which each molecule is connected to the substrate via one anchoring group.

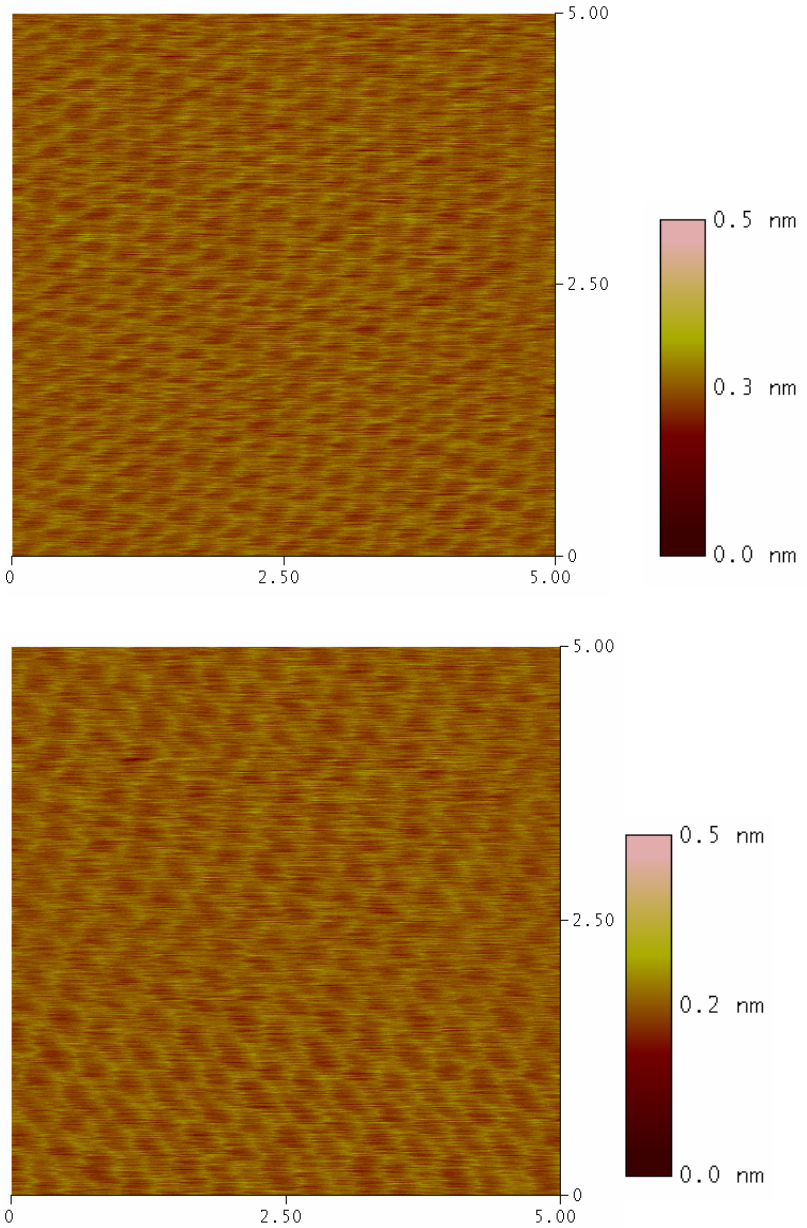

Figure 5.17. AFM unfiltered image of SAM-coated film of **3** a) 5 nm x 5 nm with set point ***1.503 V***, z scale range0.5 nm, and atomic spacing ***0.303(0.005) nm*** b) 5 nm x 5 nm with set point ***1.200 V***, z scale range0.5 nm, and benzene spacing ***0.452(0.011) nm***.

V.6. Conclusions and Outlook

AFM images of SAM-coated films of **1** and **2** were carried out using contact mode AFM, in atmospheric conditions, to understand the packing and periodicity of the molecules adsorbed on gold substrate. The first attempt to atomically and molecularly resolved images of azulene films was made in this study. Different properties may influence molecular packing including SAM formation. The experimental displacement route of SAM formation can impact the quality of the AFM images due to better molecular packing. The AFM images of the thiolate-bound SAMs on gold were made via displacement methods and compared to the analogue isocyanide preformed SAMs. The hexagonal spacings observed for the atomically resolved images of gold films were consistent with the literature. The molecular layer showed periodicity for isocyanide- bound SAMs on gold related to the ($\sqrt{3}$ x $\sqrt{3}$) R30° geometry.

AFM images of **1** and **2** show different repeat distances and unit cell lengths, which suggests different packing of the two molecules on Au (111). The AFM images of **2** showed asymmetric repeated patterns which is not observed on the **1**. This may be the result of different bindings of the thiolates and isocyanides on gold. Typically, thiols have been shown to binding in three-fold hollow sites while isocyanides are bound in an η^1 fashion, to a single Au atom.[14,25] Also, the AFM images from **1** showed lower packing density, which correlates with the observed thickness and estimated tilt angle of the molecule with respect to the gold surface. A better resolution of AFM images was observed in **2** which may be due to the better molecular packing.

To improve the packing and stability of the molecular layer, increasing how the molecules bind to the substrate may stabilize the movement of the molecules during AFM analysis. That is, increasing the coordination sites of each molecule to the gold surface, by increasing the number of thiolate or isocyanide junction groups may affect the durability of the film. A metacyclophane ring

featuring multiple isocyanide anchoring units, attached to individual four benzene rings of the molecule adsorbed on the gold film (**3**) was investigated using contact mode AFM. The repeated spacings of the molecularly resolved image showed individual benzene rings, consistent and repeated on the image. The stability enhanced by multiple isocyano anchoring units on each molecule resulted in high resolution images of **3**.

Further probing of the topography images and conductivity using STM at ambient conditions will provide information on both the charge transport and the molecular packing of the azulenyl SAMs. Current measurements using STM at a constant height when a sharp probe Pt-Ir tip is raster-scanned over the surface. providing spatially resolved conductivity. Preliminary studies using highly ordered pyrolytic graphite (HOPG) samples with well-defined surfaces have been tested on our STM in ambient conditions. The structural arrangements of the monolayers on the substrates and their molecular packing information may pave the way to experimentally probe the conductivity behavior of the isocyano- and mercaptoazulene SAMs.

V.7. References

1. Hynes, M.; Maurer, J., Photoinduced Monolayer Patterning for the Creation of Complex Protein Patterns. *Langmuir* **2012**, *28*, 16237-16242.
2. Saito, N.; Hayashi, K.; Sugimura, H.; Takai, O.; Nakagiri, N., Surface Potentials of Patterned Organosilane Self-Assembled Monolayers Acquired by Kelvin Probe Force Microscopy and Ab Initio Molecular Calculation. *Chemical Physics Letters* **2001**, *349*, 172-177.
3. Krok, F.; Sajewicz, K.; Konior, J.; Goryl, M.; Piatkowski, P.; Szymonski, M., Lateral Resolution and Potential Sensitivity in Kelvin Probe Force Microscopy: Towards Understanding of the Sub-nanometer Resolution. *Physical Review B* **2008**, *77*, 235427-235429.
4. Houston, J. E.; Kim, H. I., Adhesion, Friction, and Mechanical Properties of Functionalized Alkanethiol Self-Assembled Monolayers. *Accounts of Chemical Research* **2002**, *35*, 547-553.
5. Chockalingam, M.; Darwish, N.; Le Saux, G.; Gooding, J., Importance of the Indium Tin Oxide Substrate on the Quality of Self- Assembled Monolayers Formed from Organophosphonic Acids. *Langmuir* **2011**, *27*, 2545-2552.
6. Vickerman, J. C.; Vickerman, J. C., *Surface Analysis : The Principal Techniques*. Chichester England ; New York : John Wiley, Chichester [England] ; New York, **1997**; 457.
7. Butt, H.-J., Electrostatic Interaction in Atomic Force Microscopy. *Biophysical Journal* **1991**, *60*, 777-785.
8. Butt, H.-J., Measuring Electrostatic, Van Der Waals, and Hydration Forces in Electrolyte Solutions with an Atomic Force Microscope. *Biophysical Journal* **1991**, *60*, 1438-1444.
9. Eaton, P. J., Atomic force microscopy. West, P., Ed. Oxford : Oxford University Press: Oxford, **2010**.
10. Eaton, P. J., *Atomic Force Microscopy*. Oxford : Oxford University Press, Oxford, **2010**.
11. Attard, G., *Surfaces*. Oxford Science ; New York : Oxford University Press, Oxford ; New York, **1998**.
12. Sohn, Y.; White, J., Solely Sigma-atop Site Bonding of Phenyl Isocyanide on Au(111)? Comparison with on Cu(111). *The Journal of Physical Chemistry C* **2008**, *112*, 5006-5013.
13. Boscoboinik, J.; Kestell, J.; Garvey, M.; Weinert, M.; Tysoe, W., Creation of Low-Coordination Gold Sites on Au(111) Surface by 1,4-phenylene Diisocyanide Adsorption. *Topics in Catalysis* **2011**, *54*, 20-25.
14. Boscoboinik, J.; Calaza, F. C.; Habeeb, Z.; Bennett, D.; Stacchiola, D.; Purino, M.; Tysoe, W., One-dimensional Supramolecular Surface Structures: 1,4- diisocyanobenzene on Au(111) Surfaces. *Physical Chemistry Chemical Physics* **2010**, *12*, 11624–11629.
15. Cossaro, A.; Mazzarello, R.; Rousseau, R.; Casalis, L.; Verdini, A.; Kohlmeyer, A.; Floreano, L.; Scandolo, S.; Morgante, A.; Klein, M. L.; Scoles, G., X-ray Diffraction and Computation Yield the Structure of Alkanethiols on Gold(111). *Science* **2008**, *321*, 943-946.
16. Zharnikov, M., High-Resolution X-Ray Photoelectron Spectroscopy in Studies of Self-Assembled Organic Monolayer. *Journal of Electron Spectroscopy and Related Phenomena* **2010**, *178–179*, 380-393.
17. Sellers, H.; Ulman, A.; Shnidman, Y.; Eilers, J. E., Structure and Binding of Alkanethiolates on Gold and Silver Surfaces: Implications for Self-assembled Monolayers. *Journal of the American Chemical Society* **1993**, *115*, 9389-9401.
18. Han, P.; Kurland, A.; Giordano, A.; Nanayakkara, S.; Blake, M. M.; Pochas, C. M.; Weiss, P. S., Heads and Tails: Simultaneous Exposed and Buried Interface Imaging of Monolayers. *ACS Nano* **2009**, *3*, 3115-3121.

19. Kang, H.; Park, T.; Choi, I.; Lee, Y.; Ito, E.; Hara, M.; Noh, J., Formation of Large Ordered Domains in Benzenethiol Self-assembled Monolayers on Au(111) Observed by Scanning Tunneling Microscopy. *Ultramicroscopy* **2009**, *109*, 1011-1014.
20. Wang, Y.; Solano Canchaya, J. G.; Dong, W.; Alcamí, M.; Busnengo, H. F.; Martín, F., Chain-Length and Temperature Dependence of Self-Assembled Monolayers of Alkylthiolates on Au(111) and Ag(111) Surfaces. *The Journal of Physical Chemistry A* **2014**, *118*, 4138-4146.
21. Carro, P.; Carro, P., A Novel Model for the ($\sqrt{3} \times \sqrt{3}$)R30° Alkanethiolate–Au(111) Phase based on Alkanethiolate–Au Adatom Complexes. *Physical Chemistry Chemical Physics : PCCP* **2014**, *16*, 19017-19023.
22. Li, Y.; Li, Y., Microscopic Characterization of the Interface between Aromatic Isocyanides and Au(111): A First-Principles Investigation. *Journal of Physical Chemistry C* **2008**, *112*, 6413-6421.
23. Samant, M. G.; Brown, C.; Gordon, J., Structure of an Ordered Self-assembled Monolayer of Docosyl Mercaptan on Gold(111) by Surface X-Ray-Diffraction. *Langmuir* **1991**, *7*, 437-439.
24. Ulman, A.; Eilers, J.; Tillman, N., Packing and Molecular-Orientation of Alkanethiol Monolayers on Gold Surfaces. *Langmuir* **1989**, *5*, 1147-1152.
25. Camillone, N.; Chidsey, C. E. D.; Liu, G. Y.; Scoles, G., Substrate Dependence of the Surface Structure and Chain Packing of Docosyl Mercaptan Self-Assembled on the (111), (110), And (100) Faces of Single Crystal Gold. *The Journal of Chemical Physics* **1993**, *98*, 4234-4245.
26. Liu, G. Y.; Salmeron, M. B., Reversible Displacement of Chemisorbed N-Alkanethiol Molecules on Au(111) Surfaces. An Atomic Force Microscopy Study. *Langmuir* **1994**, *10*, 367-370.
27. Kestell, J.; Abuflaha, R.; Garvey, M.; Tysoe, W., Self-Assembled Oligomeric Structures from 1,4-Benzenedithiol on Au(111) and the Formation of Conductive Linkers between Gold Nanoparticles. *The Journal of Physical Chemistry C* **2015**, *119*, 23042-23051.
28. Hong, S.; Reifenberger, R.; Tian, W.; Datta, S.; Henderson, J. I.; Kubiak, C. P., Molecular Conductance Spectroscopy of Conjugated, Phenyl- Based Molecules on Au(111): The Effect of End Groups on Molecular Conduction. *Superlattices and Microstructures* **2000**, *28*, 289-303.
29. Poirier, G.; Fitts, W. P.; White, J., Two Dimensional Phase Diagram of Decanethiol on Au(111). *Langmuir* **2001**, *17*, 1176-1183.
30. Poirier, G., Coverage-Dependent Phases and Phase Stability of Decanethiol on Au(111). *Langmuir* **1999**, *15*, 1167-1175.
31. Fitts, W. P.; White, J.; Poirier, G., Low-Coverage Decanethiolate Structure on Au(111): Substrate Effects. *Langmuir* **2002**, *18*, 1561-1566.
32. Sotthewes, K.; Kap, Ö.; Wu, H.; Thompson, D.; Huskens, J.; Zandvliet, H. J. W., Ordering of Air-Oxidized Decanethiols on Au(111). *The Journal of Physical Chemistry C, Nanomaterials and Interfaces* **2018**, *122*, 8430-8436.
33. Schreiber, F., Structure and Growth of Self-assembling Monolayers. *Progress in Surface Science* **2000**, *65*, 151-256.
34. Yoon, H. A.; Salmeron, M.; Somorjai, G. A., Scanning Tunneling Microscopy (STM) Study of Benzene and its Coadsorption with Carbon Monoxide On Rh(111). *Surface Science* **1997**, *373*, 300-306.
35. Toriyama, M.; Maher, T. R.; Holovics, T. C.; Vanka, K.; Day, V. W.; Berrie, C. L.; Thompson, W. H.; Barybin, M. V., Multipoint Anchoring of the [2.2.2.2] Metacyclophane Motif to a Gold Surface via Self-assembly: Chemistry of a Cyclic Tetraisocyanide Revisited. *Inorganic Chemistry* **2008**, *47*, 3284-3291.

36. Love, J. C.; Wolfe, D. B.; Haasch, R.; Chabinyc, M. L.; Paul, K. E.; Whitesides, G. M.; Nuzzo, R. G., Formation and structure of self-assembled monolayers of alkanethiolates on palladium. *Journal of the American Chemical Society* **2003**, *125*, 2597-2609.
37. Henderson, J.; Feng, S.; Bein, T.; Kubiak, C. P., Adsorption of diisocyanides on gold. *Langmuir* **2000**, *16*, 6183-6187.
38. Neal, B. M.; Vorushilov, A.; Delarosa, A.; Robinson, R.; Berrie, C.; Barybin, M., Ancillary Nitrile Substituents as Convenient IR Spectroscopic Reporters for Self-assembly of Mercapto- and Isocyanoazulenes on Au(111). *Chemical Communications* **2011**, *47*, 10803-10805.

39. Bruker AFM Probes website https://www.brukerafmprobes.com/p-3710-msnl-10.aspx (accessed November 19, 2018).

Chapter VI:

Conclusions and future directions

Conclusions and future directions

The research presented herein involved self-assembly of azulenic derivatives on metallic gold, with a focus on the resulting films' stability, molecular orientation and packing within the monolayers, film thicknesses, and the influence of the anchoring groups on the physicochemical characteristics of the SAMs. The formation and thorough characterization of new azulene-based films were discussed in detail. Overall, the SAM films anchored to gold(111) substrates via thiolate or isocyanide junction groups are stable (under ambient environmental conditions). Both the ellipsometric thicknesses and RAIR data indicate that coordination of isocyanoazulenes and isocyanobiazulenes via the isocyanide junction group to the gold surface induces upright orientation of the azulenic and biazulenic scaffolds with respect to the gold surface. Upon adsorption of the isocyanoazulenes and isocyanobiazulenes on Au(111) surfaces, the ν(CN) band attributed to the isocyanide junction invariably undergoes a significant blue shift. The strengthening of the junction's C≡N bond that accompanies Au-CN bond formation reflects antibonding character of the terminal isocyano carbon atom's lone pair with respect to the C≡N bond.

The frequency window of the RAIR spectrometer employed in our laboratory did not permit observing ν(Au-S) signatures of the azulenylthiolate and biazulenylthiolate SAMs on gold(111). T chromium(0) pentacarbonyl motif attached to the azulenic scaffold via isocyanide linker was used as remote infrared reporter to facilitate probing adsorption of mercaptoazulenes and mercaptobiazulenes on gold substrates. Thus, the molecular design featured both isocyanide and thiolate anchoring groups connecting the linear 2,6-azulenic 2,6,6',2'-biazulenic bridges to the Au/Cr termini. Whereas many reports on the surface chemistry of isocyanoarenes and mercaptoarenes had been published prior to the work described in this Thesis, no compounds with

both isocyano and mercapto substituents in the same molecule had been known. SAM's of the first π-linkers featuring both -N≡C and -SH termini in the same molecule were fabricated on Au (111) by employing linear 2,6-azulenic and 2,6,6′,2′-biazulenic frameworks. The RAIR spectroscopic and ellipsometric data indicate that the molecules assume an upright orientation upon binding to the Au (111) surface via thiolate junctions. The zero-valent chromium fragment connected to the isocyanide functioned as an excellent remote spectroscopic reporter of the orientation and binding of the molecule to the gold. Another remote spectroscopic reporter, a nitrile group, was substituted on the isocyanoazulene molecules for new SAM films. The nitrile groups do not only act as spectroscopic reporters but may affect SAM formation. The cyano groups, which have been suggested that strongly interacting cyano entities may influence molecular packing, were substituted as tail ends of the molecule. The remote cyano vibrational reporters are sensitive to electronic perturbations induced by the coordination of isocyanoazulenic motif to the gold surface.

Contact mode AFM topography of the atomic and molecular images of the azulenic SAMs were investigated using SAM displacement route to prepare the films. Here SAMs of isocyanoazulene are made and completely displaced by azulenethiolate on the film. The images of isocyanoazulene film and azulenethiolate film were compared. The periodicity of the images observed for the atomic layer indicates hexagonal packing of the gold spaced by *ca.* 0.3 nm. The molecular resolution images suggested that the isocyanoazulene packed differently from the azulenethiolate on the gold substrate due to different repeat distances and unit cell lengths. The measured unit cell dimension for the isocyanoazulene was the same across the image (*ca.* 0.5 nm), while the azulenethiolate showed *ca.* 0.5 nm in one direction and *ca.* 0.3 nm in the other direction. The AFM images in ambient conditions were not trivial due to possible mobility of the molecules when the sharp probe tip is in contact with the film. Immobilizing the molecules on the film by

increasing the number of junction groups in the molecule that coordinates to the gold film may increase the durability of the film.

Future studies on the conductivity of the azulenic films using scanning tunneling microscopy are necessary for assessing the potential of using these novel materials in molecular electronics. Both conductivity and molecularly resolved image can be derived simultaneously from STM analysis. Formation of mixed molecules on the gold film using different junction groups coordinated to the same gold substrate may be interesting to study the conductivity. That is, it may be interesting to study the charge transport behavior of mixed monolayers of isocyanoazulene and mercapotazulene derivatives as seen in Figure 6.1 below. Perhaps the electron donating and withdrawing groups, isocyano and mercapto junction groups, will have different conducting properties which may be simultaneously studied on a film using the STM. Since the junction groups are different and may result in different conducting properties of the SAMs, it will be advantageous to simultaneously study the conducting properties for the purpose of molecular electronic applications. Further understanding of the azulenyl films by XPS which may provide information on the binding of the molecule to the gold film. Specifically, the XPS analyses might be useful in understanding the adsorption of azulenylthiolate SAM films.

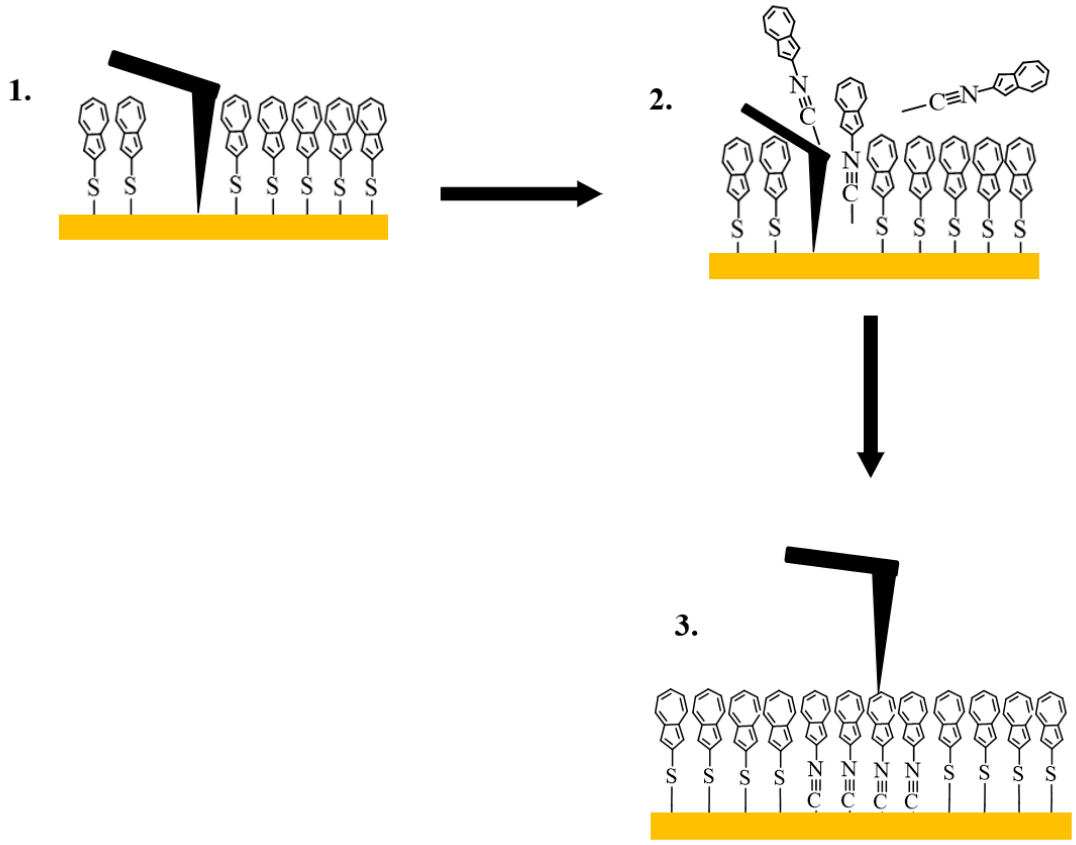

Figure 6.1. Illustration of mixed monolayers of isocyanoazulene and mercaptoazulene on gold film for STM studies.

Appendix 1

SAMs formation of 1,3-dibromo-2-isocyanoazulene (SAM 3)

SAM films were prepared by immersing freshly cleaned gold substrates, purchased from Platypus Technologies, in a 0.6 mM solution of molecules used for the formation of SAM 3 in a distilled dichloromethane for 24 hours. The films were thoroughly rinsed with distilled chloroform to remove unbound physisorbed molecules and blow dried in a flow of N_2 gas before analysis using ellipsometry and RAIR were done. No precaution to exclude air or ambient lighting were exercised for the SAM experiments. The thicknesses of the film were measured at five different spots.

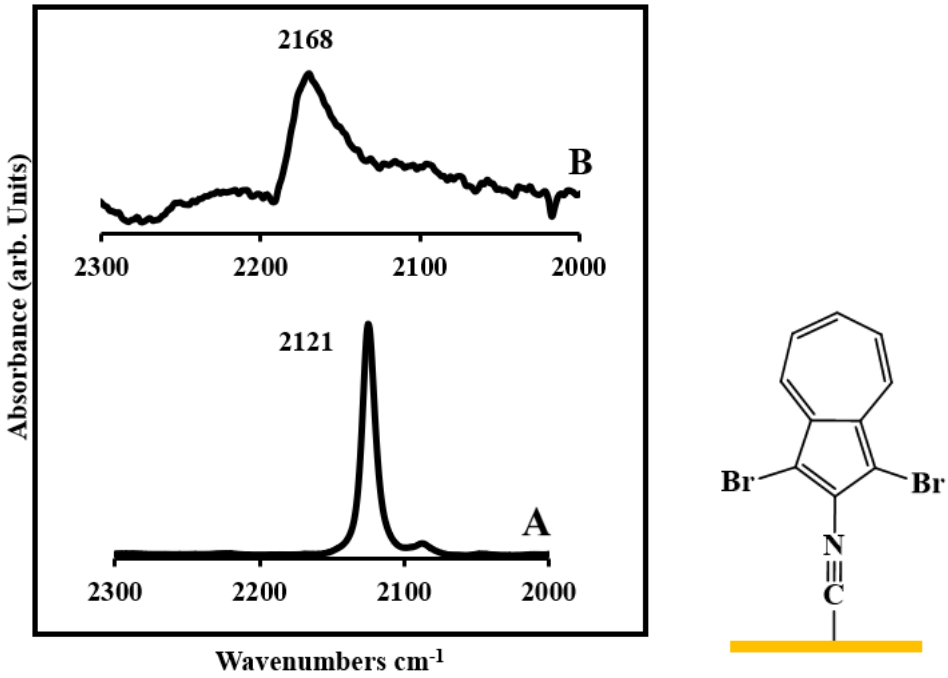

Figure 1. Solution IR in CH_2Cl_2 (A) and RAIR (B) spectra of 1,3-dibromo-2-isocyanoazulene (SAM 3) and an illustration showing the upright orientation of the molecule coordinated on gold film via the isocyanide junction group.

Appendix 2

FTIR of 2-isocyano-1,1′,3,3′-diethoxyl-6,6′-biazulene (SAM 13)

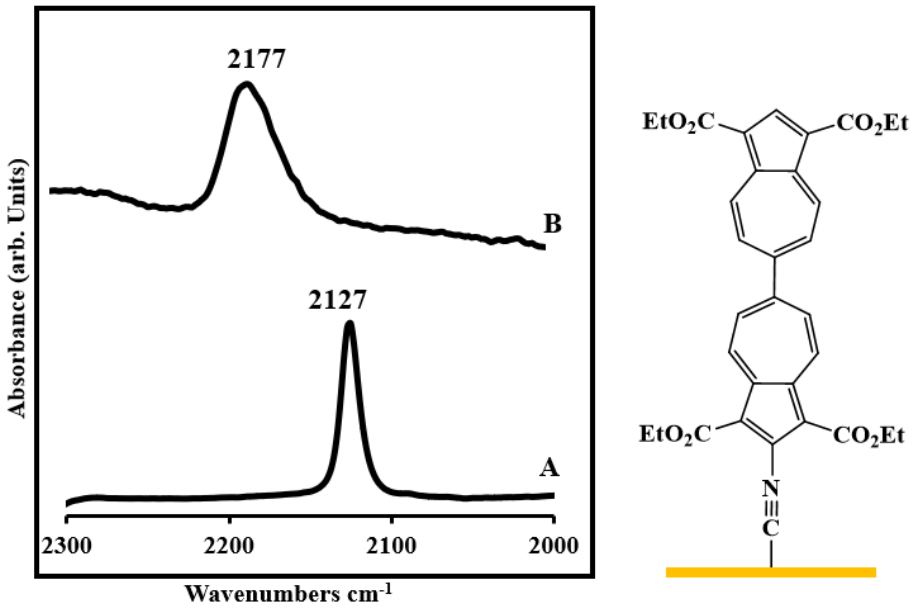

Figure 1. Solution IR in CH_2Cl_2 (A) and RAIR (B) spectra of 2-isocyano-1,1′,3,3′-diethoxyl-6,6′-biazulene (SAM 13) and an illustration showing the upright orientation of the molecule coordinated on gold film via the isocyanide junction group.

Appendix 3

FTIR of 6-isocyano-2,2′-biazulene (SAM 17)

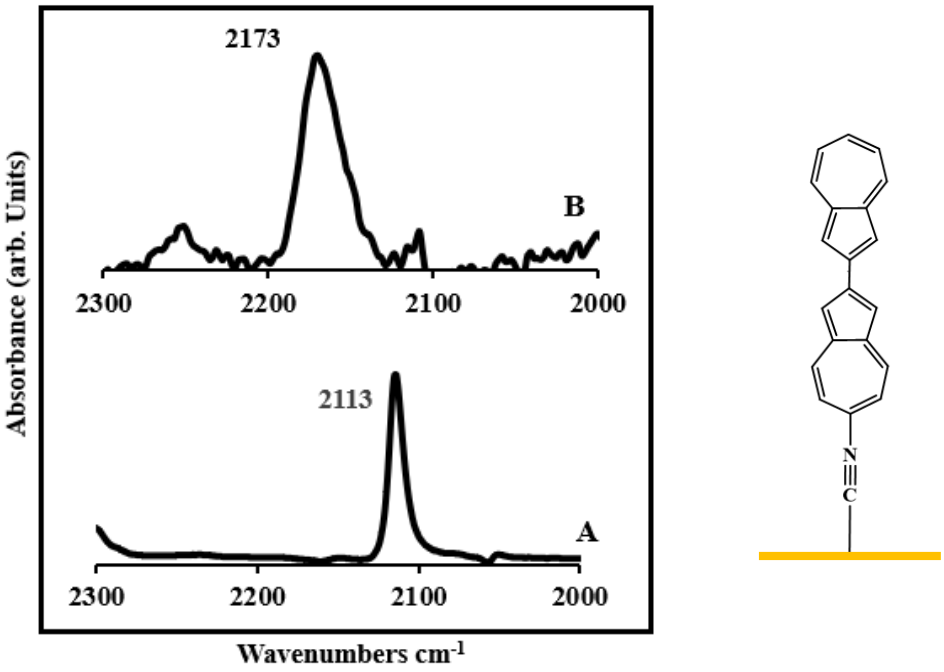

Figure 1. Solution IR in THF (A) and RAIR (B) spectra of 6-isocyano-2,2′-biazulene (SAM 17) and an illustration showing the upright orientation of the molecule coordinated on gold film via the isocyanide junction group.

Appendix 4

FTIR of 8,16,24,32-tetraisocyano[2.2.2.2]metacyclophane (3)

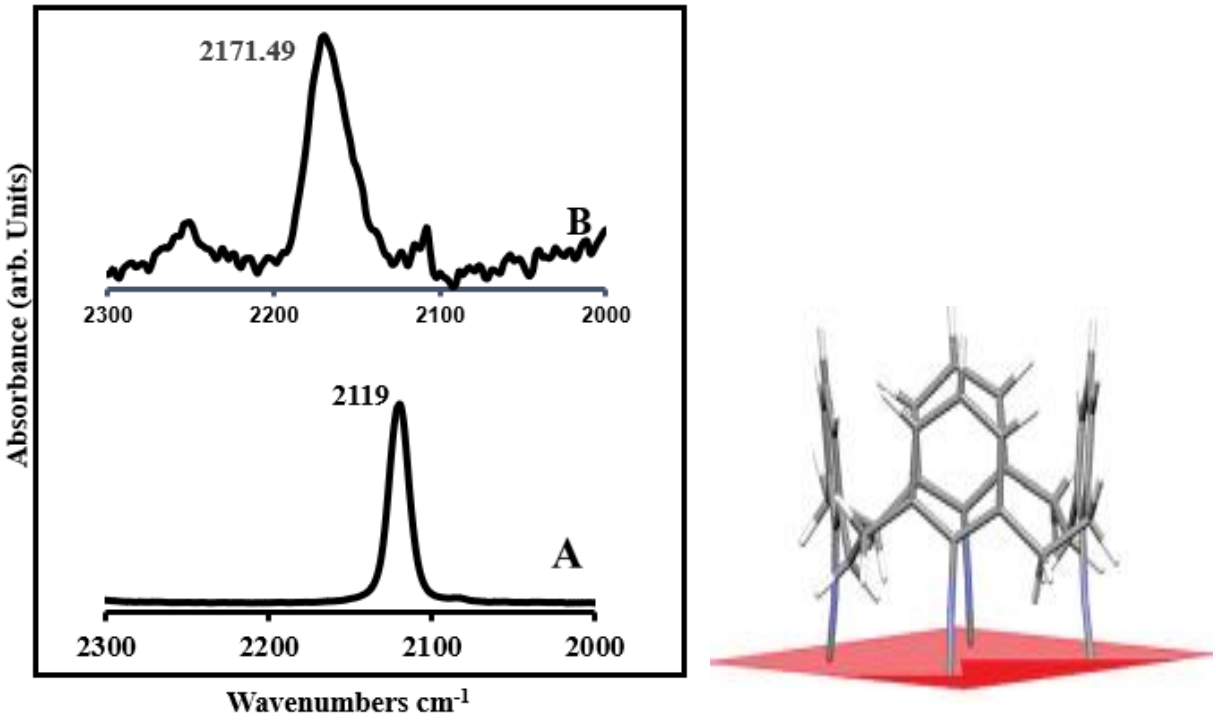

Figure 1. Solution IR in DCM (A) and RAIR (B) spectra of 8,16,24,32-tetraisocyano[2.2.2.2] metacyclophane (**3**) and an illustration showing the upright orientation of the molecule coordinated on gold film via the isocyanide junction group.